Spring 2021

# Fiber reinforced polymer bar investigation: Long-term in-situ durability and bond strength assessment in conventional and sustainable concrete

Ali Fadhil Al-Khafaji



Department: Civil, Architectural and Environmental Engineering

# FIBER REINFORCED POLYMER BAR INVESTIGATION: LONG-TERM IN-SITU DURABILITY AND BOND STRENGTH ASSESSMENT IN CONVENTIONAL AND SUSTAINABLE CONCRETE

by

ALI FADHIL AL-KHAFAJI

A DISSERTATION

Presented to the Graduate Faculty of the

MISSOURI UNIVERSITY OF SCIENCE AND TECHNOLOGY

In Partial Fulfillment of the Requirements for the Degree

DOCTOR OF PHILOSOPHY

in

CIVIL ENGINEERING

2021

Approved by:

John J. Myers, Advisor
Lesley Sneed
Guirong Yan
K. Chandrashekhara
Antonio Nanni

## PUBLICATION DISSERTATION OPTION

This dissertation consists of the following three articles, formatted in the style used by the Missouri University of Science and Technology:

Paper I, found on pages 7–43, has been published in *ACI-Material Journal*.

Paper II, found on pages 44–88, has been published in *Journal of Cleaner Production*.

Paper III, found on pages 89–131, has been published in *ASCE-Composites for Construction Journal*.

# ABSTRACT

Corrosion of steel reinforcement and carbon dioxide emissions are two major global problems. Different methods, techniques, and materials have been implemented to mitigate these problems. Glass fiber-reinforced polymer (GFRP) bar presents itself as a solid alternative to replace conventional steel reinforcement owing to its fantastic features in resisting corrosion. Its demand is progressively increasing. Cement-based concrete, on the other hand, is not eco-friendly due to the excessive amount of carbon dioxide ($CO_2$) emissions yielded from its cement production. One of the alternatives used to mitigate the use of cement in concrete is fly ash. Fly ash is considered a supplementary cementitious material (SCM) and has been only implemented partially to replace cement as a binding material in concrete, however its application has been limited to only limited doses (lower than 30%). In this study, durability and bond-slip investigations were carried out. The durability study was done on GFRP bars extracted from eleven bridges across the United States after being in service from 12 to 20 years. Several tests were conducted on the bar and the surrounding concrete to make the assessment. The tests results showed that there were slight sings for environmental attack but did not show any obvious signs for microstructural deteriorations. In addition, a bond-slip investigation was carried out to evaluate the bond performance of GFRP bars embedded in fly ash-based sustainable concrete. A high-volume fly ash (HVFA) concrete was implemented; 50% and 70% cement replaced with fly ash were used. The results showed that GFRP bars had less bond strength than that resulted from mild steel bars.

# ACKNOWLEDGMENTS

Firstly, I am extremely thankful to my lord and creator for everything I have been given and, in return, I sincerely want to use this degree and the others I obtained to improve the lives of my fellow human beings.

I also would like to express my sincere gratitude to my advisor and mentor, Dr. John J. Myers, for his guidance, encouragement, motivation and support during my PhD studies. In addition, I would like to thank the members of my advisory committee: Dr. Lesley Sneed, Dr. Guirong Yan, Dr. K. Chandrashekhara, and Dr. Antonio Nanni for their advice and assistance.

I also would like to thank GAANN program from the United States Department of Education for their great support throughout this degree. In addition, I would like to thank the department of Civil Engineering and Missouri Department of Transportation and the Tier 1 University Transportation Center RECAST at Missouri S&T for their assistance. Many thanks to the High bay laboratory staff. I also would like to thank my fellow graduate students: Hayder, Zuhair, Eli, Wei, Michael, and Nick for their help.

I would like to greatly thank my parents for their enormous support and encouragement. I would like to especially and deeply thank my Mom from the bottom of my heart for everything she has done for me since I was born. It is deeply appreciated. Finally, I also would like to thank my brother, sister, and grand mom, and aunts for their encouragement and support. Without, first, God and, second, the aforementioned people, I wouldn't have been able to reach this stage.

# TABLE OF CONTENTS

SECTION

# LIST OF ILLUSTRATIONS

PAPER I Page

PAPER II



PAPER III

# LIST OF TABLES

# NOMENCLATURE

| Symbol | Description |
|---|---|
| P | Tensile load |
| f'c | Compressive strength of concrete |
| u | Bond strength |
| $d_b$ | Bar diameter |
| $l_d$ | Embedment length |
| $A_p$ | Peak toughness |
| $A_{p50}$ | Post-peak toughness at 50% of the peak |
| $A_{p80}$ | Post-peak toughness at 80% of the peak |
| c | Concrete cover |

# 1. INTRODUCTION

## 1.1. BACKGROUND

Corrosion and carbon dioxide emissions are two global and major problems. Steel reinforcement used in concrete corrodes and when it does, it requires a considerable amount of monitoring as well as it is considered costly to repair (add ref). Failing to repair corroded reinforcement can compromise the integrity of a structure. Corrosion problems have been treated/prevented using several methods such as cathodic protection, anodic protection, epoxy-coated bars, and galvanized bars, however these methods have not been completely successful in avoiding corrosion (ref 2 ACI paper Ali). Corrosion-related repairs consume more than $8 billion per year in the United States only (NACE 2013 JCLP paper Ali). Therefore, the search for alternatives has been of main interest for many industries and scientists. One of these alternatives is called glass fiber-reinforced polymer (GFRP) and it is a corrosion-resistant material. In addition, it has magnificent characteristics including high strength to weight ratio, non-conductivity, and price competitiveness in compared with steel (ASCE-JCC part 2 Ali). Glass fiber-reinforced polymer has many applications including bridges (ASCE-JCC part 2 Ali, and part 1), barriers (El-Salakawy et al. 2005 from Benmokrane 2018), parking garages (Ahmed et al. 2017 from Benmokrane 2018), and storage structures (Mohamed and Benmokrane 2014 from Benmokrane 2018).

Even though, considerable amount of research has been carried out to evaluate the instant (i.e. freshly produced GFRP bars) chemical and mechanical properties of the

GFRP bars, very few studies were conducted to evaluate their field-based performance after being in service for several years (add ref). In addition, most of the field-based data were for bars extracted after being in service for less than one decade (add ref). The lack of long-term durability database of GFRP bars in standards and design documents could be the main reason behind the shy application of GFRP bars in the civil engineering industry. In order to encourage implementing these bars, surely more field-based and long-term data is needed. Therefore, to enrich our understating about the long-term and field-based performance of GFRP bars, a major study was carried out to investigate the durability performance of GFRP bars installed in two bridges firstly and followed by nine bridges across the United States after being in service for about two decades. Several institutional and industrial laboratories collaborated to carry out the investigation. Multiple GFRP tests were conducted to examine the microstructural, chemical, and mechanical performances of the extracted bars. Scanning electron microscopy (SEM) examination was used to evaluate the microstructural performance; energy dispersive spectroscopy (EDS), glass transition temperature ($T_g$), Fourier transform infrared spectroscopy (FTIR), fiber content, water absorption, and moisture contents were used to evaluate the chemical performance; while short bar shear and tensile tests were used to assess the mechanical performance. In addition to the GFRP bar tests, three main tests were performed on the concrete surrounding these bars to see what environment surrounded the bars and how that affected the overall performance of the bars. The concrete tests performed were: pH, carbonation depth, and chlorides content.

Besides the importance of durability investigations and since the desire for green structures has never been as high as now a day, the author also wanted to investigate the bond performance of GFRP bars in green concrete (i.e. eco-friendly). GFRP bars have been investigated in conventional concrete, but very limited research has been done on GFRP bars installed in green concrete. Production of Portland cement generates significant amount of carbon dioxide ($CO_2$) where the construction industry is responsible for about 8% of the total $CO_2$ emissions. Therefore, many research centers have dedicated a big chunk of their research to study and investigate effective concrete alternative to fully or partially avoid cement-based concrete (also called conventional concrete).

Fly ash is a supplementary cementitious material and has been used moderately in concrete, but its dose of use has been limited to around 25% (add ref). Fly ash is a byproduct resulted from burning coal (add ref). There are two main types of fly ash as per ASTM xxx (add ref); class-C and class-F. Besides the other chemical differences between these two classes, the major difference between class-C and F is the Ca level, where class-F has a Ca level of no more than 15%, while, in class-C, Ca levels could surpass 50% (add ref). Besides fly ash is considered waste and it is abundant, adding fly ash to the concrete has many advantages including: enhancing workability, lowering hydration heat, lowering early ages concrete thermal cracking, and enhancing concrete mechanical and durability performances (add ref fly ash review – Sahmaran and Li 2009). Based on the environmental protection agency (add ref – EPA 2008), the fly ash implementation in concrete lowers the CO2 emissions equivalent to emission from 2.5

million vehicles on road every year. In addition, multiple research mentioned the effectiveness of fly ash in lowering the concrete expansion through lowering the alkalis levels in the pore water solution of concrete (add ref – fly ash review). This advantage works greatly when GFRP bars used as reinforcement in fly ash-based concrete, because resin of GFRP bars (especially ester-based resins) are susceptible to alkalis (add ref – Ali ACI material). Hydroxyl group (OH) reacts with alkalis of the glass fiber and thus leaching issues will be introduced. In addition, OH group can react with alkalis in the concrete pore water solution and generates what is known by alkali hydrolysis attack (add ref – Ali - ACI Durability). Alkali hydrolysis attacks the resin of GFRP bar and thus compromises the integrity of the resin. Therefore, having fly ash in concrete can reduce the amount of alkalis and as a result the existence of fly ash will reduce the chances of leaching and alkali hydrolysis issues when GFRP bars used.

Owing to the many advantages of using fly ash in concrete, the author attempted to investigate concrete made with high-volume fly ash and reinforced with GFRP bar. Two levels of fly ash were used, 50% and 70% cement replaced with fly ash. This was the first time to investigate high-volume fly ash (HVFA) concrete with such reinforcement. This combination was selected for two reasons: first, fly ash reduces $CO_2$ emissions, and second, fly ash reduces alkalis. To assess the performance of the HVFA concrete with GFRP bars, the author chose the bond as a topic of investigation owing to its structural importance. Two sizes of GFRP bar were used, 0.50 in. (13 mm) and 0.75 in. (19 mm) as well as two length of embedment were used, 2.5 in. (64 mm) and 3.5 in. (89 mm). Pullout test was carried out to assess the bond-slip performance. Additionally,

besides the mechanical tests, microstructural and chemical tests were conducted to see if the addition of fly ash affected the GFRP bar even though the period was only limited to the curing time. The tests were SEM, $T_g$, and EDS to make the assessment. Furthermore, statistical-based models were made to predict the bond strength of the bar.

## 1.2. OBJECTIVES AND SCOPE OF WORK

This research addressed two important aspects of GFRP bars. The first aspect was the on-site long-term durability after being in-service for around two decades. This aspect will not only enrich our design standards but also will encourage the civil engineering industry to implement GFRP bars in their constructions. The majority of the available data are based on bars with five-to-ten years of service, so this study is very important and adds a lot information to the database.

The second aspect is the bond performance of the GFRP bars when installed in fly-ash based concrete. Replacing cement with fly ash can significantly reduce the amount of the $CO_2$ emissions. Fly ash-based concrete is considered green (e.g. eco-friendly) concrete. In addition, fly ash reduces the alkalinity level in concrete and that works great when GFRP bars used as reinforcement because the latter is sensitive to alkalis. Having a perfect bond between concrete and its reinforcement is essential for a structure integrity, therefore the topic of bond between GFRP bars and fly ash-based concrete was investigated in this study. Since fly ash has been only used in low dosage (around 25% maximum) and has many benefits, high-volume fly ash (HVFA) concrete was selected as the concrete of investigation.

## 1.3. LAYOUT OF THE DISSERTATION

Section 1 includes the background information, studies objectives and scopes, and layout of the dissertation.

Paper I includes: introduction; research significance; sample extraction, preparation, and conditioning; concrete examinations; GFRP bar examinations; conclusions and recommendations.

Paper II includes: introduction; experimental work; materials, mixture proportions, fresh and hard properties; GFRP rebar tests; test setup and procedure; test results and discussion; GFRP rebar test results and evaluation; statistical analyses and discussions; comparison with previous studies; and conclusions.

Paper III includes: introduction; bar testing program; GFRP test results and discussion; and conclusions and recommendations.

Appendix describes paper IV and V. Paper IV includes: introduction; selected bridges; sample extraction; sample inventory and distribution; challenges and solutions; concrete tests procedure; concrete tests results; and conclusions. Paper V includes: introduction; pullout bond experiment; mixtures and materials; setup and procedure of pullout test; test results and discussions; and conclusions.

# PAPER

## I. ASSESSMENT STUDY OF GFRP REINFORCEMENT USED IN TWO CONCRETE BRIDGES AFTER MORE THAN FIFTEEN YEARS OF SERVICE

Ali F. Al-Khafaji [1]; John J. Myers [1]; and Antonio Nanni [2]

[1] Missouri University of Science and Technology, Rolla, MO 65409, USA

[2] University of Miami, Coral Gables, FL 33124, USA

## ABSTRACT

Corrosion in reinforced concrete (RC) represents a serious issue in steel reinforced concrete structures, therefore finding an alternative to replace steel reinforcement with a non-corrosive material is necessary. One of these alternatives is glass fiber-reinforced polymer (GFRP) that arises as not only a feasible solution but is also economical. The objective of this study is to assess the durability of GFRP bars in concrete bridges exposed to a real-time weather environment. The first bridge is Southview Bridge (in Missouri State) and its GFRP bars have been in service for more than 11 years; the second bridge is Sierrita de la Cruz Creek Bridge (in Texas State) and its GFRP bars have been in service for more than 15 years. In order to observe any possible mechanical and chemical changes in the GFRP bars and concrete, several tests were conducted on the GFRP bars and surrounding concrete of the extracted cores. Carbonation depth, pH, and chlorides content were performed on the extracted concrete

cores to evaluate the GFRP-surrounding environment and see how they influenced certain behaviors of GFRP bars. Scanning electron microscopy (SEM) was performed to observe any microstructural degradations within the GFRP bar and on the interfacial transition zone (ITZ). Energy dispersive spectroscopy (EDS) was applied to check for any chemical elemental changes. In addition, glass transition temperature (TA) and fiber content tests were carried out to assess the temperature state of the resin and check any loss in fiber content of the bar after these years of service. The results showed that there were no microstructural degradations in both bridges. EDS results were positive for one of the bridges, and they were negative with signs for leaching and alkali-hydrolysis attack on the other. Fiber content results for both bridges were within the permissible limits of ACI440 standard. Carbonation depth was found only in one of the bridges. In addition, there were no signs for chlorides attack in concrete. This study adds new evidence to the validation of the long-term durability of GFRP bars as concrete reinforcing used in field applications.

## 1. INTRODUCTION

Corrosion of steel reinforcement represents a major issue within the civil engineering industry, as the cost of repairs in the United States, Canada, and several European countries makes up a substantial percentage of the infrastructure-allocated expenditures of these countries [1]. Several methods such as cathodic protection, epoxy coated bars, and galvanized steel were implemented, yet these methods have not been

entirely successful to stop corrosion [2]. Thus, considering the difficulties and costs of corrosion repairs, the direction to find non-corrosive alternative materials are of primary importance to replace steel reinforcement. One of these alternatives is glass fiber reinforced polymer (GFRP). GFRP bars have been applied successfully as a main reinforcement in quite a few concrete structures. As they have high strength to weight ratio and are non-corrosive, in addition to being economically feasible [3]. Some of these GFRP-reinforced concrete structures include barriers [4], parking garages [5], storage structures for wastewater treatment [6], and marine structures [7]. However, the use of GFRP as a main reinforcement requires additional field validation [8]. Despite the fact that there has been significant research on laboratory-based chemical and mechanical testings, creep, and natural weathering of composites, limited research closely related to real-time field exposure scenarios has been performed. Thus, field-related durability data needs to be proactively gathered and made available for standard writing organizations [9].

Using accelerated laboratory tests to assess the GFRP durability performance by exposing GFRP-reinforced concrete to an alkaline environment does not resemble the conditions of those exposed to a real-time field exposure [2]. Accelerated tests are significantly harsher on GFRP bars than real-time filed exposure. In 1998, Porter and Barnes [10] conducted accelerated experiments on GFRP bars to determine their long-term tensile strength. Alkaline solution was used on the bars with a temperature of 60° C (140° F) for three months. The test results showed that after alkaline exposure, the residual strengths of bars were between 34 and 71%. In 2004, Nkurunziza et al. [11] implemented the combined effect of sustained loadings (up to 40%), chemical solution (de-ionized

water or alkaline solution), and high temperature (between 55° C (131° F) to 75° C (167° F)) on 9.5-mm diameter GFRP bars. The test results showed that de-ionized water-exposed and alkaline-exposed specimens lost 4% and 11% of their original strength respectively.

On the other hand, a more reliable indication of the durability of GFRP bars can be taken from monitoring the performance of existing GFRP-reinforced concrete structures. Therefore, durability studies on GFRP bars extracted from bridges have become the preferred process of evaluation. In 2007, Mufti et al. conducted a durability study on GFRP bars extracted from five bridges across Canada after being in service for over 8 years [12]. Several tests were performed on the specimens to investigate their microstructural, chemical, and mechanical performance. The results showed that, from the SEM examination, a decent bond observed between the GFRP and concrete, while from Fourier transformed infrared spectroscopy and differential scanning calorimetry tests, neither hydrolysis nor significant changes in glass transition temperature took place. Gooranorimi et al. 2016 assessed the durability of GFRP bars in an existing bridge in the State of Texas, USA. After 15 years of service, tests were conducted on these bars including scanning electron microscopy (SEM), energy dispersive x-ray spectroscopy (EDS), short bar shear (SBS), fiber content, and glass transition temperature (TA). The test results showed no microstructural deteriorations in the bars, and no change in their chemical compositions. The TA and the fiber content results were close to the control bars values, while the short bar shear results were inconclusive [8].

In this study, another durability study was carried out on GFRP specimens extracted from the same bridge that Goornorimi et al. [8] used to conduct their study, but this time the specimens were taken from another location of the bridge. In addition, another bridge in a different state (Missouri State) was added to the list of durability investigation to enrich and validate the current durability documents. Several GFRP bars extracted from the two bridges, that have been in-service over eleven and fifteen years, were investigated. The tests were conducted on the GFRP bars, including: SEM, EDS, Fourier-Transform Infrared spectroscopy (FTIR), TA, and fiber content. The test results were compared to control bars available from one bridge and to test results conducted on the same bridges but on different cores. Control bars are similar to those installed in the bridge, but they were tested at the same year of GFRP bars installation. Besides the GFRP tests, concrete surrounding the GFRP bars were also evaluated to observe the environment surrounding the GFRP bars and thus to see how they influenced a certain behavior/failure of the bar. The concrete tests involved carbonation depth, pH, and chlorides content and were performed on portions of the cores that contained the GFRP bars.

## 2. RESEARCH SIGNIFICANCE

The significance of this research is to provide more technical information about the durability of GFRP bars. Durability data of GFRP bars embedded in concrete structures and have been in service for a decade or more is very limited. To encourage the

construction industry to implement GFRP bars, a more-detailed and updated durability information needs to be present in the design standards and guidelines. Therefore, this study attempts to add more information to the durability performance of GFRP bars used as a reinforcement material for structural applications.

## 3. SOUTHVIEW AND SIERRITA DE LA CRUZ CREEK BRIDGES

Southview Bridge is located on Carter Creek in Rolla, Missouri, shown in Figure 1.A. The original bridge was one-lane and consisted of four box culverts and topped with steel reinforced concrete deck of a 254 mm (10 in.) thickness. An expansion occurred in 2004 by replacing the existing sidewalk with a new one and adding another lane that consisted of four-box culverts and topped with glass fiber reinforced concrete deck. The expansion phase involved removing the curb from the existing deck to allow extending the bridge total width from 3.9 m (12.8 ft) to 11.9 m (39 ft). The new resulting width of the bridge is 9.1 m (30 ft) 13. GFRP reinforcement with 19 mm (3/4 in.) diameter was used as a main reinforcement and 13 mm (1/2 in.) diameter was implemented for shrinkage and temperature reinforcement in the deck [2]. Also, 10-mm (3/8 in.) diameter GFRP bars were used as prestressing tendons. Figure 2 shows the cores locations. The bridge is exposed to a range of temperature between -5° to 35° C (22° to 95° F) during the year. Also, it experiences regular wetting, drying, freezing, and thawing cycles. In addition, deicing salt is sprayed in winter months.

The temperature range and precipitation (from 1981 to 2015) are shown in Figure. 3. The second investigated bridge was Sierrita de la Cruz Creek Bridge and is located north-west of Amarillo, Texas. Figure.1. B. shows the Sierrita de la Cruz Bridge. The bridge was severely corroded, so it was considered structurally deficient, therefore a bridge replacement was necessary.


Figure 1. (A) Southview Bridge, Rolla, MO. (B) Sierrita de la Cruz Creek Bridge, Amarillo, TX

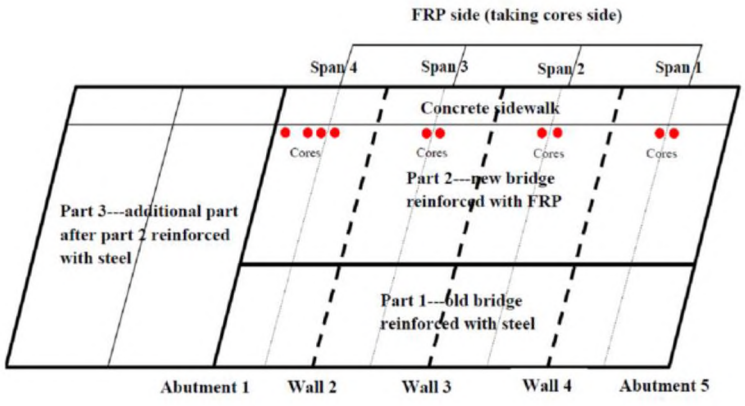


Figure 2. Cores locations of Southview Bridge

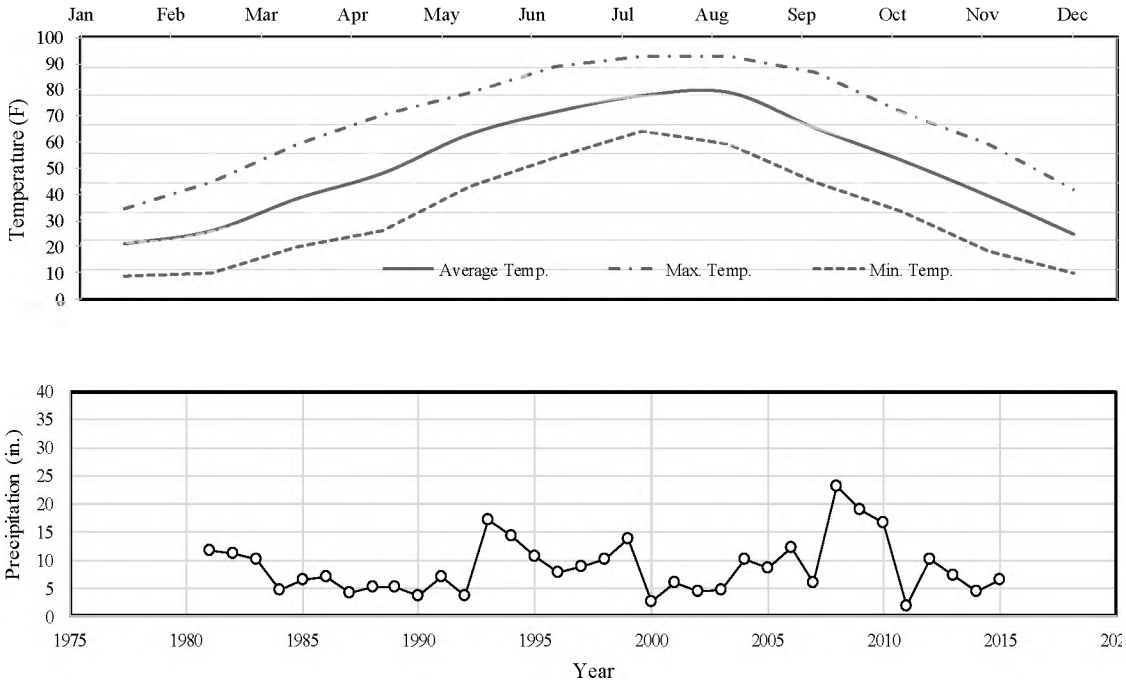


Figure 3. Temperature range and precipitation of Rolla, MO. from 1980 to 2015[36,37]

This bridge was the first bridge in the State of Texas that implemented GFRP bars. The GFRP reinforcement was used in the deck of the bridge and the construction work took place in 2000. The Bridge is 24 m (79 ft) long and 14 m (46 ft) wide. GFRP bars with 16 mm (5/8 in.) and 19.0 mm (3/4 in.) diameter were used in only two spans out of the seven spans total. To assess and monitor the behavior of GFRP bars, witness GFRP bars were implanted during construction at the overhang, midspan, and control joints where they were planned to be extracted at different times of their service life without compromising the structural integrity of the bridge deck [8]. Figure. 4 shows the location of the cores. It should also be noted that these locations were seated where de-icing salts tend to concentrate along the guard rail from roadway salt spray. The temperature in Amarillo ranges from -3° to 39° C (26° to 102° F). In addition, the bridge

is exposed to frequent wetting, drying, freezing, and thawing cycles. Figure. 5 shows the temperature range and precipitation (from 1981 to 2015) of Amarillo, Texas.

Sand coating was used in all GFRP bars installed in these bridges to provide a proper bond to surrounding concrete. In addition, the GFRP bars were made of E-glass fibers and vinyl-ester resin.

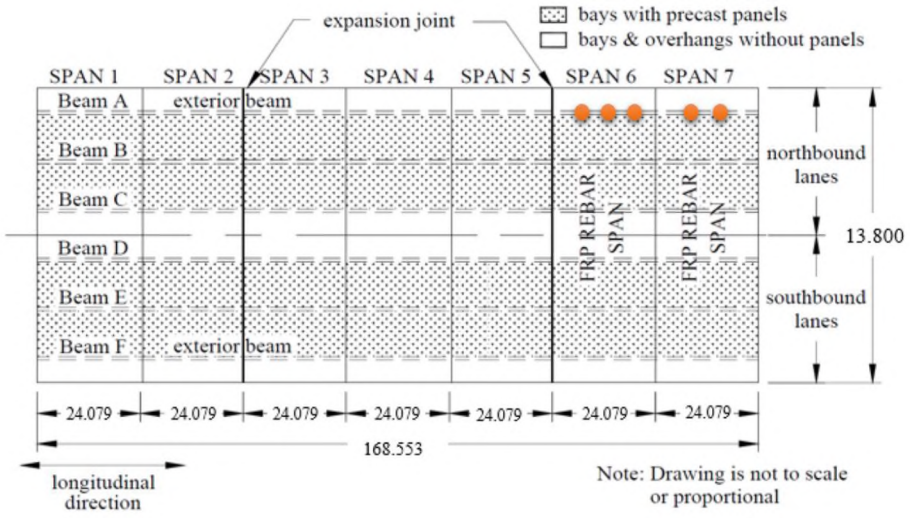


Figure 4. Cores locations of Sierrita de la Cruz Creek Bridge

## 4. SAMPLE EXTRACTION, PREPARATION, AND CONDITIONING

Concrete cores of 102 mm (4 in.) diameter with encapsulated GFRP bars were extracted from the bridges in 2015. A total of ten cores were taken from the deck of Southview Bridge in the following manner: two cores from each of span one, two, and three, and four cores from span four.

On the other hand, five cores were extracted from the overhang of Sierrita de la Cruz Bridge. In both bridges, the core holes filled immediately after the core extraction with a fast-curing durable cementitious grout.

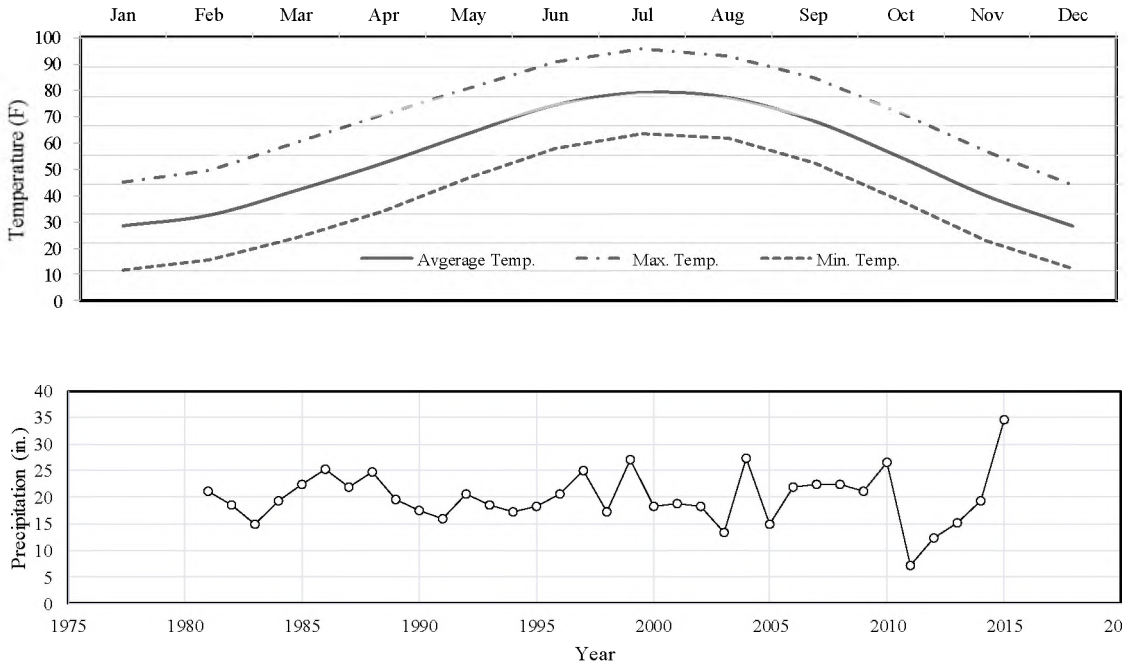


Figure 5. Temperature range and precipitation of Amarillo, TX. from 1980 to 2015[36,37]

The extracted cores were then sent to the laboratories of the collaborated universities. Two cores, CM1 and CM2, from Southview Bridge and one core, CT, from Sierrita de la Cruz Bridge were sent to the laboratory of Missouri S&T for examinations. In both bridges, all the extracted GFRP bars were 19 mm (3/4 in.) diameter. Figure. 6 shows one core from each bridge and Table 1 shows the GFRP bars information. The preparation of a specimen varies from one test to another. Since some of the tests required only a tiny piece of material to study, each core was cut into

several slices parallel to bar-length orientation. Next, each slice that contained GFRP bar was cut into several slices until what was left is a GFRP bar with a little concrete surrounding it. Some of these little pieces were kept whole with no concrete removed and some had the concrete stripped from the GFRP bar.

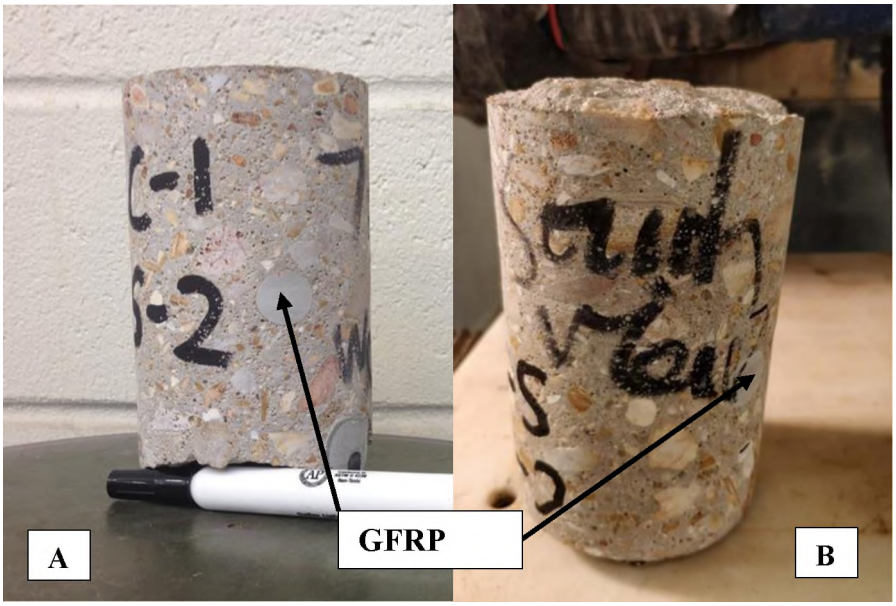


Figure 6. Cores from (A) Southview Bridge, Rolla, MO. (B) Sierrita de la Cruz Creek Bridge, Amarillo, TX

Table 1. Properties of GFRP bars used in the bridges

| Bridge Location | Bridge | Cores ID | GFRP Reinforcement Number & Diameter | Fiber Type | Resin Type | Bridge's Core Location |
|---|---|---|---|---|---|---|
| Missouri | Southview | CM1 | #6 (0.75 in.) (19 mm) | E-glass | Vinyl ester | Midspan |
| | | CM2 | #6 (0.75 in.) (19 mm) | E-glass | Vinyl ester | Midspan |
| Texas | Sierrita de la Cruz Creek | CT | #6 (0.75 in.) (19 mm) | E-glass | Vinyl ester | Bridge Overhang |

It completely depends on the test that was being conducted on that piece. Figure 7 depicts some of the samples preparations. In SEM and EDS, after cutting the GFRP specimens to a 13-mm (1/2 in.) thick piece, the surface of GFRP specimens was smoothed using different levels of sandpaper (e.g. NO: 180, 300, 600, 800, and 1200 Grit) and was then polished for an extra surface smoothness. After that, an oven at 50° C (122° F) was used to keep the specimens dry. Also, since GFRP is nonconductive material, a gold coating was used on the specimens to make it conducive and sensitive to electrons that will be exerted from the SEM apparatus. For FTIR test, very tiny chunks, around 5 mg (0.0002 oz.), were cut from the GFRP specimens and were then grinded with KBr to enhance the level of spectrum detection [12]. The mix was then compressed in order to make a thin film to be used later in the FTIR device. In TA test, small chunks, about 15 mg (0.0005 oz.), were taken from the GFRP specimens and were then placed inside an aluminum pan that was later on sealed mechanically and situated inside the DSC device for TA testing. Preparations for the fiber content test is mentioned in its section. Specimens were conditioned first by keeping them in a hermetically sealed environment and second, for two days before testing, by exposing them to 40° C (104° F) temperature to maintain a controlled (i.e. standardized) environment.

## 5. CONCRETE EXAMINATION

In order to have a complete assessment of the GFRP bars, the surrounding concrete had been examined too. The tests used for concrete in this study were, pH, chlorides content, and carbonation depth.


Figure 7. Preparations of Specimens: (A) air drying, (B) oven drying, (C) sonic bath, (D) drilling to get concrete powder

**pH Test**: The test of pH quantifies alkalinity level in concrete. In Portland cement-based concrete, pH of concrete ranges between 11-12 [14]. The value of pH on concrete surface falls as a result of the reaction of the carbon dioxide from the atmosphere and alkalis in the concrete. To measure pH level, there are two methods; Grubb procedure and ASTM F710 [15]. The Grubb procedure was applied in this study where powder, about 2 grams, were taken from the surface of concrete core and then mixed with distilled water in a 1:1 mass ratio. After mixing the distilled water with the concrete powder, a 60-sec set-time was given to mixture to let it become a thick muddy-like solution. Next, pH strips were used to determine the alkalinity of the solution. The test was conducted three times per core. For Southview Bridge, pH test results were 13, 12.9, and 13.2 which were considered high for such concrete. It could be due to the ingress of hydroxide ion from exposing the concrete to an alkaline-based environment. In Sierrita de la Cruz Creek Bridge, the pH results were 11, 11.1, and 11.1 which satisfied the expectation for that type of concrete and age. Figure.8 shows concrete pH measurements of one of the specimens. Table 2 shows the pH test results.

Table 2. Concrete test results

| **Bridge** | **Cores ID** | **pH** | **Carbonation Depth mm (in)** | **Chloride Content (%)** |
|---|---|---|---|---|
| Southview | CM1 | 13 | 0 (0) | 0.0033 |
| | CM2 | 13 | 0 (0) | 0.0094 |
| Sierrita de la Cruz Creek | CT | 11-12 | 13 (0.5) | 0.0031 |

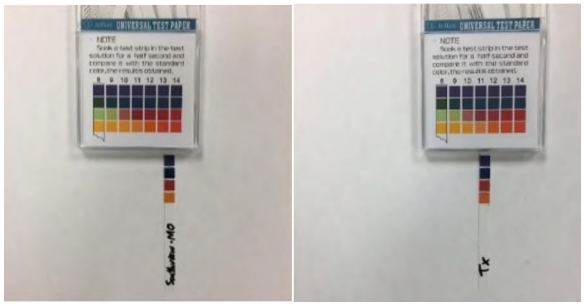

Figure 8. pH test measurements: (A) Southview Bridge (B) Sierrita de la Cruz Creek Bridge

**Carbonation Depth**: Concrete cover provides a protective layer to steel reinforcement against corrosion, but the cover is normally exposed to the atmosphere. Carbonation takes place when carbon dioxide in the atmosphere reacts with alkalis of concrete [2]. It lowers concrete pH from about 12 to 9 or less, which makes the concrete layer relatively acidic. It has been proposed that corrosion happens when the carbonation depth is equal to the concrete depth [16]. There are several factors that influence the carbonation rate including: the mix design, cement composition, concrete porosity, ambient temperature, $CO_2$ concentration, relative humidity, and existing cracks [17]. In order to conduct the test, RILEM 1988 [18] was used where the depth of carbonation was determined by spraying a 1% of phenolphthalein-70% ethyl alcohol solution to a fresh cut of the concrete surface. The solution is colorless as long as the ambient atmosphere is acidic. However, once it hits an alkaline environment where the pH is around 9 or over, it will turn purple. The results of the carbonation depth indicated that, in Southview Bridge, there was no carbonation depth found, but in Sierrita de la Cruz Creek Bridge, a carbonation depth of 13 mm (1/2 in.) was observed. Even though, the pH results of Sierrita de la Cruz Creek Bridge were not low enough to induce carbonation attack,

carbonation was detected. It is most likely because the collected powder was from unaffected area, therefore its pH came out relatively high. Figure.9 and Table 2 show the carbonation depth results.

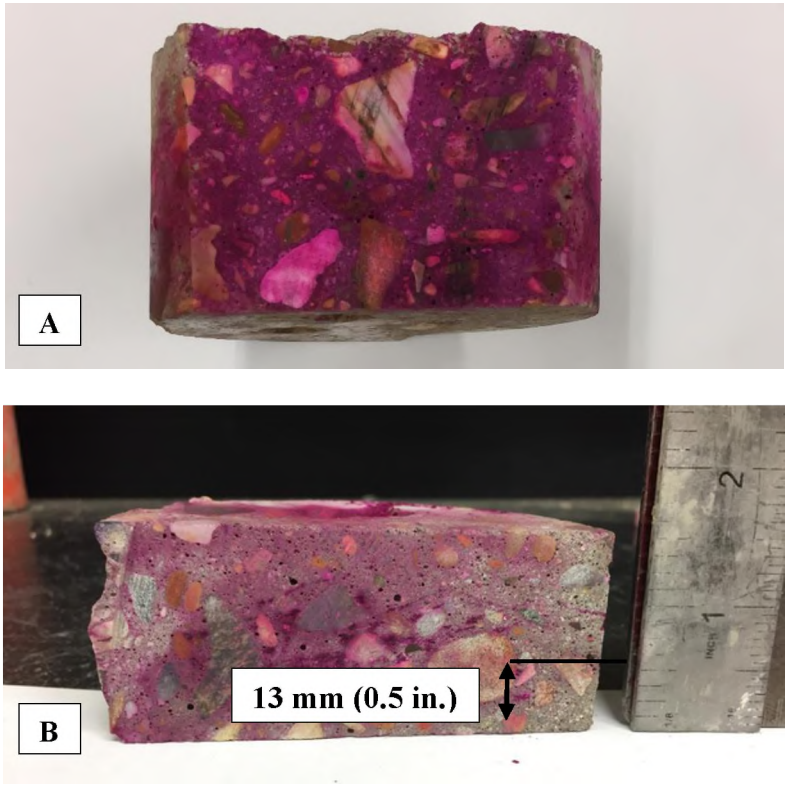


Figure 9. Carbonation depth test (A) Southview Bridge, (B) Sierrita de la Cruz Creek Bridge

**Chloride Content**: Chloride testing is crucial for concrete as chloride is considered one of the main causes of reinforcement corrosion [17]. Chlorides attack the light oxide film that forms over the reinforcement due to the alkaline-based environment of concrete and therefore result in corrosion of reinforcement. There are two techniques to determine chlorides content, namely acid-soluble and water-soluble techniques. Acid-

soluble analysis is used to determine the total content of chlorides including both chlorides trapped inside the concrete voids and the ones that damage the oxide film of reinforcement [19]. The water-soluble method provides only the chlorides content that deteriorated the oxide film. In this study, the acid-soluble approach was used to determine chlorides content. In order to implement this approach, rapid chlorides testing (RCT) equipment was implemented. A 1.5-grams (0.05 oz.) of concrete powder was taken from the cores at three different locations. They were then put into small coned-shaped containers and pressed in using a short plastic wire. After that, the powder was emptied in chloride-agent vails and left out to react with the agent. After 24 hours, the calibration step took place where different concentrations of chlorides were used. A voltage reading in mV was measured from each concentration and then used to draw a chlorides content curve. After that, an mV reading was taken from each vail tested and then compared to the curve to find the chlorides content concentrations. The degree of significance of these resulted concentrations was then compared to an associated chart to see if the content is high, low, or negligible. Per Broomfield, the chlorides content can be neglected as long as the content is less than 0.03%, content is considered low when it is between 0.03-0.06%, is considered moderate if it is between 0.06-0.14%, and is high if it's over 0.14% [20]. In both bridges, it was found that the chlorides content was within the negligible rates, as every vial had less than 0.03%. Table 2. Shows the chlorides content results.

## 6. GFRP EXAMINATION

Five tests were conducted on the GFRP bars to assess their durability performance.

The tests were as follows: scanning electron microscopy (SEM), Fourier transform infrared spectroscopy (FTIR), energy dispersive spectroscopy (EDS), glass transition temperature (TA), and fiber content.

**Scanning Electron Microscopy (SEM)**: In order to observe any existence of microstructural degradations, SEM test was carried out. Two 25.4 × 25.4 × 6.35 mm (1 × 1 × 0.25 in.) slices were taken from Southview Bridge core and one 25.4 × 25.4 × 6.35 mm (1 × 1 × 0.25 in.) slice was taken from Sierrita de la Cruz Creek Bridge core. Before using the SEM test, the samples were prepared following the procedure mentioned in section three of this article. Different magnification grades were employed to examine not only the GFRP bars but also the interfacial transition zone (ITZ) between the concrete and GFRP bar. The main reason for the scanning was to see if there was any microstructural degradation in the GFRP bars and areas in the vicinity of concrete in terms of fiber and resin morphological changes and/or cracks. Images were taken from different locations in each specimen to give a comprehensive view of the specimen. The SEM images depicted that there were no microstructural degradations in fibers, resin, and the neighboring areas of the GFRP bars. Fibers were not damaged and no loss in the cross-sectional area of fiber took place. Furthermore, there was no bond loss between the fibers and resin, and there were no gaps at GFRP-concrete interface (Interfacial

Transition Zone). Figure.10 shows representation of the scanned images. It is important to note that, in SEM analysis, sample preparation is very crucial and has a significant impact on the results, as lack of proper preparation may give false results. For example, exposing a specimen to high temperatures (over 55° C (130° F)) at the conditioning stage may result in gaps at the interfacial transition zone of GFRP and concrete. Furthermore, uncontrolled pressure at sand papering stage may damage cross section of fiber and leave dents in the matrix. Figure. 11 shows an example of a damaged specimen. One good indication that the damage was due to preparation was that there were cracks all over the specimens and they were distributed evenly.

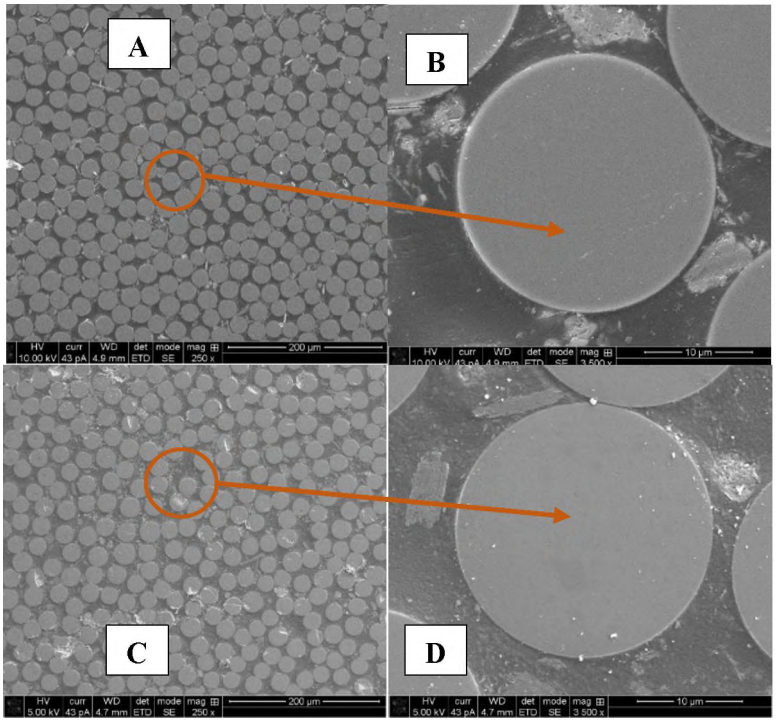


Figure 10. SEM images of the undamaged specimens (A) Sierrita de la Cruz at 250x magnification, (B) Sierrita de la Cruz at 3500x magnification, (C) Southview at 250x magnification, (D) Southview at 3500x magnification

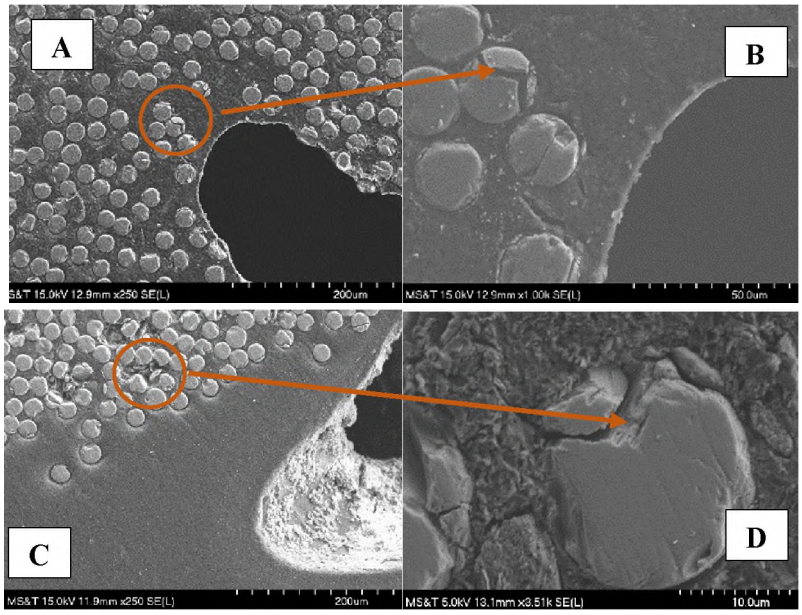


Figure 11. SEM images of some of the cracked specimens- (A) Southview at 250x magnification, (B) Southview at 3500x magnification, (C) Sierrita de la Cruz at 250x magnification, (D) Southview at 3500x magnification

**Energy Dispersive X-Ray Spectroscopy (EDS)**: This test was used to determine site specific elemental concentrations. Concrete pore solution is highly alkaline, as it has $Na^+$, $K^+$, and $OH^-$. It is known that Si of fiber dissolves in high alkaline [12]. In addition to alkalis coming from concrete pore water solution, there are alkalis that are a constituent of the fiber itself. When there is an abundant of $OH^-$, the pH rises, and leaching process might occur. Leaching is the process of extracting alkalis out of fiber resulting in affecting Si network of fiber and thus forming SiOH product. The produced SiOH is a gel type product that is less dense than the original Si network and has the ability to transform water and alkalis [21 22]. In addition to the investigation of main elements of fiber and resin matrix, EDS was implemented to check for alkalis attack. EDS cannot detect

elements with atomic number lower than Na, therefore OH cannot be detected, but they might defuse together for neutrality [12]. That said, appearance of Na, Ca, and/or K in the resin matrix can be a sign of alkalis migration from concrete pore solution to the glass fibers. A 10 to 20 KeV electron beam was applied on the same specimens used for SEM analyses. In EDS test, the results were shown as plot where its y-axis shows the number of X-rays sent by the apparatus and its x-axis shows the level of energy of those counts.

In both bridges, the fibers chemical composition showed no signs of zirconium (Zr), therefore it confirms that the GFRP bars were not alkaline-resistant (AR)[22]. Additionally, the main elements of fiber including Al, Ca, Si, Na, O were found. Besides these elements, Mg was found too in both bridges and that indicates the GFRP bars were not ECR-glass [8]. Elements such as Au and Pd were also detected in the resin and fiber, which is an indication for coating (gold sputtering) to make the surface of GFRP bar from non-conductive to semi-conductive, so the SEM and EDS apparatus can work. For the resin matrix, the main element, C, was found in both bridges. In Sierrita de la Cruz Creek Bridge, alkaline elements such as Na, Mg, Al, and Ca were found in the resin. In addition, Si was found too. The appearance of alkaline and Si in resin are not welcomed, as their existence can be an indication for alkali-hydrolysis attack and a leaching problem [22]. However, in Sierrita de la Cruz Bridge, these elements were found in the control bars too, therefore there is a significant chance that these observed elements were part of filler. Figure. 12 shows the EDS results of the fiber and resin of Sierrita de la Cruz Creek Bridge. Additionally, and to support this claim, the pH of the bridge was not even high enough to induce alkali-hydrolysis attack. Furthermore, carbonation depth was observed,

and thus, these signs moderately confirm that these elements were part of the filler of GFRP bar. In Southview bridge, alkaline elements and Si were found in the resin as well.

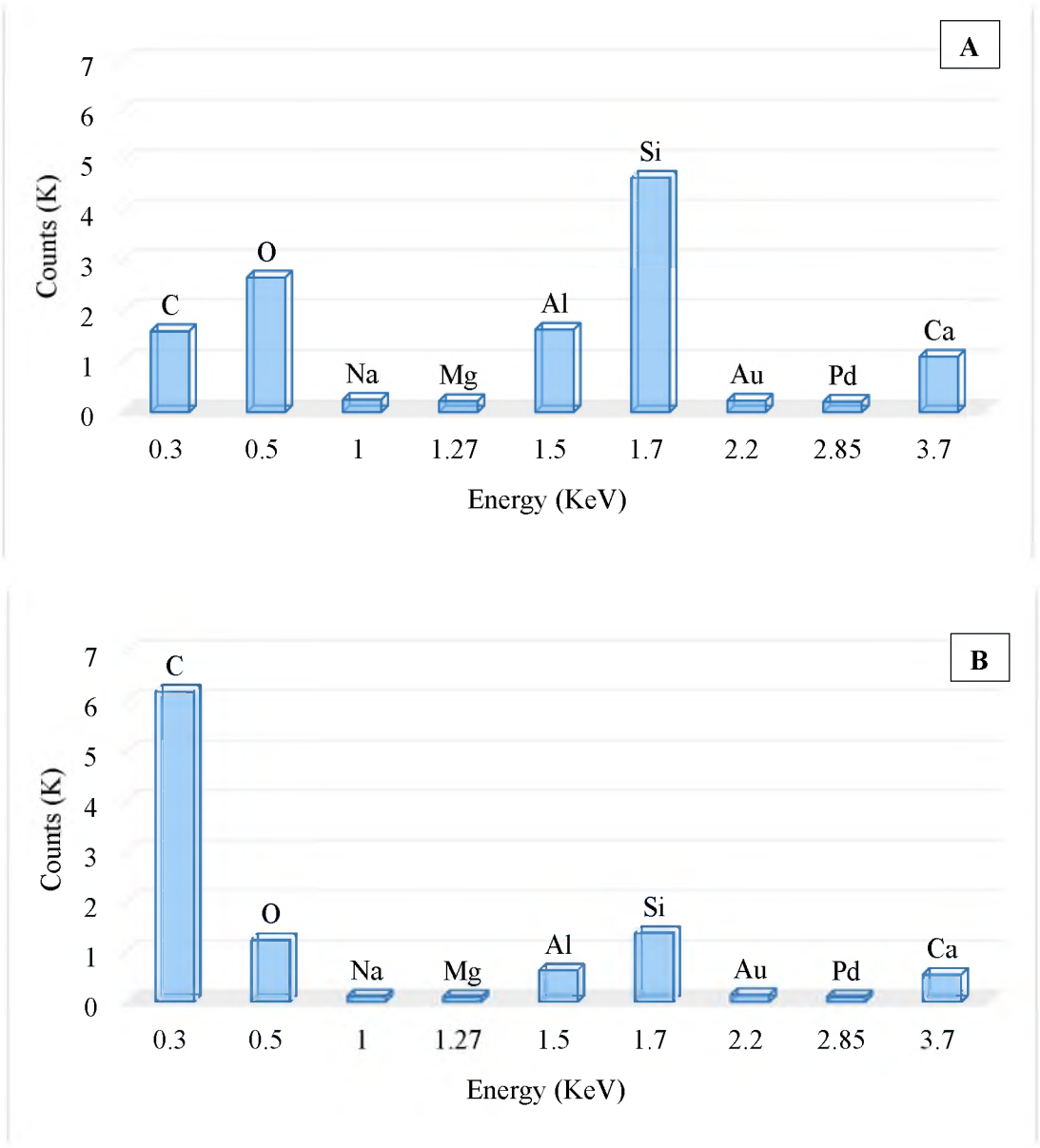


Figure 12. EDS analysis of Sierrita de la Cruz Creek Bridge (A) fiber (B) resin

The difference this time from Sierrita de la Cruz Bridge is that the tested pH of Southview Bridge was high and carbonation was not observed. Additionally, Na was observed only in the resin. Thus, the appearance of Na and Si in the resin can clearly indicate to an alkaline-hydrolysis attack and leaching problem. To contrast, Si sometimes is used as part of a filler in resin. Bank et al [1998] [23] stated that the existence of Al, Si, and $PO43^-$ in the resin matrix is a sign of a filler. These two elements, Al and Si, and one compound, $PO43^-$, form a filler called alumino-silicate phosphate (ASP). Each of Al, and Si were seen in the resin, but there were no signs for the $PO43^-$. Therefore, to make sure these alkalis and Si from alkalis attack, FTIR test was carried out to observe the level of OH in the resin matrix. EDS results of Southview Bridge are shown in Figure. 13.

**Fourier Transform Infrared Spectroscopy (FTIR)**: Glass fiber is weak against alkaline and acid environment. In fact, glass fibers do not do well if the alkaline concentration is 2 mol/l or more. Hydroxyl group (OH) is very active in alkaline environment and can induce alkali-hydrolysis attack on resin. Cross-links in thermoset resins, such as vinyl-ester, are the weakest connection in the resin structure and are the ones susceptible to damage if alkali- hydrolysis attack takes place [12]. When attack occurs, resin degrades and loses its ability to transfer stress properly to the fibers and thus GFRP system fail. FTIR test was applied to monitor the changes in the amount of OH. If alkali-hydrolysis occurs, new OH are generated and as a result infrared band of OH increases and becomes higher than the normal infrared band of OH [24].

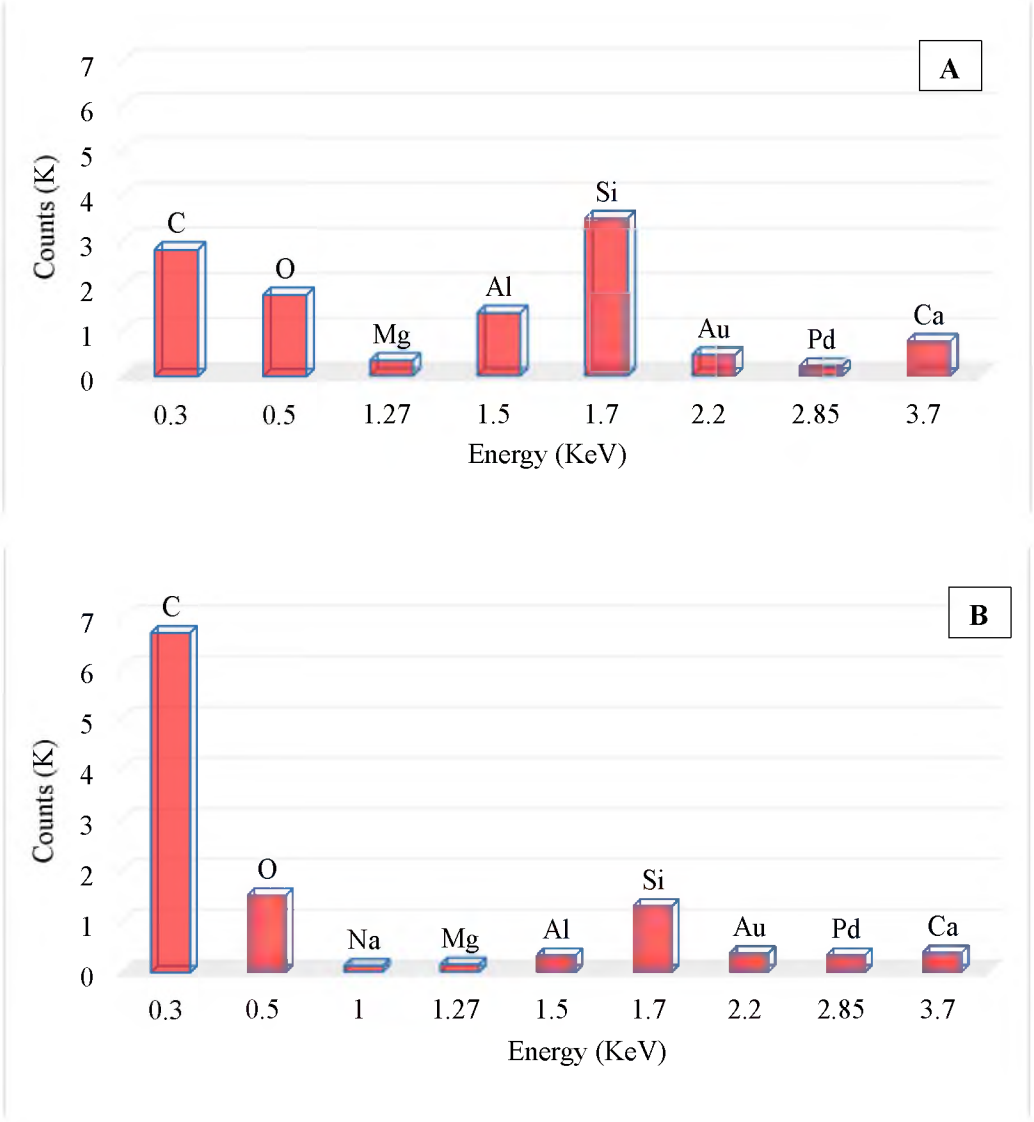


Figure 13. EDS analysis of Southview Bridge (A) fiber (B) resin

Additionally, since EDS only works with elements having an atomic number equal or higher than Na, and OH has an atomic number smaller than that of Na, FTIR was used to check for OH level. The normal range of the Hydroxyl group (OH) is between 3000 and 3600 $cm^{-1}$ [25]. To conduct the test, little fractures about 2 grams from

the GFRP bar were taken and were then ground with the bromide potassium (KBr), because it does not have bands that fall in the mid-IR region of the spectrum. Hence, preparation as halide disks misses significantly less information. Then the ground powder was compressed to form a light transparent sheet that was placed later in the FTIR device to obtain the measurement. The output reading was in terms of plot between the intensity and wavenumber that presents the inverse of the wavelength.

In the Southview Bridge, OH was found to be a little over 3700 $cm^{-1}$, which now clearly indicates that alkali-hydrolysis and leaching were taking place. Regarding Sierrita de la Cruz Creek Bridge, OH was found to be about 3600 cm-1, which met the normal range of OH group. It was anticipated to be on the high side, because even though carbonation was found when its concrete was tested, the pH test was not lower than 11. Representative results are shown in Figure 14.

**Glass Transition Temperature (TA)**: Glass transition temperature can be defined as the temperature region where the resin physical characteristics change from hard to soft material [26]. The importance of TA comes from its indication for material thermal stability, polymer structure, and mechanical properties. In composites, there are two glass transition temperatures, one for fiber and the other for resin. Since the TA of the fiber is substantially higher than that of the resin matrix, only the resin is of main concern during the investigation of TA. Surrounding environment of composites has significant impact on TA, as it can substantially reduce it [27]. To contrast, wet environment where OH is abundant, can be very deleterious on TA due to plastification.

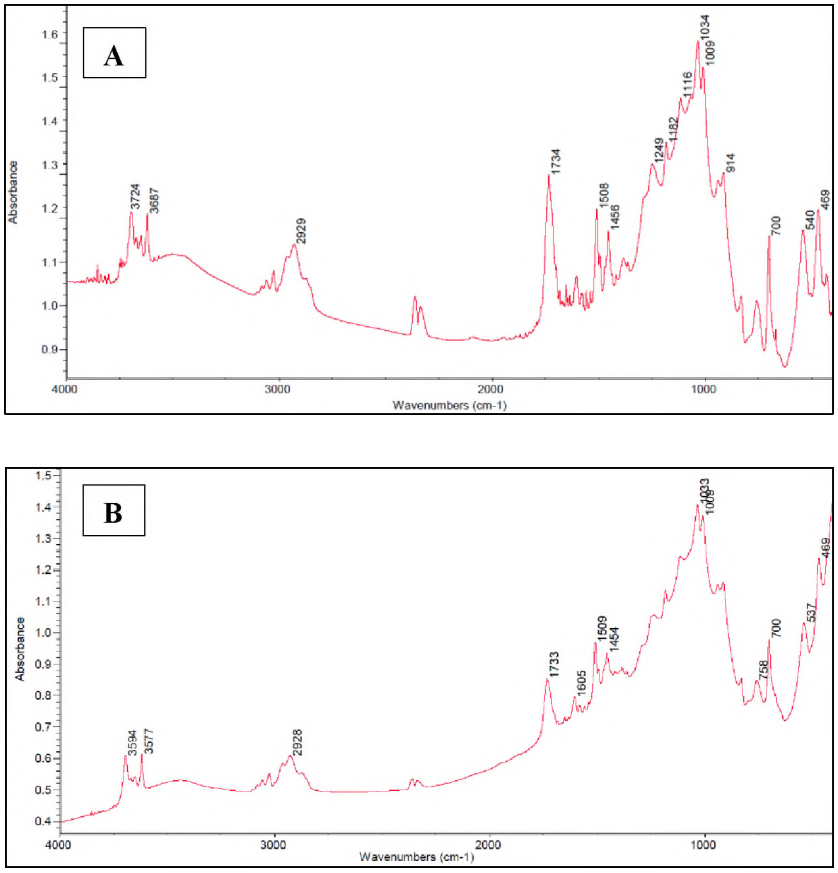


Figure 14. FTIR analysis of (A) Southview Bridge (B) Sierrita de la Cruz Creek Bridge

The OH group is the reason for plastification, as it can induce alkali-hydrolysis attack on resin. This attack destroys the Van der Waals bonds of resin, and thus plastification takes place [12]. In addition, Micelli and Nanni [9] stated that there are solid signs that the deterioration rate of polymer composites subjected to fluid environment is highly related to the rate of fluid sorption, which is strongly affected by elevated temperatures.

Frequent exposure of composite to high temperature can lead to what is called thermal softening (Reduction in TA) [27]. Thermal softening results in reduction of not only

elastic modulus, but also fiber strength. The matrix properties of polymeric composites are considerably affected by temperature increase rather than fiber properties. It was found that the axial mechanical properties (strength and modulus) of fibers, situated on 0° C (32° F) degree to the applied load, were not affected by the increase in temperature. However, those situated perpendicular to the other fibers had mechanical properties that were significantly affected by the temperature increase. In addition, it was found that resin (vinyl-ester) of composites can resist high temperature up to 40° C, however the exposure should not be for a long term [27].

Another important aspect in TA is level of curing. In 2015, Kumar et al. [28] discussed in their work the effect of curing ratio on TA, as it was found that composites with optimum cure ratio were expected to have a higher TA than those with lower cure ratio. Kumar et al. also defined the optimum curing ratio as the level of curing required in a material to achieve its mechanical, thermal, and durability properties for a certain application [25]. In addition, ACI-2008 permitted any composite product as long as it is 100% cured [29]. In contrast, CSA-2010 permitted only GFRP bars with curing ratio of at least 95% [30]. Glass transition temperature tests can be performed using either dynamic mechanical analysis (DMA) or differential scanning calorimetry (DSC). In this study, DSC was used to evaluate the TA temperature of both bridges. ASTM-E1640 was used as a standard [31]. The specimens were cut into very little chunks containing about 10 mg (0.0004 oz.) each of the GFRP bars. Next, they were placed inside a TA instrument for TA measurement where the temperature ramp was 5° C (41° F) per minute. The temperature was elevated up to 200° C (392° F) from room temperature and then cooled

back down using the same ramp of 5° C (41° F) per minute. All the results showed a significant reduction in TA temperature of about 25° C (77° F) from the original TA for vinyl-ester resin which is about 100° C. This reduction could be due to the increase in OH. Regarding the Sierrita de la Cruz Creek Bridge, vinyl-ester was also used for the resin matrix of the bar. TA results for this bridge were about 70° C (176° F) which is 10° C (212° F) less than the TA conducted on control bars. However, the FTIR results exhibited that OH levels were within normal range [32] (3000-3600 $cm^{-1}$), and the EDS test did not show any change in the chemical properties of either the fiber or the resin. The hygrothermal environment that surrounded the GFRP bars could be the reason behind this reduction of the TA magnitude. Results are shown in Table 3.

Table 3. Test Results of Glass Transition Temperature (TA)

| | | | |
|---|---|---|---|
| **Southview Bridge** | CM1 | Number of samples | 3 |
| | | Average Temp. °C (°F) | 72 (162) |
| | | Coefficient of variation % | 6.94 |
| | CM2 | Number of samples | 3 |
| | | Average Temp. °C (°F) | 75 (167) |
| | | Coefficient of variation % | 3.32 |
| **Sierrita de la Cruz Creek Bridge** | TA-Control Bars | Number of samples | 3 |
| | | Average Temp. °C (°F) | 81 (178) |
| | | Coefficient of variation % | 16.9 |
| | CT | Number of samples | 3 |
| | | Average Temp. °C (°F) | 74 (165) |
| | | Coefficient of variation % | 9.19 |

CM1 and 2: Cores from Southview Bridge tested in for this study at Missouri S&T
TA-Control Bars: Control cores from Sierrita de la Cruz Creek Bridge
CT: Cores from Sierrita de la Cruz Creek Bridge tested at Missouri S&T

**Fiber Content Test**: fiber content is directly related to the mechanical performance of GFRP bars [25]. This test can be utilized only with polymer-matrices and with fibers where a high-temperature exposure does not affect them [33]. The fiber content test, also called the Burn-off, is designed to determine the ignition loss of cured resin. ASTM D2584 was applied to conduct the experiment [34]. The specimens were cut into little pieces of about 5 grams (0.18 oz) each and then weighed. The specimens were then burnt in a muffle furnace at 575° C (1010° F) until the resin was disappeared. After that, the burnt specimens were then weighed again. The percentage weight difference yields the fiber content. The results are shown in Table 4.

Table 4. Test Results of Fiber Content Test

| | | | |
|---|---|---|---|
| **Southview Bridge** | CM1 | Number of samples | 3 |
| | | Fiber Content % | 69.9 |
| | | Resin Content % | 30.1 |
| | | Coefficient of variation % | 4.32 |
| | CM2 | Number of samples | 3 |
| | | Fiber Content % | 71.8 |
| | | Resin Content % | 28.2 |
| | | Coefficient of variation % | 3.34 |
| **Sierrita de la Cruz Creek Bridge** | α – Control Bars | Number of samples | 2 |
| | | Fiber Content % | 80.5 |
| | | Resin Content % | 19.5 |
| | | Coefficient of variation % | 2.2 |
| | CT | Number of samples | 3 |
| | | Fiber Content % | 81.6 |
| | | Resin Content % | 18.4 |
| | | Coefficient of variation % | 3.07 |

CM 1 and 2: Cores from Southview Bridge tested in for this study
α – Control Bars Control cores from Sierrita de la Cruz Creek Bridge
CT: Cores from Sierrita de la Cruz Creek Bridge tested at Missouri S&T

The results of Southview Bridge showed a fiber content percentage of 70% and 72% for the CM1 and CM2 specimens, respectively. Even though, there were no control bars, but the results were in match with fiber content limit stated in ASTM D7957 standard for GFRP bars in concrete [35]. Despite the fact that there were signs for leaching in Southview Bridge specimens, there were no signs for a loss in the fiber content. It is most likely because the leaching process was at its early stage, as the Si levels in resin, from the EDS test, were not high. For Sierrita de la Cruz Creek Bridge, the results showed a fiber content of 82% which was close to tests conducted on control bars.

This result was expected in that bridge, as there were no signs for any chemical changes. Therefore, it can be concluded that there was no loss in the fiber content of both bridges.

## 7. CONCLUSIONS AND RECOMMENDATIONS

Glass fiber reinforcement is a promising solution to replace steel reinforcement and hence avoid corrosion problems. However, GFRP has not been studied thoroughly especially when it comes to durability performance under field conditions. Thus, in this study, durability of GFRP bars taken from two bridges in the United States after over 11 and15 years of service were evaluated. The experiments were performed on two bridges: Southview Bridge in the state of Missouri and Sierrita de la Cruz Creek Bridge in the state of Texas. The following observations and recommendations can be drawn from these tests:

1. pH of concrete: For Southview Bridge, the pH level was 13 which is high for such a concrete (i.e. for most bridge decks in USA, a-6000 psi cement-based reinforced concrete). High pH indicates high OH and increases the chance for resin and fiber attacks. For Sierrita de la Cruz Creek Bridge, it was about 11 to 12 which is within the normal range for such concrete.

2. Carbonation Depth: Carbonation is something undesirable in RC structures, as they can lead to corrosion issues. For Southview Bridge, the tests were conducted on different parts of the core and showed no significant depth of carbonation. For the Sierrita de la Cruz Creek Bridge, carbonation was present with depth of 13 mm (0.5 in.) from the weather-exposed surface. It is believed that it took place due to the alkaline environment surrounding the concrete.

3. Chlorides Content: For both bridges, the test results showed that chlorides were within the negligible limits (less than 0.03%).

4. Scanning Electron Microscopy (SEM): For both bridges, no microstructural degradation was found in the GFRP bars where the scanning was conducted. All fibers were complete and the resin was properly and fully bonded to the fibers. Also, there was no loss in the cross-sectional area of fibers. In addition, the interfacial transition zone (ITZ) between the concrete and the glass fiber matrix was fully intact. However, cracks did appear in one specimen, but are believed to be due to the improper preparation of the sample.

5. Energy Dispersive X-Ray Spectroscopy (EDS): This test was conducted to observe the chemical elemental changes in the bar. In both bridges, the main elements of

fibers were found including: Al, Ca, and Si. In addition, the main element of resin, C, was found too. No Zr was found in both bridges which confirms those bars were not alkali-resistant. Also, it indicates that the bars tested were vinyl ester-based bars as per their manufacturer claim. In both bridges, Mg was found and that confirms that there were not ECR-glass fibers. No signs for chemical attack was found in Sierrita de la Cruz Creek Bridge, even though alkaline was found not only in fibers but also in resin. It was believed those alkalis in resin were due to filler of the GFRP. On the other hand, the EDS results of Southview Bridge showed significant signs for alkali-hydrolysis attack as Na was found only in the resin. Also, Si was detected in the tested resin as well which it can be taken as a clear sign for leaching.

6. Fourier Transform Infrared Spectroscopy (FTIR): In Southview Bridge, the results showed that the spectra of the OH group was high (a little over 3700 cm-1) which confirms that the alkalis elements found in EDS test of resin were from alkali-hydrolysis attack. For Sierrita de la Cruz Creek Bridge, the results were within the normal range at around 3600 $cm^{-1}$. Also, it was expected to be normal as the pH test was not high.

7. Glass Transition Temperature (TA): Glass transition temperature of both bridges were less than control bars and the ASTM standard of GFRP bars in concrete. For Sierrita de la Cruz Creek Bridge, TA results were about 70° C (158° F) and were less than the controlled ones that scored 80° C (176° F). This reduction is possibly due to the hygrothermal environment that surrounds the bridge. For the Southview Bridge, there were no control bars, but since vinyl-ester was used as a resin in this bridge, the results

were instead compared to the ASTM-E1640 standard that states a TA of 100° C (212° F) for such a resin. The TA for the tested specimens was found to be around 75° C (167° F), much lower than the ASTM standard. This significant reduction is due to alkali-hydrolysis attack and the moderately high temperatures that the bridge has been exposed to.

8. Fiber Content: For both bridges, the results were in agreement with the fiber mass content limit mentioned in ASTM D7957 for quality control and certification. It was expected to not see any fiber content issues with Sierrita de la Cruz Creek Bridge, as no indications for chemical changes were detected. However, for Southview Bridge, it was expected to see fiber content changes, but apparently there were no changes due to the early stage of the leaching attack.

Sample size presented itself as a critical limitation in this study. Even though all the required tests were properly conducted, the number of specimens needed to affirm certain behavior could not be achieved. The conclusions determined in this study cannot be generalized due to the limited sample size of some of the tests but lays the foundation and framework to collect and develop durability data sets. To increase the current durability data reliability, definitely more bridges should be considered for this kind of research in the future in order to improve durability-related requirements in the design codes and standards.

## ACKNOWLEDGMENTS

The authors gratefully wish to acknowledge the support from the ReCAST Tier 1 University Transportation Center at the Missouri University of Science and Technology (Missouri S&T), the United States Department of Education GAANN Program, The American Concrete Institute (ACI) Foundation as well as Owens Corning for their contributions to sample extraction. The opinions expressed in this study are those of the authors and do not necessarily reflect the views of sponsoring agencies.

## REFERENCES

1. Mufti, A., Onofrei, M., Benmokrane, B., et al. "Report on the studies of GFRP durability in concrete from field demonstration structures," *Proceedings of the 3rd International Conference on Composites in Construction - CCC 2005*, No. May 2014, 2005, pp. 11–13.

2. Wang, W. "Durability Behavior of Fiber Reinforced Polymer and Steel Reinforced Polymer for Infrastructure Applications." Missouri University of Science and Technology, 2017.

3. Achillides, Z. and., and Pilakoutas, K. "Bond Behavior of FRP Bars Under Direct Pullout Conditions.pdf," *Journal of Composites for Construction.*, V. 8, No. April, 2004, pp. 173–81.

4. El-Salakawy, E., Benmokrane, B., … R. M.-S., et al. "Concrete Bridge Barriers Reinforced with Glass Fiber-Reinforced Polymer Composite Bars," *ACI Structural Journal*, V. 100, No. 6, 2003, pp. 815–24.

5. Ahmed, E. A., Benmokrane, B., and Sansfaçon, M. "Case Study: Design, Construction, and Performance of the La Chancelière Parking Garage's Concrete Flat Slabs Reinforced with GFRP Bars," *Journal of Composites for Construction*, V. 21, No. 1, 2017, p. 05016001.

6. Mohamed, H. M., and Benmokrane, B. "Design and Performance of Reinforced Concrete Water Chlorination Tank Totally Reinforced with GFRP Bars: Case Study," *Journal of Composites for Construction*, V. 18, No. 1, 2014, p. 05013001.

7. Manalo, A., Benmokrane, B., Park, K., et al. "Recent Developments on FRP Bars as Internal Reinforcement in Concrete Structures," *Constr. Aust.*, V. 40, 2014, pp. 46–56.

8. Gooranorimi, O., Bradberry, T., Dauer, E., et al. "FRP Reinforcement for Concrete: Performance Assessment and New Construction," v. vol. I, 2016.

9. Micelli, F., and Nanni, A. "Durability of FRP rods for concrete structures," *Construction and Building Materials*, V. 18, No. 7, 2004, pp. 491–503.

10. Porter, M., and Barnes, B. "Accelerated Durability of FRP Reinforcement for Concrete Structures." 1st International Conference on Durability of Fiber Reinforced Polymer for Construction. 1998. pp. 191–202.

11. Nkurunziza, G., Benmokrane, B., Debaiky, A., et al. "Effect of Creep and Environment on Long-Term Tensile Properties of Glass FRP Reinforcing Bars." 4th International Conference on Advanced Composite Materials in Bridges and Structures, Calgary, Alberta. 2004.

12. Mufti, A., Onofrei, M., Benmokrane, B., et al. "Durability of GFRP reinforced concrete in field structures." Proceedings of the 7th International Symposium on Fiber Reinforced Polymer Reinforcement for Concrete Structures - FRPRCS-7. 2007. pp. 889–895.

13. Fico, R., Galati, N., Prota, A., et al. "Southview Bridge Rehabilitation in Rolla, Missouri," 2006, 1–194 pp.

14. Grubb, J., Limaye, H., and Kakade, A. "Testing pH of Concrete: Need for a Standard Procedure," *Concrete International*, V. 29(4), 2007, pp. 78–83.

15. ASTM-F710. "Standard practice for preparing concrete floors to receive resilient flooring.," *ASTM*, 2008.

16. Nanni, A., De Luca, A., and Zadeh, H. "Reinforced Concrete with FRP Bars," CRC Press, 2014, 1–406 pp.

17. Sagues, A. "Carbonation in concrete and effect on steel corrosion," 1997.

18. RILEM. "CPC-18 Measurement of Hardened Concrete Carbonation Depth," *Materials and Structures*, V. 21, No. 6, 1988, pp. 453–5.

19. Transportation, M. D. of. "Self-Consolidating Concrete ( SCC ) for Infrastructure Elements Report E – Hardened Mechanical Properties and Durability Performance," Rolla, 2012.

20. Broomfield, J. P. "Corrosion of Steel in Concrete," 2nd edition, Taylor and Francis, 2007, 1–294 pp.

21. Barkatt, A. "Issues in predicting long-term environmental degradation of fiber-reinforced plastics.," *Environmental effects on engineered materials*, 2001, pp. 419–458.

22. Kamal, A. S. M., and Boulfiza, M. "Durability of GFRP rebars in simulated concrete solutions under accelerated aging conditions," *Journal of Composites for Construction*, V. 15, No. 4, 2011, pp. 473–81.

23. Bank, L. C., Puterman, M., and Katz, A. "The Effect of Material Degradation of Bond Properties of FRP Reinforcing Bars in Concrete.," *ACI Materials Journal*, V. 95, No. 3, 1998, pp. 232–43.

24. Robert, M., Cousin, P., and Benmokrane, B. "Durability of gfrp reinforcing bars embedded in moist concrete," *Journal of Composites for Construction*, V. 13, No. 2, 2009, pp. 66–73.

25. Benmokrane, B., Nazair, C., Loranger, M. A., et al. "Field Durability Study of Vinyl-Ester-Based GFRP Rebars in Concrete Bridge Barriers," *Journal of Bridge Engineering*, V. 23, No. 12, 2018, pp. 1–13.

26. Epoxy Technology Inc. "Glass Transition Temperature for Epoxies," *Available in URL: http://www.epotek.com*, 2012, pp. 1–2.

27. Nkurunziza, G., Debaiky, A., Cousin, P., et al. "Durability of GFRP Bars: A Critical Review of the Literature," *Progress in Structural Engineering and Materials*, V. 7, No. 4, 2005, pp. 194–209.

28. Kumar, D. S., Shukla, K. K., Mahato, D. K., et al. "Effect of Post-Curing on Thermal and Mechanical Behavior of GFRP Composites." 4th National Conference on Processing and Characterization of Materials. 2015.

29. ACI-318. "Building Code Requirements for Structural Concrete (ACI 318-08) and Commentary," 2008, 471 pp.

30. CSA. "Specification for Fibre Reinforced Polymers," CSA (Canadian Standards Association), 2010.

31. ASTM-E1640. "Standard Test Method for Assignment of the Glass Transition Temperature By Dynamic Mechanical Analysis," *ASTM*, 2013.

32. Mohrig, J. R., Hammond, C. N., and Schatz, P. F. "Techniques in Organic Chemistry," Third, W.H.Freeman and Company, 2006, 468 pp.

33. Agarwal, B., Broutman, L., and Chandrashekhara, K. "Analysis and Performance of Fiber Composites," 3rd edition, Wiley, 2015, 576 pp.

34. ASTM-D2584. "Standard Test Method for Ignition Loss of Glass Strands and Fabrics 1," *ASTM*, 2005.

35. ASTM-D7957. "ASTM D7957 - Standard Specification for Solid Round Glass Fiber Reinforced Polymer Bars for Concrete Reinforcement," *ASTM*, 2017.

36. NCDC. "National Climatic Data Center." Available at: http://www.ncdc.noaa.gov.

37. NWSF. "National Weather Service Forecast." Available at: http://www.weather.gov.

# II. EVALUATION OF BOND PERFORMANCE OF GLASS FIBER REBARS EMBEDDED IN SUSTAINABLE CONCRETE

Ali F. Al-Khafajia [1]; John J. Myers [1]; Hayder H. Alghazali [2]

1 Missouri University of Science and Technology, Rolla, MO 65409, USA

2 Lecturer of Civil Engineering, University of Kufa, Najaf, Iraq

## ABSTRACT

This paper presents experimental and statistical investigations of the bond performance of sand-coated glass fiber rebars (GFRP) embedded in three types of concrete. The need for corrosion-free materials has become more wanted to avoid the high-cost of corrosion repairs. Glass fiber is a strong candidate to replace steel reinforcement in concrete structures due to its cost-effectiveness and great corrosion resistance. On the other hand, the production of cement generates substantial amount of carbon dioxide, therefore other alternatives are in high demand. Fly ash is considered one of these alternatives used to fully or partially replace cement in concrete to avoid the problem of carbon dioxide emission. In this study, other than conventional concrete (CC), 50% and 70% replacement of cement with fly ash were implemented as two types of high-volume fly ash concrete (HVFAC). Twenty-four cylindrical specimens were pullout-tested following the Réunion Internationale des Laboratoires et Experts des Matériaux, systèmes de construction et ouvrages (RILEM) recommendations. The parameters evaluated in this study were: rebar type, rebar diameter, and concrete type. In

addition to the experimental work, statistical analyses were conducted including predictions of GFRP's bond strength, peak toughness, and post-peak toughness. Test results showed that, despite the type of concrete used, peak bond strengths of GFRP rebars were lower than those of mild steel, but the post-peak strength were higher in GFRP bars. In addition, GFRP rebars were microstructurally and chemically examined, and there were no visual signs of any microstructural and chemical attack resulted from the fly ash-based concrete.

## 1. INTRODUCTION

Corrosion and carbon dioxide emission are the main problems with conventional concrete reinforced with mild steel. Corrosion is a serious problem, if it is neglected long enough, it can cause structural deficiency. In addition, corrosion cost of remedy is very high and requires continuous monitoring [1]. There are approximately 600, 000 bridges in the Unites States where 235,000 were made from steel reinforced conventional concrete. About 15% of them are considered structurally deficit due to reinforcement corrosion [1]. Per National Association of Corrosion Engineers (NACE), annual direct cost estimates a total of $8.3 billion [2]. To avoid corrosion issues of mild steel reinforcement, glass fiber (GFRP) rebars have been used as an excellent alternative. Over the course of the past 25 years, GFRP rebars have gained foothold within the construction industry owing to its high corrosion resistivity and economic feasibility [1][3][4][5]. Economically speaking, steel price per one meter is $0.20 while for GFRP bars, it is $0.25 per one meter, so even

though steel is cheaper but GFRP bars are three times lighter than steel, therefore, delivery and labor costs are cheaper in GFRP bars [6][7][8].

The other problem comes from conventional concrete when cement represents its only binding material. Globally, cement production has grown very fast in recent years and has been considered the third-largest source of anthropogenic emissions of carbon dioxide [9]. Cement has been used as a building material since ancient times, but it was following World War II that the production of cement accelerated quickly worldwide, with present levels of global production equivalent to more than half a ton per person per year [9]. There have been several alternatives put forward to replace Portland cement with eco-friendly binding material in concrete. One that has been widely accepted is fly ash which is a by-product of coal-burning thermal power stations [10]. Fly ash is defined in ASTM C618-08 [11] as "the finely divided residue that results from the combustion of ground or powdered coal and that is transported by flue gases". There are mainly three types of fly ash products: class N, F, and C. The difference between one and another is the chemical compositions [12]. The usage of fly ash in concrete structures has been limited to only 15-30% cement replacement [13]. Recent studies showed that implementing a high dose (up to 75%) of cement replacement with fly ash can produce an excellent concrete in terms of both strength and durability. High-volume fly ash concrete (HVFA concrete) offers a feasible alternative to Portland cement-based concrete and is considerably more sustainable. As for the costs, Portland cement cost ranges from $50 to $70 per ton while the fly ash cost ranges from $15 to $40 per ton [14]. ACI 232.2R defines HVFAC as the concrete that has at least 50% fly ash [12][15]. A

significant amount of research was performed on both fresh and hardened properties of HVFAC, but very limited research has been done on structural behavior [16]. Naik et al. [17] conducted a pullout test using 10, 20, and 30% fly ash replacement of cement and concluded that the bond strength increased with increasing the fly ash percentage up to 20% maximum. Gopalakrishnan et al. [18] studied a pullout test of a concrete with only 50% fly ash replacement and they concluded that the bond strengths of the 50% fly ash were in agreement with those conducted on conventional concrete. Another study on HVFA concrete was performed in 2014 by Arezoumandi et al. to assess the bond strength of mild steel reinforcement in HVFA concrete. They applied three levels of fly ash in their concrete: 0.0%, 50%, and 70% replacement of Portland cement with class C fly ash and used pullout test to perform the bond assessment [19]. The results indicated that the bond strength increased by increasing the level of fly ash. In 2018, Al-Azzawi et al. conducted a study about the factors affecting the bond strength between the fly ash-based geopolymer concrete (FBGC) and steel reinforcement [20]. The investigators used five different sources of fly ash type F, three fly ash contents: 300, 400, and 500 kg/m3 (18, 25, and 31 lb/ft3), and three proportions of alkaline activators. The pullout test was implemented to assess FBGC bond performance with steel reinforcement. The study concluded that the increase in the fly ash content in the FBGC highly increased the bond strength between the FBGC and steel reinforcement.

The GFRP bond with CC has been investigated by several researchers. Zenon Achillides and Kypros Pilakoutas conducted pullout tests on cube specimens using different kinds of fiber reinforced polymers including GFRP rebars [3]. They found that

bond strength of GFRP appeared to be close to those resulted from mild steel. Another pullout study was made by Ginghis Maranan [21] on GFRP rebars with geopolymer concrete. They studied the bond performance using sand-coated GFRP rebars implanted in geopolymer concrete with compressive strength of 33 MPa (4786 psi). The effect of several parameters such as the rebar diameter and embedment length were investigated. It was found that the bond strength of GFRP rebars in geopolymer concrete was fairly close to those resulted from using ordinary steel reinforcement in geopolymer concrete. Additional study was done by El-Refai et al. to assess the bond durability of basalt fiber-reinforced polymer rebars using the pullout test [22][23]. They investigated the effect of five different accelerated environments on the bond strength of two types of basalt rebars and one type glass fiber rebars. The study concluded that bond-slip responses of all specimens were controlled by the rebar surface treatment and its manufacturing quality. Also, glass fiber rebars exhibited less bond strength than that of basalt fiber rebars. Besides the experimental analyses, Garcia-Taengua et al. conducted both experimental and statistical analyses on bond of reinforcing rebars embedded in steel fiber reinforced concrete. Pullout test was carried out to make the bond assessment; three parameters were selected in their study: compressive strength, rebar size, and concrete cover. Their statistical analyses involved developing predictive models of bond strength and toughness. They concluded that compressive strength had a major impact on bond strength, and increasing in rebar size resulted in a higher bond strength [24].

In this investigation, the study novelty was represented by evaluating the bond performance of GFRP rebars embedded in sustainable concrete (HVFA concrete). The

bond performance was analyzed mechanically and chemically in addition to being analyzed statistically. In this study, 50% and 70% fly ash replacement of Portland cement were investigated using mild steel reinforcement and glass fiber rebars (GFRP). Two rebar diameters were utilized for both GFRP and mild steel; 13 mm (1/2 in.) and 19 mm (3/4 in.). Twenty-four specimens were tested where twelve of them were used as control specimens and the others (involved GFRP rebars) were considered for comparison purposes. In addition, statistical investigation was made to assess the bond performance including making bond strength predictive models, toughness and post-peak toughness models.

## 2. EXPERIMENTAL WORK

Bond behavior between reinforcement and concrete can be investigated via different tests including pull out test, beam-end specimen, beam anchorage, and beam splice specimens. In this study, pullout specimen test was considered to study the bond strength of cylindrical concrete specimens. The only drawback with this test is that in concrete members, the steel and concrete are exposed to the same type of stress, either both in compression, or both in tension, while in this test, concrete is in compression and steel is in tension. Therefore, the pullout test is not recommended by the ACI 408R-03 [25] to find the development length of reinforcement. On the other hand, when it comes to determining relative performance between different types of concrete or different types of reinforcing rebar coating, the pullout test is valid [26][27]. In this study, pullout test

was conducted to evaluate the bond strength of GFRP rebars embedded in conventional (CC) and high-volume fly ash (HVFAC) concrete. The results were then compared to those resulted from using ordinary steel reinforcement in conventional concrete and HVFAC.

RILEM 7-11-128 [28] was used to design the pullout specimens. The embedment length of the reinforcement was ten times the rebar diameter. Half of the embedment length was debonded using a section of polyvinyl chloride pipe (PVC) to ensure the slip failure is the controlling mode of failure among other types of failures (e.g. splitting). To maintain a proper cover, RILEM recommends a distance of no less than 4.5 times the rebar diameter measured from the center of the reinforcing rebar to the outer edge of the specimen. In this study, the RILEM 7-11-128 cover requirements was exceeded with a distance of 305 mm (12 in.) to avoid any potential failure by splitting and ensure that only slip failure controls. Figure 1 shows a sketch of the test specimen with the applied forces.

## 3. MATERIALS, MIXTURE PROPORTIONS, AND FRESH AND HARDENED PROPERTIES

ASTM Type I/II Portland cement and ASTM Class C fly ash were used. Table 1 shows the chemical and physical properties of the cement and fly ash. Natural sand was used as a source of fine aggregate and crushed dolomite, 19 mm (3/4 in.) size-diameter, was used as a coarse aggregate. The steel rebars used were 13 mm (1/2 in.) and 19 mm (3/4 in.). They met the requirements of ASTM A615-09 [29] and were 414 MPa (Grade

60) material. Each of the rebar's rib spacing, height, and relative area was in agreement with ACI 408R-03 [25] and ASTM A615-09 [29]. On the other hand, all the GFRP rebars were 100 Aslan from Owens Corning [30] where they were made based on the ASTM D7205 [31] standards FRP rebars were also 13 mm (1/2 in.) and 19 mm (3/4 in.) diameters. Their mechanical and physical properties are shown in Table 2.

Table 1. Chemical and physical properties of cementitious materials

| Properties | Unit | Cement | Fly Ash |
|---|---|---|---|
| $SiO_2$ | % | 19.4 | 35.17 |
| $Al_2O_3$ | | 4.58 | 21.07 |
| $Fe_2O_3$ | | 3.20 | 6.58 |
| CaO | | 62.7 | 26.46 |
| MgO | | 3.27 | 6.22 |
| $SO_3$ | | 3.19 | 1.43 |
| $Na_2O$ | | - | 1.91 |
| $K_2O$ | | - | 0.44 |
| $Na_2O$ eq. | | 0.50 | 1.31 |
| Loss in ignition | | 2.31 | 0.12 |
| Fineness (+325 Mesh) | | 98.4 | 15.2 |
| $C_3S$ | | 58.0 | - |
| $C_2S$ | | - | - |
| $C_3A$ | | 7.00 | - |
| $C_4AF$ | | - | - |
| Vicat set time, initial | Minutes | 90.0 | - |
| Vicat set time, final | | 195 | - |
| Specific gravity | - | 3.15 | 2.68 |

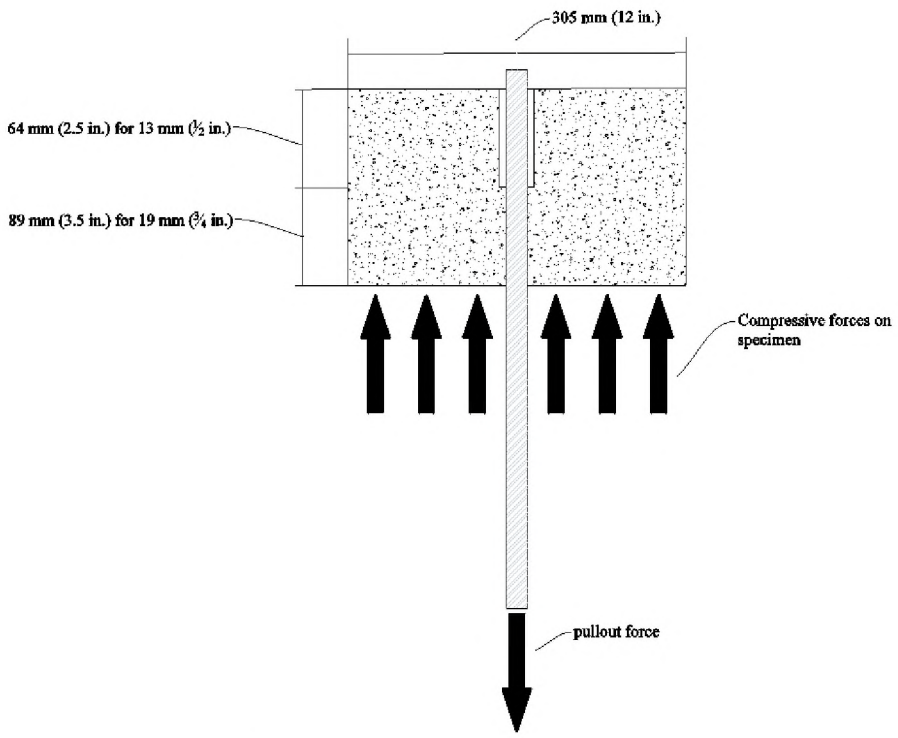


Figure 1. Test specimen's dimensions and forces

Table 2. Manufacturer's, Owens Corning, mechanical and physical properties of GFRP rebars

| Rebar size mm (in.) | Nominal Area $mm^2$ ($in^2$) | Guaranteed Tensile Strength MPa (ksi) | Ultimate Tensile Load kN (kips) | Modulus of Elasticity GPa (ksi) | Ultimate Strain (%) |
|---|---|---|---|---|---|
| 13 (1/2) | 127 (0.20) | 758 (110) | 95.90 (21.55) | 46 (6672) | 1.64% |
| 19 (3/4) | 285 (0.44) | 690 (100) | 196.60 (44.20) | 46 (6672) | 1.49% |

A 35 MPa (5 ksi) was the design compressive strength of the concrete. To achieve that strength, a water-cement ratio of 0.40 was implemented as well as air-entraining additive of 161 $gm/m^3$ (0.27 $lb/yd^3$) was applied [32]. Table 3 shows mixture of concrete.

Table 3. Mixture proportions of concrete

| Concrete Type | Water kg/m$^3$ (lb/yd$^3$) | Cement kg/m$^3$ (lb/yd$^3$) | Fly Ash kg/m$^3$ (lb/yd$^3$) | Fine Aggregate kg/m$^3$ (lb/yd$^3$) | Coarse Aggregate kg/m$^3$ (lb/yd$^3$) | Air-Entraining Additive g/m$^3$ (lb/yd$^3$) |
|---|---|---|---|---|---|---|
| CC | 176 (297) | 449 (756) | 0 (0) | 657 (1107) | 993 (1674) | 161 (0.27) |
| 50% HVFAC | 176 (297) | 222 (378) | 224 (378) | 641 (1080) | 993 (1643) | 161 (0.27) |
| 70% HVFAC | 176 (297) | 128 (216) | 320 (540) | 657 (1107) | 993 (1674) | 161 (0.27) |

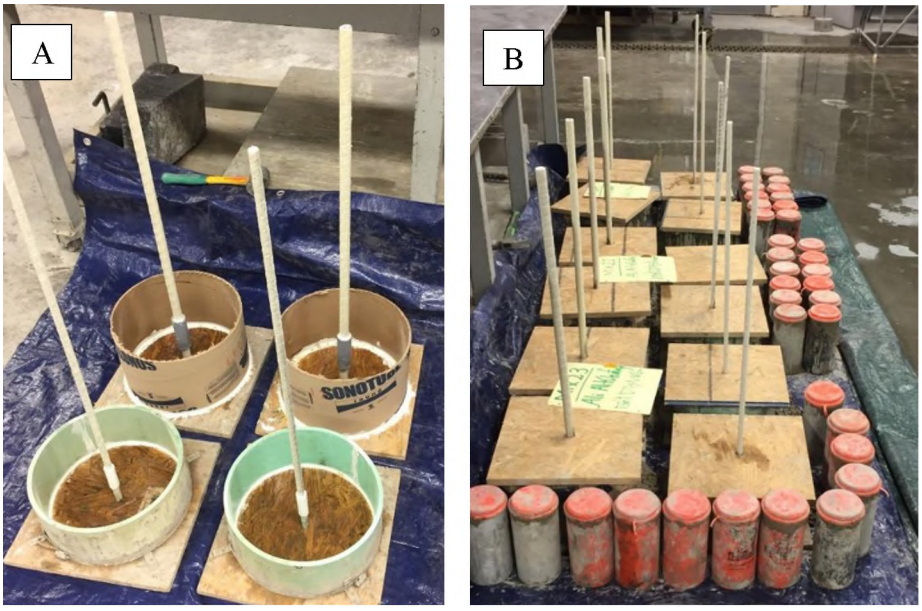


Figure 2. Specimens at the pouring day: (A) Specimens' Molds (B) Specimens after pouring

After casting, the specimens were covered with a plywood center-hole cover to not only protect the specimen's top surface from dirt but also to make sure the rebar was centered while the concrete was gaining strength. Also, the quality control assurance companion cylinders (ASTM C39-12 and C496-11) [33][34] were taken and stored in

secure environment. Table 4 shows fresh and hardened concrete properties. Figure 2 shows the specimens. Specimens and cylinders demolding were conducted after 24 hours from casting. After that, all the specimens were labeled and moved inside the curing room. Figure 3 shows specimens inside the curing room.

Figure 3. Specimens in curing room

The specimens were tested at age of 56 days, while the companion cylinders were tested for compressive strength at 3, 7, 28, and 56 days and for tensile strength at only 28 and 56 days. GFRP's specimens were sleeved with steel tubes in order to avoid grip slippage and/or rebar crushing when the test was conducted. A sleeved GFRP specimen is shown in Figure 4. The sleeve was made from steel tube where, for 13 mm (1/2 in.) rebar,

a 19 mm (3/4 in.) tube was used with a thickness of 2.87 mm (0.113 in.) and, for 19 mm (3/4 in.) GFRP rebar, a 25.4 mm (1.0 in.) tube was used with the same thickness as the one used for the 13 mm GFRP bar. Skia-Dur 30 epoxy was used to attach steel tube to the GFRP rebar to prevent crushing of the GFRP rebar during pullout testing.

Figure 4. GFRP's specimen steel grip

Table 4. Fresh and hardened concrete properties

| Property | Specification | Age of Test, Days | CC | 50% HVFAC | 70% HVFAC |
|---|---|---|---|---|---|
| Slump, mm (in.) | ASTM C143 | - | 114 (4.5) | 120 (4.7) | 127 (5.0) |
| Air Content, % | ASTM C231 | - | 4 | 5 | 4.5 |
| Unit Weight, $kg/m^3$ ($lb/ft^3$) | ASTM C138 | - | 2390 (149) | 2360 (147) | 2340 (146) |
| Splitting Tensile Strength, Mpa (psi) | ASTM C496 | 28 | 1.59 (231) | 1.63 (236) | 1.41 (205) |
| | | 56 | 1.72 (249) | 1.66 (241) | 1.42 (206) |
| Compressive Strength, MPa (psi) | ASTM C39 | 28 | 36.5 (5290) | 30.4 (4411) | 29.6 (4300) |

## 4. GFRP REBAR TESTS

To fully assess the performance of bond between the GFRP rebars and concrete, the rebars were subjected to several tests before and after the pullout tests were carried out. These GFRP tests included: scanning electron microscopy (SEM), energy dispersive spectroscopy (EDS), and glass transition temperature (Tg). Although these tests conducted when the time factor is significantly involved, they were chosen in this investigation to observe any minimal chemical and microstructural changes of the rebar properties after being in contact with fly ash for almost two months. In addition, the bond between conventional concrete and GFRP rebars have been moderately studied, but the fly ash with GFRP rebar has not yet, therefore this study carried out those tests to evaluate the rebars.

The results of these tests do not necessarily reflect the time factor as much they give an idea about what changes can be expected when the GFRP rebar is surrounded with fly ash-based concrete. The tests are as follows:

**Scanning Electron Microscopy (SEM):** This test was performed to observe any microstructural degradation that may have taken place from fly ash-based concrete and GFRP rebar [35]. Four specimens were cut from the rebars and were then prepared for SEM. Sample preparation included cutting rebar to 6.4 mm (0.25 in.) thick and then sandpapering it using several grades up to 1200 (US system). Sonic bath was employed between the sandpapering stages to remove any dirt stuck on the sample. Additionally, the sample was polished to a 0.2 μm and was then coated with gold to make it conductive and ready to receive the SEM device's electrons. Before entering the sample in SEM, the sample was preconditioned in an oven for 48 hours at $40^{o}$ C ($104^{o}$ F).

**Energy Dispersive Spectroscopy (EDS):** This test was performed to check for any changes in the chemical elemental concentration of rebar. The pore water solution of conventional concrete is highly alkaline and the latter is one of the GFRP's enemies as it induces with hydroxyl group (OH) what is known as alkali-hydrolysis attack. This attack destroys the ester bonds of resin and resulted in deteriorating the integrity of the composite system [35][36]. On the other hand, several investigations stated the effectiveness of fly ash in reducing the amounts of alkalis available in the pore solution and that should help minimizing the chance to subject GFRP rebar to alkali hydrolysis attack [37]. Since the fly ash-based concrete to GFRP rebar contact time was too short, the EDS test was focused only on the exterior sides of the rebar to see if there is any signs

of chemical elemental changes of rebar and/or chemical elemental intruders arriving from concrete to the rebar. In addition to alkali-hydrolysis attack, having an environment where OH heavily thrives increases the chances for leaching problem [38]. Leaching is the process of extracting alkalis that are constituents of fibers leaving the fibers of rebar generating a gel-type product (SiOH) that works as a medium to transfer more OH and alkalis to the rebar [38][39]. In this study, the same specimens used in SEM analyses were implemented in EDS tests. A 10-20 KeV electron beam was applied on the specimens. The specimens before and after pullout tests was tested in EDS. The outside edges of the rebar was of the main interest (locations of concrete-to-rebar contact).

**Glass transition temperature (Tg):** This temperature represents the range of temperature in which the state of the rebar changes from solid to more-like plastic stage [40]. Glass transition temperature can be considered not only an indicator for thermal stability, but also polymer structure [35][41]. Environment surrounding GFRP rebar has substantial effect on Tg, as it can decrease it. Furthermore, high OH environment can decrease Tg due to plastification [42][43]. In addition, in 2004, Micelli and Nanni reported that there are strong signs of increase deterioration rate of composite polymer exposed to fluid environment (high OH) [42]. Generally, there are two techniques to check for Tg, one is called DMA which stands for Dynamic Mechanical Analysis, and the second is DSC which stands for Differential Scanning Calorimetry. In this study, DSC was employed to investigate Tg following ASTM E1356 standards [44]. The samples were cut into little bites containing about 10 mg (0.0004 oz.) each of the GFRP rebar. After that, they were installed inside a Tg apparatus where a ramp of temperature

of 5° C (41° F) per minute was employed. The temperature was elevated up to 200° C (393° F) and then cooked back down using the same temperature ramp. The tests of were carried out before and after the pullout tests were conducted to see if there were any effects from fly ash-based concrete the rebar.

## 5. TEST SETUP AND PROCEDURE

A-890 kN (200 kips) universal machine was used to conduct the pull-out tests. The specimens were flipped upside down in which the rebar side was facing down. A thin piece of rubber was used beneath the specimen to ensure the specimen was rested evenly. The free end of the rebar was clamped into grips of the universal machine. On top of the specimen, a liner variable differential transformer (LVDT) was placed directly on the exposed piece of the rebar to record the slippage. To make sure enough data points were stored and to avoid any dynamic effects, a loading rate paced at 2.5 mm/min (0.01 in./min) was employed. The data acquisition system was linked to a computer and used to record rebar slippage as a function of load. The specimens were loaded in tension to its maximum capacity and were then left under loading until complete slippage occurred in order to gain enough data to draw the bond-slip curve. Figure 5 depicts the test specimen and the setup used respectively in this study.

# 6. TEST RESULTS AND DISCUSSIONS

Glass fiber rebars with 13 mm (1/2 in.) diameter produced less peak bond strength than that of mild steel, however glass fiber rebars yielded higher post-peak bond strength than that of mild steel. Glass fiber rebars with 19 mm (3/4 in.) diameter produced less peak and post-peak bond strength than steel rebars. All the specimens experienced a pullout mode of failure. Splitting mode of failure did not occur, as it was intentionally avoided when the specimens were made by significantly increasing the cover dimension.

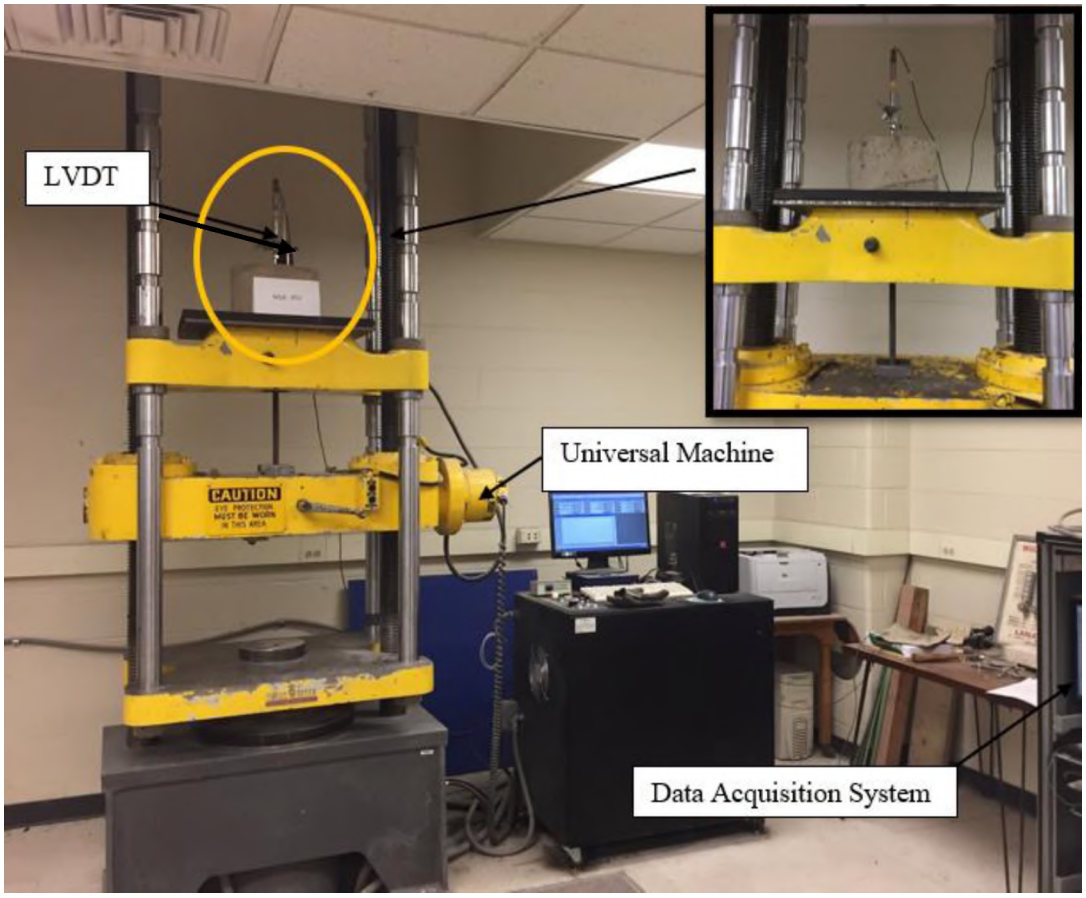


Figure 5. Test setup

Figure 6 shows a GFRP rebar from a failed specimen. The results were normalized to compensate for the differences between the field and design compressive strengths. ACI 318-14 [45] and AASHTO (American Association of State Highway and Transportation Officials) [46] recommend using the inverse square root of the compressive strengths to perform the normalization while, ACI 408R-03 [25] endorses the forth root. The results are shown in Table 5.

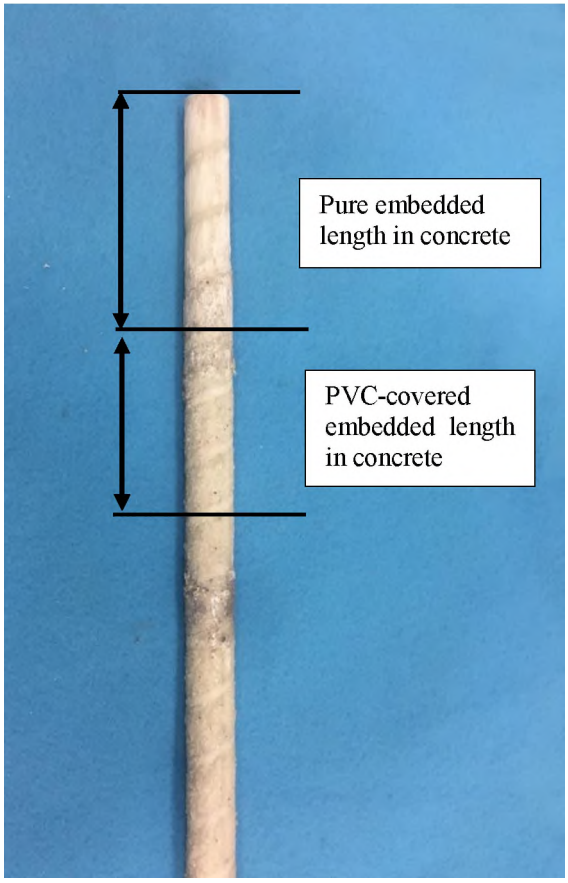


Figure 6. Failed specimen's rebar

The design compressive strength of all concrete was 35 MPa (5 ksi), but there was a slight difference in the tested concrete compressive strengths and that was reflected on the results of pullout test. Conventional concrete (CC) yielded the highest bond strength and the 70% HVFAC yielded the lowest, as the bond strength is significantly affected by and directly proportional to compressive strength, and since CC had the highest compressive strength, the highest bond strength was found in that concrete.

The bond strength of GFRP rebars were less than that of mild steel because GFRP rebars relied only on the friction resistance (chemical and mechanical) to resist the pullout force, while mild steel rebars, in addition to these forces, relied on the bearing forces generated on the surface deformations of rebar. These surface deformations act as anchor in concrete and therefore a substantial resistance can be generated. Once the cracks occur along the rebar deformations' surface, they will drive the failure mode to a shear failure (also called: slippage or pullout) ACI 408R-03 [25]. In this study, it was noticed that the larger the rebar size was, the bigger the gap between the bond strength of GFRP and mild steel of that rebar size. In addition, the bigger the rebar size was, the bigger the size its surface deformations (higher bearing forces), and thus a higher anchorage is developed. That was the reason behind having a significant gap in bond strength curve when 19 mm (3/4 in.) rebars were used and having a not as significant gap as that of 19 mm (3/4 in.) rebars when 13 mm (1/2 in.) rebars were implemented. The smaller rebar deformations were, and the smaller the bearing resistance and the more friction-based resistance. A steady linear elastic trend of load-slip curve was noticed for both types of rebars before the peak load was reached. The post-peak load-slip curve

behavior was nonlinear, and each type of rebar acted a little differently from the other. GFRP rebars exhibited a steady loss of strength, while mild steel exhibited a sharp loss (significant drop in the curve). It was believed that the steady loss in strength was merely due to the chemical and mechanical friction between the rebar's surface and the concrete, while the sharp loss of strength exhibited by the steel rebars was due to the principle cracks generated from the shear forces resulting from the action of bearing and friction forces on rebar's deformations. That said, having principle cracks along the length of the rebar's surface reduced the effect of the frictional resistance and as a result a sharp loss in strength took place. Figure 7 shows the pullout failure mechanism in steel and GFRP rebar. In addition to the bond strength, peak and post-peak toughness were measured. Figure 8, 9, and 10 illustrate the experiment results in each type of concrete used. Toughness is presented by the area under load-slip (or stress-strain) diagram [47]. Toughness can be used as an indication for material ductility. It is inversely proportional to ductility; the higher the toughness is, the more ductile the material. In this study, three levels of toughness were measured; peak and post-peak toughness (at 50% and 80% of the peak). Toughness results were based off of only pullout mode of failure. In addition, toughness calculations were only done to glass fiber rebars, as mild steel rebars have already been extensively studied [24]. The results are shown in Table 6. Peak toughness is presented by the area under load-slip diagram up to the peak load only, and since the bond strength's peak load is highly affected by the compressive strength of concrete, the higher the compressive strength of concrete is, the higher the peak toughness. Also, it was noticed that the slope of the load-slip curve, before reaching the peak point, did not

change significantly in all types of concrete used. Thus, peak toughness behavior is directly proportional to the compressive strength of concrete. Consistently with the findings in relation to peak toughness, it was found that compressive strength had the most significant impact on result of post-peak toughness. Increasing compressive strength from 21 MPa to 41 MPa (3000 psi to 6000 psi) increased the Ap80 by 102% and Ap50 by 248%. Even though there was only 30% difference between the post-peak at 80% and that at 50%, the percentage difference in toughness between them was almost 150%. When the rebar size increased from 9.5 mm (3/8 in.) to 25.4 mm (1.0 in.), the Ap80 increased by 228%, while the Ap50 increased by 249%, so there was only an increment of 25%. That clearly states the impact of the compressive strength on post-peak toughness result.

## 7. GFRP REBAR TEST RESULTS AND EVALUATION

To fully assess the performance of GFRP bars, a microstructural and chemical investigations were performed via conducting SEM, EDS, and Tg tests. The following was observed:

In SEM analysis, it was found that all fibers were intact with no cracks, the resin was not cracked and fully surrounded fibers with no gaps. Some voids were noticed but this is normal and comes from rebar manufacturing. The circumference parts of rebar were of the main focus due to its contact with fly ash and did not have any significant cracks neither in fibers nor in resin. It is important to note that some specimens did have

some cracks, however those were believed due to inappropriate preparation of sample, as they were observed in the middle section of the rebar and the time of exposure to concrete was too short to make such damage if it were from pore water solution of concrete, therefore, it was believed they were due to inappropriate preparation. Figure 11 shows a sample specimen. In EDS, the search for chemical intruders or changes was of main interest. This test was conducted control rebar and pullout rebar. In all tests, the main elements of fibers were detected including Al, Ca, and Si. Additionally, the main element of resin, carbon (C), was seen too. Sodium (Na), however, was detected in both fiber and resin, but that does mean there was an alkali-hydrolysis attack as Na was detected in control bars too. When EDS test was conducted, the main focus was intended to be at the circumference parts of the rebar as in SEM tests so as to see if there were any chemical changes and/or migrants from concrete into the rebar. No abnormal chemical elemental changes were noticed, thus it appears either the time (56 days) is too short for a chemical change to happen, or HVFA concrete was good enough to prevent alkalis migration to the rebar. Figure 12 shows a sample EDS specimen for control and after-pullout-test specimens. In Tg test, the experiment was performed on control rebar and pullout rebar. All the results were in agreement with ASTM standard and those results confirm that there was no chemical attack resulted from the surrounded concrete. Table 7 shows $T_g$ results for control and after-pullout-tests specimens.

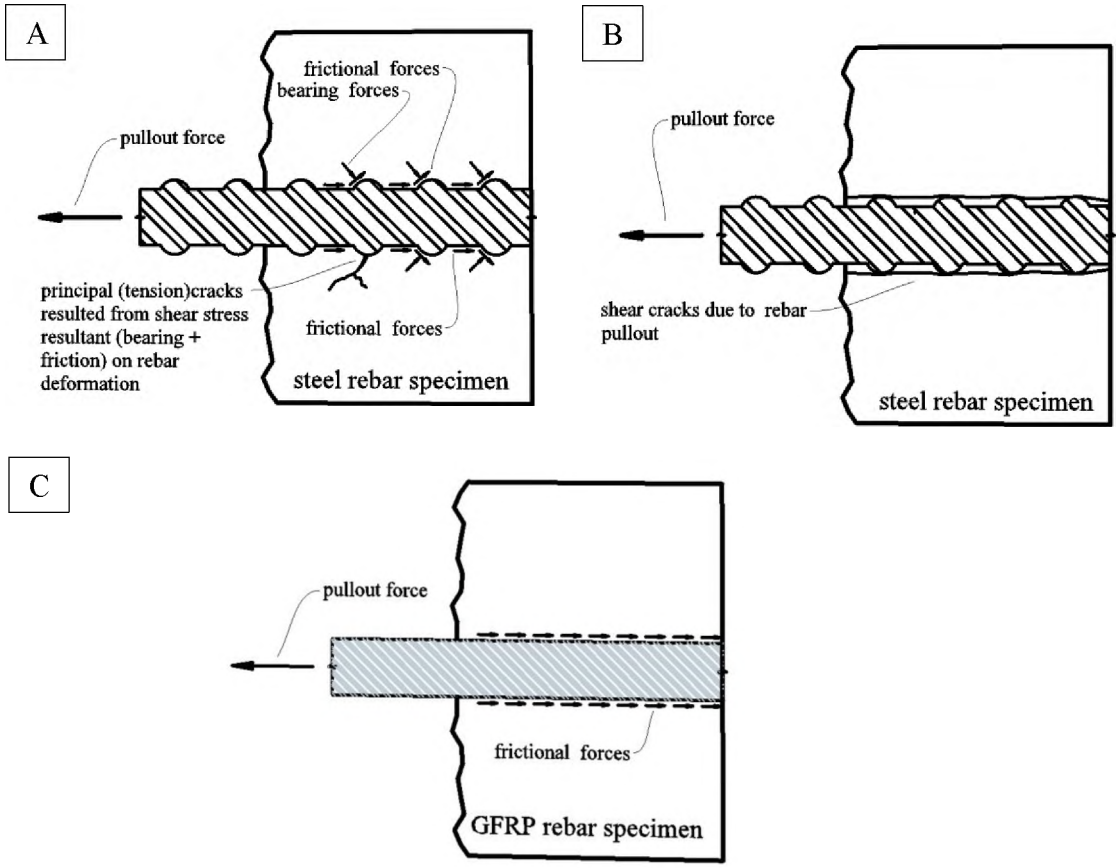


Figure 7. Pullout failure mechanism (A) forces and cracks generation – steel (B) rebar pullout – steel (C) rebar forces and pullout failure - GFRP

Table 5. Pullout test results

| Concrete Type | Bar Size mm | Bar Type | P (kN) | f'c test (MPa) | $\frac{P}{\sqrt{\frac{fc'(design)}{fc'(test)}}}$ (MPa) | P avg. (kN) | Coefficient of Variation (%) | $\frac{P}{\sqrt{\frac{fc'(design)}{fc'(test)}}}$ (MPa) | P avg. (kN) | Coefficient of Variation (%) |
|---|---|---|---|---|---|---|---|---|---|---|
| CC | 13 | Steel | 66 | 35.38 | 67 | 63 | 8 | 66 | 63 | 8 |
| | | | 59 | | 59 | | | 59 | | |
| | | GFRP | 54 | 35.38 | 54 | 49 | 14 | 54 | 49 | 14 |
| | | | 44 | | 44 | | | 44 | | |
| | 19 | Steel | 171 | 35.38 | 172 | 160 | 11 | 172 | 160 | 11 |
| | | | 148 | | 148 | | | 148 | | |
| | | GFRP | 110 | 35.38 | 110 | 115 | 6 | 110 | 115 | 6 |
| | | | 119 | | 120 | | | 119 | | |
| 50% HVFAC | 13 | Steel | 70 | 35.11 | 70 | 71 | 3 | 70 | 71 | 3 |
| | | | 72 | | 73 | | | 73 | | |
| | | GFRP | 45 | 35.11 | 45 | 40 | 16 | 45 | 40 | 16 |
| | | | 36 | | 36 | | | 36 | | |
| | 19 | Steel | 160 | 35.11 | 160 | 162 | 2 | 160 | 162 | 2 |
| | | | 164 | | 164 | | | 164 | | |
| | | GFRP | 112 | 35.11 | 112 | 108 | 6 | 112 | 108 | 6 |
| | | | 103 | | 103 | | | 103 | | |
| 70% HVFAC | 13 | Steel | 71 | 34.05 | 70 | 73 | 5 | 71 | 73 | 5 |
| | | | 76 | | 75 | | | 76 | | |
| | | GFRP | 34 | 34.05 | 33 | 35 | 8 | 34 | 36 | 8 |
| | | | 38 | | 37 | | | 38 | | |
| | 19 | Steel | 158 | 34.05 | 156 | 156 | 0 | 157 | 157 | 0 |
| | | | 159 | | 157 | | | 158 | | |
| | | GFRP | 79 | 34.05 | 78 | 83 | 8 | 79 | 83 | 8 |
| | | | 89 | | 88 | | | 88 | | |

Note: 1 mm = 0.04 in., 1 N = 0.22 lb., 1 MPa = 145 psi

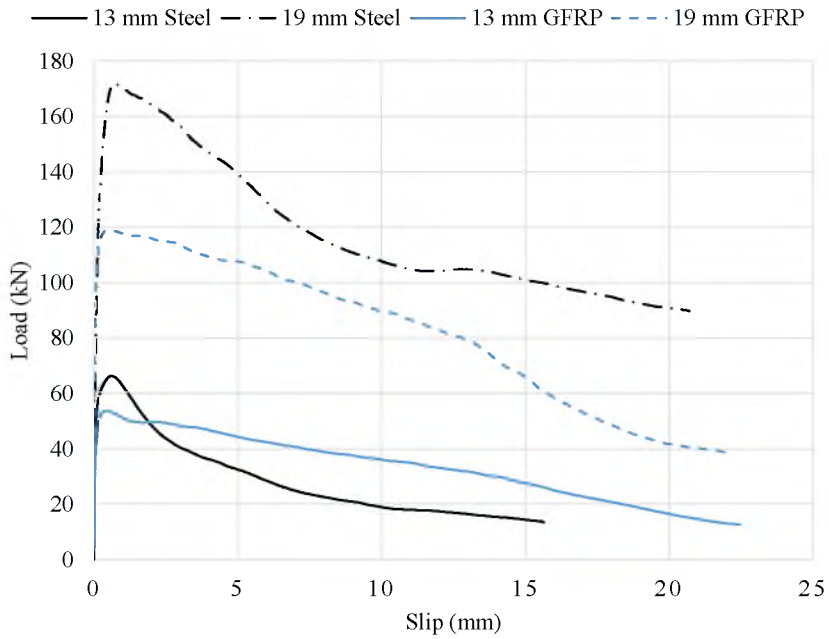


Figure 8. Pullout results of steel and GFRP rebars in conventional concrete (CC)

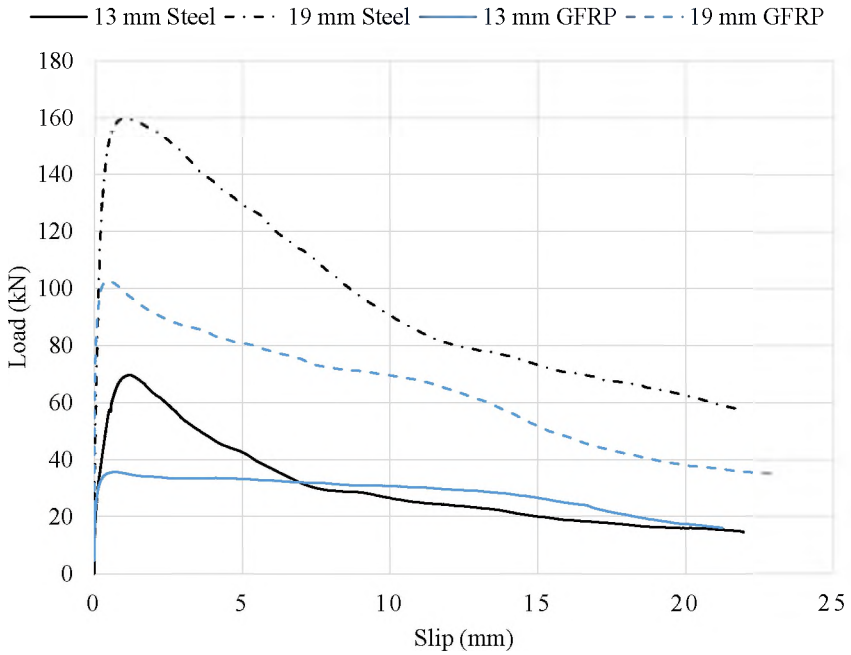


Figure 9. Pullout results of steel and GFRP rebars in 50% high volume fly ash

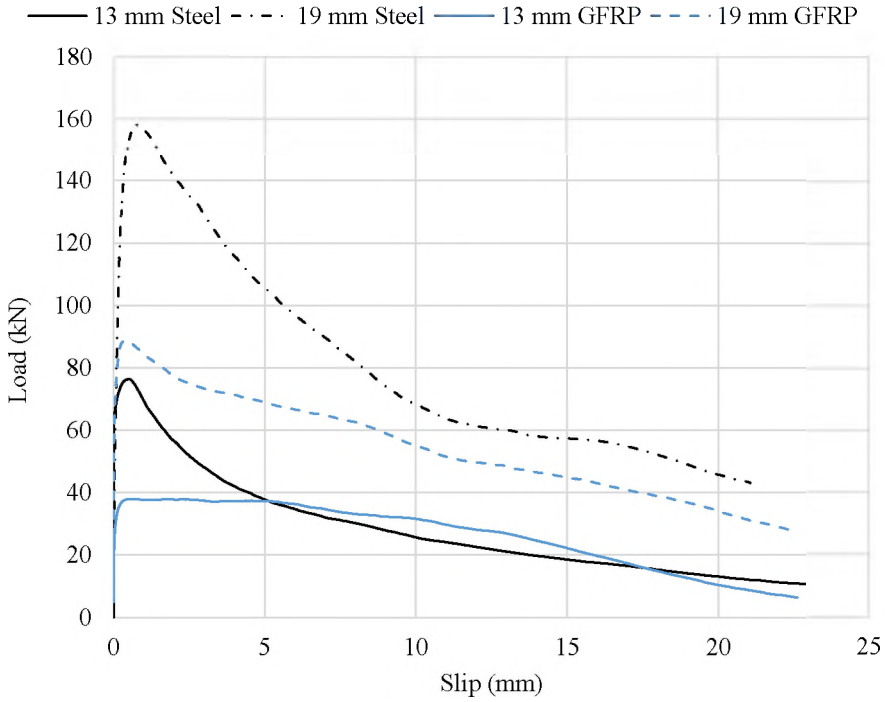


Figure 10. Pullout results of steel and GFRP rebars in 70% high volume fly ash

Table 6. Toughness results of GFRP rebars

| Concrete Type | Rebar Size mm (in.) | Specimen Number | $A_{peak}$ kN.m (in.lb) | $A_{80\%}$ kN.m (in.lb) | $A_{50\%}$ kN.m (in.lb) |
|---|---|---|---|---|---|
| CC | 13 (1/2) | 1 | 0.010 (92) | 0.14 (1232) | 0.30 (2654) |
| | | 2 | 0.012 (104) | 0.22 (1967) | 0.28 (2515) |
| | 19 (3/4) | 1 | 0.030 (261) | 0.54 (4828) | 0.82 (7257) |
| | | 2 | 0.025 (219) | 0.48 (4233) | 0.74 (6566) |
| 50% HVFAC | 13 (1/2) | 1 | 0.010 (89) | 0.13 (1184) | 0.26 (2187) |
| | | 2 | 0.007 (65) | 0.18 (1594) | 0.25 (2205) |
| | 19 (3/4) | 1 | 0.022 (194) | 0.37 (3270) | 0.69 (6192) |
| | | 2 | 0.020 (179) | 0.25 (2175) | 0.52 (4628) |
| 70% HVFAC | 13 (1/2) | 1 | 0.005 (45) | 0.15 (1291) | 0.21 (1863) |
| | | 2 | 0.006 (53) | 0.16 (1445) | 0.22 (1967) |
| | 19 (3/4) | 1 | 0.013 (115) | 0.35 (3113) | 0.47 (4132) |
| | | 2 | 0.014 (127) | 0.30 (2633) | 0.43 (3797) |

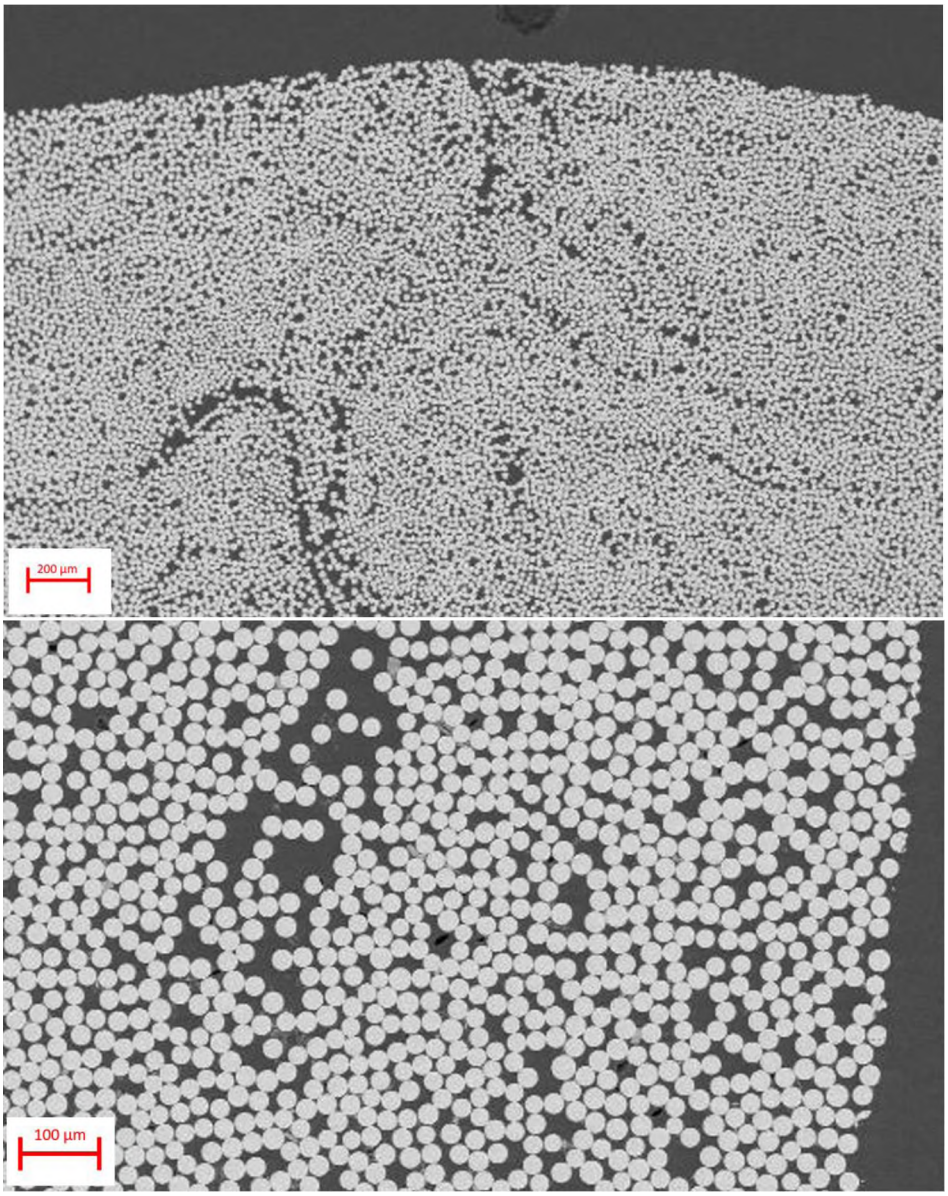


Figure 11. Sample specimen subjected to SEM analysis after pullout test

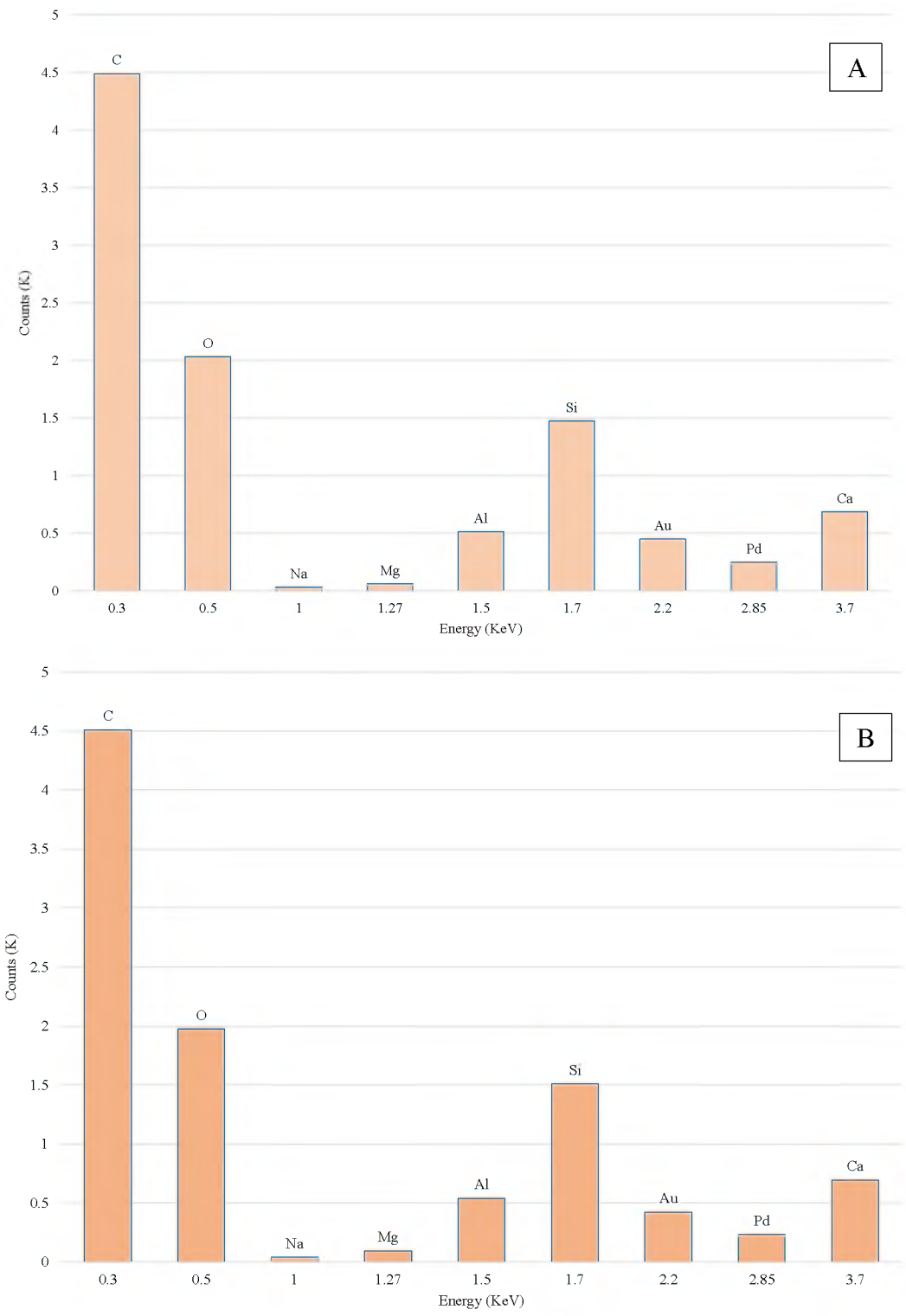


Figure 12. A sample EDS specimen for (A) control and (B) after-pullout-test

Table 7. Glass transition temperature ($T_g$) for control and after-pullout-test specimens

| | Specimen | Net Weight (mg) | $T_g$° C |
|---|---|---|---|
| Control Specimen | CB-1 | 13.3 | 110 |
| | CB-2 | 16.6 | 105 |
| | CB-3 | 15.6 | 108 |
| After-Pullout-Test | AP-1 | 14.2 | 100 |
| | AP-2 | 11.2 | 110 |
| | AP-3 | 19.1 | 110 |

## 8. STATISTICAL ANALYSES AND DISCUSSIONS

To fully assess the performance of GFRP bars, a microstructural and chemical investigations were performed. Besides the experimental analyses performed on the collected data, statistical analyses were used to assess the performance of GFRP rebars. Only GFRP rebars were used in this section, as mild steel rebars have been extensively investigated [24]. There are extremely limited number of data about the bond-slip between GFRP rebars and HVFA concrete. Therefore, there is only the current pool of data to conduct statistical work, but the authors still think that they can still be used for comparisons purposes with the current experimental data and also be used in the future as a basis for other researchers to build their work on. Multiple linear regression was used to predict the GFRP's bond strength considering the effects of compressive strength and rebar diameter to embedment length ratio. Rebar diameter and embedment length factors were involved as a ratio for two reasons; first, most of the ACI 408R-03 [25] equations (the previous work) involved that ratio, and second, in this study, that ratio was fixed; meaning every time 13 mm (1/2 in.) rebars were used, an embedment length of 77 mm (3

in.) was used (the same took place with 19 mm (3/4 in.) rebars). In addition, concrete cover was not considered in the predictive model, as its effect was purposely eliminated as mentioned earlier in Section 5. After removing the terms that were statistically insignificant, the following bond strength model was obtained for the data collected in this study:

$$u = \frac{(f_c')^{1.8}}{25}\left(\frac{d_b}{l_d}\right)^{2.5} \quad ------ (1)$$

Where $u$ is the bond strength in psi units (conversion: 1 MPa = 145 psi), $f'c$ is the concrete compressive strength (psi), $d_b$ is the rebar diameter (in.) (conversion: 1 mm = 0.04 in.), and $l_d$ is the embedment length (in.). The goodness-of-fit plot of the model was good, as there were fair data scattering and no clustering. This plot was used to show the relationship between the predictive and experimental model where the solid line presents the predictive model and the dots presents the experiment results of bond strength. The coefficient of determination, R-squared, of the model was 0.83 which is considered fairly well (above 0.70). The model was based off of a 95% level of confidence. The effect of each factor in the model was assessed relying on the p-values, which resembles the chance that variation was as a result of random variation obtained from the model. The statistical findings of this study were consistent with the experimental findings. It was found that compressive strength had the most significant impact. Other factors such as rebar diameter and embedment length by themselves were not significant, however the ratio of rebar diameter to embedment length was fairly significant after the compressive strength significance.

The goodness-of-fit plot of the bond strength is shown in Figure 13 (A). In addition to the bond strength prediction, peak and post-peak toughness were modeled in this study. Figure 14 shows the measured toughness levels. The following model was obtained for peak toughness ($A_p$) with an R-squared = 0.92:

$$A_p = 2857(f_c')^{2.86}\left(\frac{d_b}{l_d}\right)^{15.62} \quad ------ (2)$$

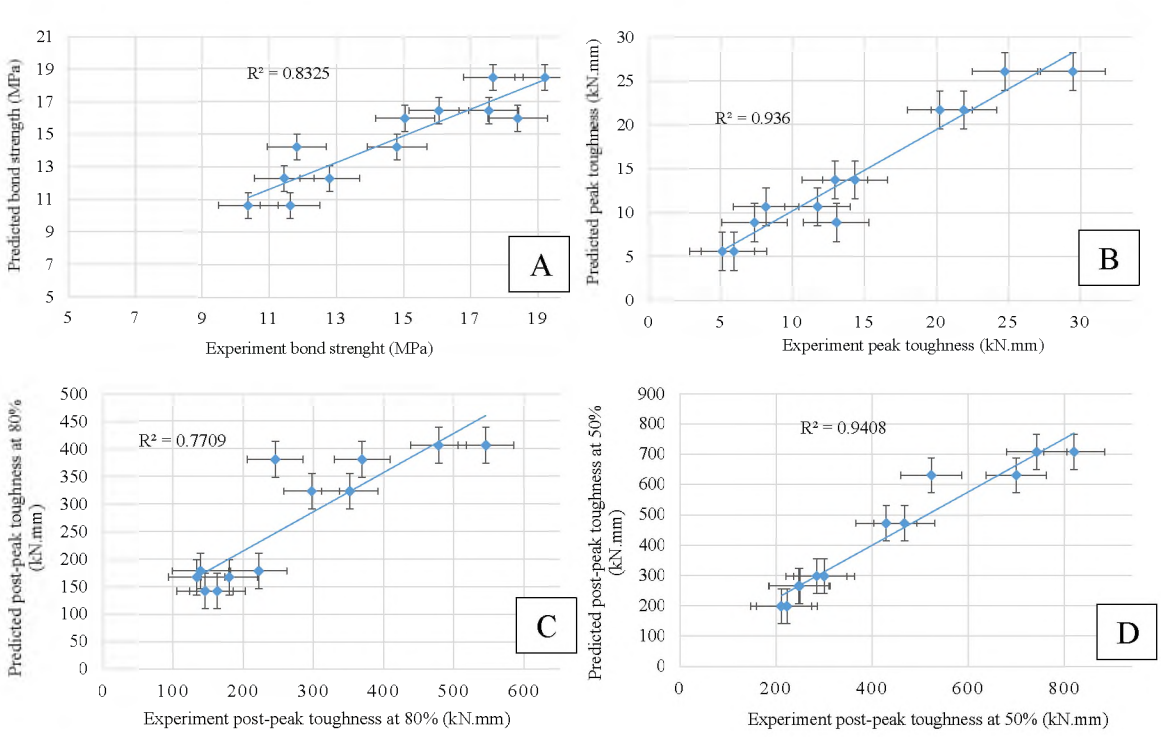


Figure 13. Goodness-of-fit: (A) bond strength, (B) peak toughness, (C) post-peak toughness at 80%, (D) post-peak toughness at 50%

For the post-peak toughness at 50% of the peak ($A_{p50}$), the following was obtained with an R-squared = 0.96:

$$A_{p50}=458\times10^{6}(f_c')^{1.8}\left(\frac{d_b}{l_d}\right)^{15.17} \quad ------ (3)$$

For the post-peak toughness at 80% of the peak ($A_{p80}$), the following was obtained with an R-squared = 0.80:

$$A_{p80}=40049\times10^{6}(f_c')^{1.02}\left(\frac{d_b}{l_d}\right)^{14.4} \quad ------ (4)$$

All the equations above are in psi-in. units. Therefore, for conversion, 1 MPa = 145 psi, and 1 mm = 0.04 in. The goodness-of-fitness plots for the peak and post-peak toughness exhibited good data scatter. In addition, R-squared of the both models were high. Toughness models were also built based off of 95% level of confidence. The good-of-fitness plots of the both types of toughness are shown in Figure. 13 (B), (C), and (D) show the goodness-of-fit plot of toughness. Besides the two models above, there were other models built to investigate toughness involving other factors such as rebar diameter and embedment length (terms by themselves and not ratio). However, they were found to be statistically insignificant, so they were eliminated; also, their R-squared were substantially low. Compressive strength was found to be the most significant factor on both peak and post-peak toughness and then followed by the rebar diameter to embedment length ratio. Decreasing compressive strength or using smaller rebar diameter lead to lower toughness and vice versa.

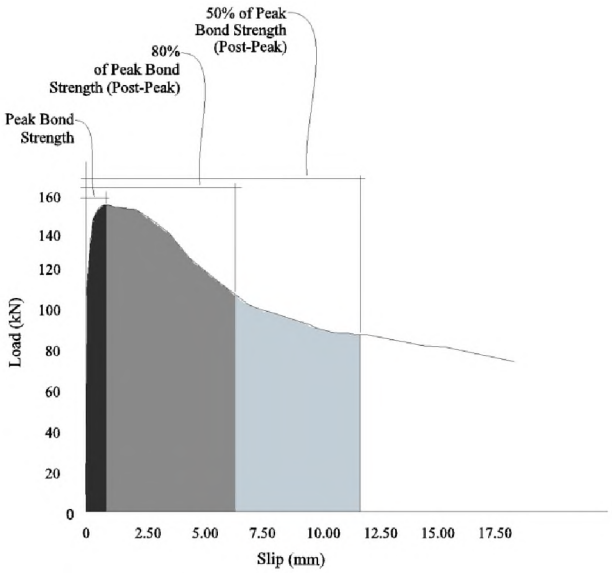


Figure 14. Measured toughness levels

## 9. COMPARISON WITH PREVIOUS STUDIES

To assess the effectiveness of the statistically-based bond strength model, other statistical predictions were made from other related studies and then were compared to the one made for this study. In 2004, Achillides and Pilakoutas conducted a bond-slip study on FRP bars (including glass fiber) in conventional concrete [3]. The parameters of their study were type of rebar, length of embedment, and compressive strength. A multiple variable regression was implemented to gain a model of their work. The following model was found:

$$u_{Achillides} = 25\,(f'c)^{0.55}\left(\frac{d_b}{l_d}\right)^{0.33} \quad ------(5)$$

where $u_{Achillides}$ is the bond strength based on Achillides and Pilakoutas data (psi). In 2012, Volz et al. conducted a thorough investigation about the HVFA concrete including its

bond-slip performance [32]. They investigated the effect of: 50% and 70% cement replacement with fly ash, size of rebar, and compressive strength on bond performance. The following was predicted from their data:

$$u_{Volz} = 1.5 \times 10^5 (f'c)^{0.1} (\frac{d_b}{l_d})^3 \quad ------(6)$$

where $u_{Volz}$ is the bond strength based on Volz et al. data (psi). Besides comparing with Achillides and Volz models, the current models was also compared to the ACI318 model. For comparison purposes, concrete compressive strength, embedment length, and rebar diameter were selected to check their influences on bond strength. The ACI318 bond strength equation [29][30] is as follows:

$$u_{ACI} = (1.2 + 3\frac{c}{d_b} + 50\frac{d_b}{l_d})\sqrt{f'c} ------(7)$$

where $u_{ACI}$ is the bond strength (psi), and $c$ is the concrete cover (in.). Since the cover was not taken as a parameter in any of ours, Achillides, and Volz studies, it was taken as a constant in this analysis to minimize its effect on the outcome of the bond strength model. The first parameter considered was the effect of concrete compressive strength and is shown in Figure. 15 (A). It can be seen from this Figure that the compressive strength effect had the most influence in our equation (Ali), and the least influence in Volz's equation. ACI and Achillides exhibited the same behavior where both equations had similar trend and small slopes. The reason for that is, in both equations, the powers of the compressive strengths were close to each other, a power of 0.5 in ACI and 0.55 in Achillides. In addition, Ali's equation had the highest influence from the compressive strength; because it had the highest power of compressive strength. Also, it was noticed

from the equations and the Figure that compressive strength was directly proportional to the bond strength despite the difference in its rate of influence on bond strength results. Furthermore, Anderson-Darling test was carried out for the four models to assess their distribution trend. The results showed that all models were normally distributed with p-values ranging from 0.054 to 0.184 (the data is normal as long as P-Value $\geq$ 0.05)[48].A divergence in the distribution curve of all four models was noticed when the compressive strength value is below or beyond their design range (20 - 40 MPa (3000 - 6000 psi)). The reason for divergence is that these models were based off of that range of compressive strength that imitates what used commonly in the construction industry. The second parameter in this investigation was the rebar diameter and is shown in Figure. 15 (B). Ali, Volz, and Achillides models showed that the higher the rebar diameter was, the higher the bond strength. Particularly, Ali and Volz equations had sort of similar curves where their slopes are close to each other, because the power of rebar diameters were close to each other. On the other hand, ACI equation exhibited a different behavior where it showed that rebar diameter is indirectly proportional to the bond strength. Even though the rebar diameter in the ACI's equation was presented in the nominator one time and in the denominator at another, the rebar diameter acted as if it was only placed in the denominator as it reduced the bond strength. The reason of that was due to the higher ratio of cover to rebar diameter than the rebar diameter to embedment length ratio. Therefore, the rebar diameter the higher it went, the lower the bond strength was. If a smaller cover was used, a smaller ratio of cover to rebar diameter would have been resulted, and thus a higher rebar diameter to embedment length ratio achieved and

therefore the influence of rebar diameter on bond strength results could have been positive. The normality test for the bar diameter showed that all models exhibited a normal distribution, however since there are only few rebar sizes available and used commercially, having a normal distribution does not truly reflect the effect of rebar diameter ($d_b$) on bond strength. The third factor investigated was the length of embedment where again Ali and Volz equation exhibited the same trend due to the close power of development length. In all equations, the embedment length was indirectly proportional to the bond strength, because it was in the denominator in all equations. The embedment length effect is shown in Figure. 15 (C). In addition, the normality test was carried out and it was found that all four models had a normal distribution. The p-values ranged from 0.15 to 0.78 which is considerably higher than the normalization limit of 0.05. Table 8 Normally dist. shows the Anderson-Darling test results of all models.

In addition to these statistical analyses, two sample t-tests were carried out to check for significance of the developed models. Each model was tested for significance with ours where the null hypothesis presumed that there is no significant difference and the alternative called for the otherwise. In addition, a 95% confidence interval was implemented in the analysis of t-tests. The t-test was carried out three times and was based on the most influential factor of bond strength which was compressive strength. The assessment of significance of bond strength was made by comparing our bond strength model (Ali) to ACI, Mehdi, and Zenon models. The analysis results showed that all models were statistically insignificant when compared to ours. In all models the p-value was less than 0.05 which calls for abandoning the null hypothesis and accepting the

alternative one. Furthermore, despite that all models exhibited insignificance, Mahdi's model was statistically the closest in terms of behavior to ours, probably owing to the similarities represented by concrete type (partially similar), specimen geometry, rebar dimeter, and embedment length. Figure. 16 shows the t-test results resembled by box plots.

To summarize, all the equations were made using multiple variable regression. Three factors were investigated from the previous studies. The factors were compressive strength, rebar diameter, and embedment length. It was found the higher the compressive strength and rebar diameter were, the higher the bond strength, and the lower the embedment length was, the higher the bond strength.

## 10. CONCLUSIONS

Corrosion is a serious matter in civil engineering industry, thus GFRP rebars have come out as an alternative to avoid corrosion issues related to mild steel reinforcement. Portland cement, on the other hand, is not eco-friendly material due to its high level of $CO_2$ emissions, therefore other alternatives such as fly ash has been increasingly more considered as an effective substitution to reduce cement consumption. Two HVFA concrete levels were considered: 50% and 70%.

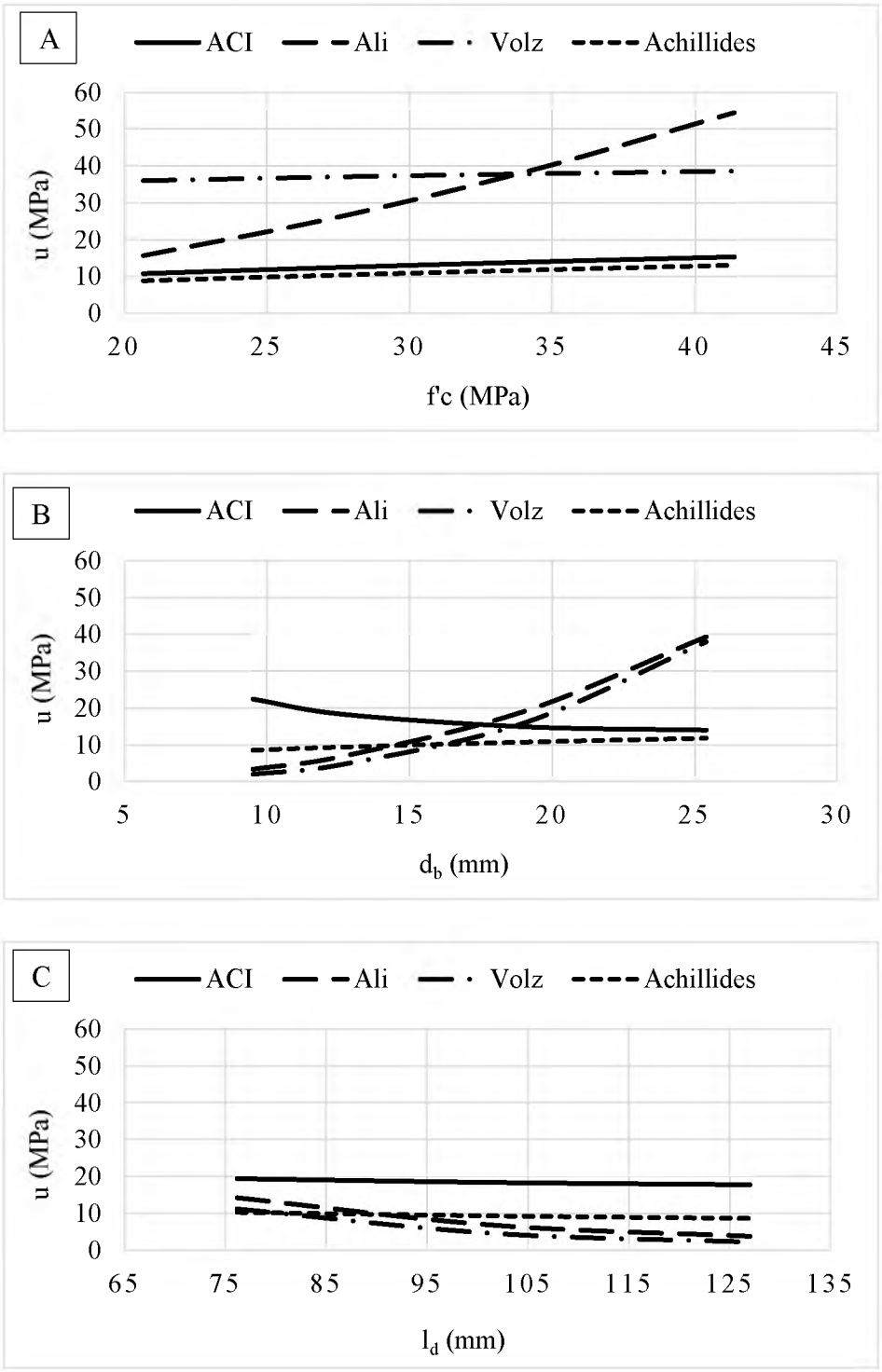


Figure 15. (A) bond strength vs compressive strength, (B) bond strength vs rebar diameter, (C) bond strength vs embedment length
Conversion: 1 MPa = 145 psi, 1 mm = 0.04 in.

Pullout tests were conducted to enrich our understanding of the bond performance of GFRP rebars in different types of concrete. The following were concluded from this study:

a) GFRP rebars exhibited less peak bond strength, but higher post-peak bond strength.

b) All the specimens experienced a pullout mode of failure.

c) The higher the rebar diameter was, the higher the bond strength.

d) The higher the compressive strength was, the higher the bond strength.

e) Rebar deformation of mild steel was the main reason for the higher peak bond strength; because of the anchorage effect from the surface deformations of rebar.

f) Mild steel rebars exhibited sharp loss of bond strength after peak load was reached due to the principle cracks generated from the rebar deformations.

g) GFRP rebar exhibited steady loss of strength after peak load was reached due to the frictional resistance generated between the sand-coated surface of the rebar and concrete.

h) CC had the highest bond strength and 70% HVFAC had the lowest, as the highest compressive strength was found in CC and the lowest in 70% HVFAC.

i) Microstructural and chemical examinations of GFRP rebars did not show any obvious signs for microstructural degradations or chemical changes.

j) Toughness and post-peak toughness were measured; they were found to be highly affected by the compressive strength and rebar diameter used.

k) Multiple regression analysis was utilized to build predictive models of bond strength, peak toughness, and post-peak toughness.

l) The predictive models of bond strength, toughness, and peak-toughness were consistent with what were found in the experiments.

m) Compressive strength and rebar diameter to embedment length ratio were the most influential factors in bond strength and toughness.

n) Comparison with previous studies showed that compressive strength and rebar diameter increase the bond strength while the embedment length decreased it.

o) The hypothesis test results between the current bond strength equation and the previous work-based bond equations showed non-significance.

The current and the future trend of research are leaning toward investigating and implementing more green and sustainable materials. The construction industry is still shy when it comes to applying new materials, therefore, to encourage them, more research-based data (implemented in codes and design standard) needs to be available. That said, more comprehensive studies about such materials are required. Regarding this study, the authors definitely see lots of areas where improvement and thorough investigations are needed such as involving different types of fly ash (in terms of types, change in chemical concentrations within a certain type). In addition, the type of reinforcement (materials and geometry) can be investigated. To improve our understanding to the bond behavior and increase the current database for such topic, the same study conducted herein can be investigated using the same and different variables.

# REFERENCES


[1] A. Nanni, A. De Luca, and H. Zadeh, *Reinforced Concrete with FRP Bars*. CRC Press.

[2] NACE, "Corrosion Costs and Preventive Strategies in The United States," *Corros. Costs Prev. Strateg. United States*, no. NACE, 2013, doi: FHWA-RD-01-156.

[3] Z. and Achillides and K. Pilakoutas, "Bond Behavior of FRP Bars Under Direct Pullout Conditions.pdf," *J. Compos. Constr.*, vol. 8, no. April, pp. 173–181, 2004, doi: 10.1111/j.1574-6968.2001.tb10907.x.

[4] O. A. Dissertations and M. Khatibmasjedi, "Scholarly Repository Sustainable Concrete Using Seawater and Glass Fiber Reinforced Polymer Bars," 2018.

[5] H. Urbancova, "Competitive Advantage Achievement through Innovation and Knowledge," *J. Compet.*, vol. 5, no. 1, pp. 82–96, 2013, doi: 10.7441/joc.2013.01.06.

[6] Composite Group Chelyabinsk, "Comparative technical characteristics of GFRP bar and steel reinforcement." [Online]. Available: http://compositegroupworld.com/produktsiya/stekloplastikovaya-armatura.html.

[7] S. Skapa, "Investment Characteristics of Natural Monopoly Companies," *J. Compet.*, vol. 4, no. 1, pp. 36–43, 2012, doi: 10.7441/joc.2012.01.03.

[8] M. Vochozka, Z. Rowland, P. Suler, and J. Marousek, "The Influence of the International Price of Oil on the Value of the EUR / USD THE INFLUENCE OF THE INTERNATIONAL PRICE OF OIL ON THE VALUE OF THE EUR / USD EXCHANGE RATE," *J. Compet.*, no. June, 2020, doi: 10.7441/joc.2020.02.10.

[9] R. M. Andrew, "Global CO2emissions from cement production," *Earth Syst. Sci. Data*, vol. 10, no. 1, pp. 195–217, 2018, doi: 10.5194/essd-10-195-2018.

[10] A. Bilodeau and V. M. Malhotra, "High-Volume Fly Ash System: Concrete Solution for Sustainable Development," *ACI Mater. J.*, vol. 97, no. 1, pp. 41–48, Jan. 2000, doi: 10.14359/804.

[11] ASTM, "Standard Specification for Coal Fly Ash and Raw or Calcined Natural Pozzolan for Use in Concrete," *Annu. B. ASTM Stand.*, pp. 3–6, 2010, doi: 10.1520/C0618.

[12] ACI 232.2R, "ACI 232.2R-96 (Reapproved 2002) 'Use of fly ash in concrete,'" *Am. Concr. Inst.*, vol. 96, no. Reapproved, pp. 1–34, 2002.

[13] E. E. Berry, R. T. Hemmings, M.-H. Zhang, B. J. Cornelius, and D. M. Golden, "Hydration in High-Volume Fly Ash Concrete Binders," *ACI Mater. J.*, vol. 91, no. 4, pp. 382–389, Jul. 1994, doi: 10.14359/4054.

[14] Anon, "Fly Ash.," *Concr. Constr. - World Concr.*, vol. 30, no. 4, 1985.

[15] Y. Esen, "The effect of cure conditions and temperature changes on the compressive strength of normal and fly ash added concretes," *Int. J. Phys. Sci.*, vol. 5, no. 17, pp. 2598–2604, 2010.

[16] T. J. Looney, M. Arezoumandi, J. S. Volz, and J. J. Myers, "An Experimental Study on Bond Strength of Reinforcing Steel in Self-Consolidating Concrete," *Int. J. Concr. Struct. Mater.*, vol. 6, no. 3, pp. 187–197, 2012, doi: 10.1007/s40069-012-0017-9.

[17] S. V. Naik TR, Singh SS, "Concrete compressives strength, shrinkage and bond strength as affected by addition of fly ash and temperature," *Univ. Wisconsin*, 1989.

[18] Gopalakrishnan S., "Demonstration of utilising high volume fly ash based concrete for structural applications," *Struct. Eng. Res. Centre; Chennai, India*, 2005.

[19] M. Arezoumandi, T. J. Looney, and J. S. Volz, "Effect of fly ash replacement level on the bond strength of reinforcing steel in concrete beams," *J. Clean. Prod.*, vol. 87, no. 1, pp. 745–751, 2015, doi: 10.1016/j.jclepro.2014.10.078.

[20] M. Al-Azzawi, T. Yu, and M. N. S. Hadi, "Factors Affecting the Bond Strength Between the Fly Ash-based Geopolymer Concrete and Steel Reinforcement," *Structures*, vol. 14, no. January, pp. 262–272, 2018, doi: 10.1016/j.istruc.2018.03.010.

[21] G. Maranan, A. Manalo, K. Karunasena, and B. Benmokrane, "Bond Stress-Slip Behavior: Case of GFRP Bars in Geopolymer Concrete," *J. Mater. Civ. Eng.*, vol. 27, no. 1, p. 04014116, 2015, doi: 10.1061/(ASCE)MT.1943-5533.0001046.

[22] S. Soares, N. Freitas, E. Pereira, E. Nepomuceno, E. Pereira, and J. Sena-Cruz, "Assessment of GFRP bond behaviour for the design of sustainable reinforced seawater concrete structures," *Constr. Build. Mater.*, 2019, doi: 10.1016/j.conbuildmat.2019.117277.

[23] H. Mazaheripour, J. A. O. Barros, J. M. Sena-Cruz, M. Pepe, and E. Martinelli, "Experimental study on bond performance of GFRP bars in self-compacting steel fiber reinforced concrete," *Compos. Struct.*, vol. 95, pp. 202–212, 2012, doi: 10.1016/j.compstruct.2012.07.009.

[24] E. Garcia-Taengua, J. R. Martí-Vargas, and P. Serna, "Bond of reinforcing bars to steel fiber reinforced concrete," *Constr. Build. Mater.*, vol. 105, pp. 275–284, 2016, doi: 10.1016/j.conbuildmat.2015.12.044.

[25] ACI 408R, "ACI 408R-03," *Am. Concr. Inst.*, pp. 1–49, 2003.

[26] G. J. Al-Sulaimani, M. Kaleemullah, I. A. Basunbul, and Rasheeduzzafar, "Influence of Corrosion and Cracking on Bond Behavior and Strength of Reinforced Concrete Members," *ACI Struct. J.*, vol. 87, no. 2, pp. 220–231, Mar. 1990, doi: 10.14359/2732.

[27] B. Benmokrane, 0. Chaallal, and R. Masmoudi, "Flexural Response of Concrete Beams Reinforced with FRP Reinforcing Bars," *ACI Struct. J.*, vol. 93, no. 1, pp. 46–55, Jan. 1996, doi: 10.14359/9839.

[28] RILEM and T. R. for the T. and U. of C. Materials, "RILEM 7-II-128. RC6: Bond Test for Reinforcing Steel - Pullout Test," 1994.

[29] ASTM A615, "Standard Specification for Deformed and Plain Carbon-Steel Bars for Concrete Reinforcement," *ASTM*, doi: 10.1520/A0615.

[30] C. C. S. Owens, "ASLAN 100 Glass fiber reinforced polymer (GFRP) rebars," pp. 5–6.

[31] ASTM-D7205, "Standard Test Method for Tensile Properties of Fiber Reinforced Polymer Matrix," *ASTM*, vol. i, no. Reapproved 2011, pp. 1–13, 2011, doi: 10.1520/D7205.

[32] B. Volz, Jeffery; Myers, John; Richardson, David; Arezoumandi, Mahdi; Beckemeier, Karl; Davis, Drew; Holman, Kyle; Looney, Trevor; and Tucker, "Design and evaluation of a high-volume fly ash (HVFA) concrete mixes," 2012.

[33] ASTM-C496, "Splitting Tensile Strength of Cylindrical Concrete Specimens," *ASTM Stand.*, vol. i, pp. 1–5, 2011, doi: 10.1520/C0496.

[34] ASTM-C39/C39M, "Standard Test Method for Compressive Strength of Masonry Prisms," *ASTM Int.*, no. C, pp. 1–10, 2015, doi: 10.1520/C0039.

[35] A. F. Al-Khafaji and J. J. Myers, "Durability assessment of non-steel reinforcement after more than ten years of service," *Adv. Eng. Mater. Struct. Syst. Innov. Mech. Appl. - Proc. 7th Int. Conf. Struct. Eng. Mech. Comput. 2019*, pp. 1566–1569, 2019, doi: 10.1201/9780429426506-270.

[36] G. Nkurunziza, A. Debaiky, P. Cousin, and B. Benmokrane, "Durability of GFRP Bars: A Critical Review of the Literature," *Prog. Struct. Eng. Mater.*, vol. 7, no. 4, pp. 194–209, 2005, doi: 10.1002/pse.205.

[37] T. Hemalatha and A. Ramaswamy, "A review on fly ash characteristics – Towards promoting high volume utilization in developing sustainable concrete," *Journal of Cleaner Production*. 2017, doi: 10.1016/j.jclepro.2017.01.114.

[38] A. S. M. Kamal and M. Boulfiza, "Durability of GFRP rebars in simulated concrete solutions under accelerated aging conditions," *J. Compos. Constr.*, vol. 15, no. 4, pp. 473–481, 2011, doi: 10.1061/(ASCE)CC.1943-5614.0000168.

[39] A. Barkatt, "Issues in predicting long-term environmental degradation of fiber-reinforced plastics.," *Environ. Eff. Eng. Mater.*, pp. 419–458, 2001.

[40] Epoxy Technology Inc., "Glass Transition Temperature for Epoxies," *Available URL http//www.epotek.com*, pp. 1–2, 2012.

[41] W. Wang, "Durability Behavior of Fiber Reinforced Polymer and Steel Reinforced Polymer for Infrastructure Applications," Missouri University of Science and Technology, 2017.

[42] F. Micelli and A. Nanni, "Durability of FRP rods for concrete structures," *Constr. Build. Mater.*, vol. 18, no. 7, pp. 491–503, 2004, doi: 10.1016/j.conbuildmat.2004.04.012.

[43] F. Micelli and J. J. Myers, "Durability of FRP-Confined Concrete," *Inst. Civ. Eng.*, vol. 161, no. 4, pp. 173–185, 2008.

[44] ASTM International, "ASTM E1356-08 Standard Test Method for Assignment of the Glass Transition Temperatures by Differential Scanning Calorimetry," *ASTM Int.*, vol. 08, no. Reapproved, pp. 1–4, 2014, doi: 10.1520/E1356-08R14.2.

[45] ACI 318, *Building code requirements for structural concrete (ACI 318-14) : an ACI standard : commentary on building code requirements for structural concrete (ACI 318R-14), an ACI report*. 2014.

[46] AASHTO, *American Association of State Highway and Transportation Officials*, 4th ed. Washington, D.C., 2007.

[47] R. A. K. J. T. Black, *DeGarmo's Materials and Processes in Manufacturing*. Wiley.

[48] D. C. Montgomery, *Design and Analysis of Experiments*, 8th ed. John Wiley & Sons Inc, 2013.

# III. DURABILITY ASSESSMENT OF 15–20-YEAR-OLD GFRP BARS EXTRACTED FROM BRIDGES IN THE US. II: GFRP BAR ASSESSMENT

Ali F. Al-Khafaji[1], Rudy T. Haluza[2], Vanessa Benzecry[3], John J. Myers[1], Charles E. Bakis[2], and Antonio Nanni[3]

[1]Department of Civil, Architectural and Environmental Engineering, Missouri University of Science and Technology, Rolla, MO, 65409, USA

[2] Department of Engineering Science and Mechanics, Pennsylvania State University, University Park, PA, 16802, USA

[3] Department of Civil, Architectural and Environmental Engineering, University of Miami, Coral Gables, FL 33146, USA

## ABSTRACT

A multi-laboratory investigation of the durability of glass fiber-reinforced polymer (GFRP) bars extracted from 11 15-20 years old bridges in the United States was performed. Part 1 (Benzecry et al. 2020) of this two-paper series describes the bridges and presents data on the condition of their concrete, while Part 2 focuses on the condition of the bars. Constituent content, maximum water absorption, as-received moisture content, glass transition temperature, short bar shear strength and tensile strength were evaluated. Scanning electron microscopy and energy dispersive spectroscopy were also performed. The fiber mass content of all bars was close to or greater than that specified in the current ASTM E1309 (ASTM 2010) GFRP bar standard. Scanning electron microscopy and energy dispersive spectroscopy showed only slight signs of degradation, predominantly near the outer radius of the bars. The loss of short

beam shear strength was slight to moderate in bars with control data for comparison. Tensile strength, which could only be evaluated in one bridge, showed a reduction of only 4.2% after 17 years of service. Overall, it is concluded that GFRP bars can be considered a promising replacement for steel reinforcement in bridge decks subjected to real-time field exposure.

## 1. INTRODUCTION

Corrosion-related damage in steel-reinforced concrete structures is expensive to repair and often demands expensive continuous monitoring (Nanni et al. 2014). There are more than 600,000 bridges in the United States built with steel-reinforced concrete (RC) and the estimated direct cost of repairs of these bridges is US$8.3 billion (Koch et al. 2016). Glass fiber-reinforced polymer (GFRP) composite reinforcement bars have emerged as a potentially more durable replacement for steel in RC structures (ACI 2015). GFRP bars have many benefits such as low cost-to-performance ratio, noncorrosive behavior, and high strength-to-weight ratio (ACI 2015).

The pore water solution of concrete is highly alkaline with a pH between 10.5 and 13.5 (Diamond 1981) (Taylor 1987). Exposure to alkalis can deteriorate the tensile and longitudinal shear strength of GFRP bars (Nkurunziza et al. 2005). There are two major mechanisms for an alkali environment to damage fibers: (1) chemical attack on the glass fibers by alkalis, and (2) concentration of hydration products at the interface between fiber and matrix (Mufti et al. 2007b) (Murphy et al. 1999). Although the resin matrix of

composites gives a certain level of protection to the fibers from alkalis and moisture, migration of chemicals through resin, void, or cracks to the fiber surface is still possible (Nkurunziza et al. 2005). While numerous aspects of GFRP structural behavior are still examined, confirming long-term durability is perhaps the most substantial barrier to increase its acceptance in the industry (Gooranorimi et al. 2017). Other barriers include concerns regarding brittleness, and its initial cost compared to mild steel (Gooranorimi et al. 2017).

The performance of GFRP bars under laboratory-controlled aggressive environmental conditions (sometimes called "accelerated testing") has been investigated by evaluating the tensile strength, tensile elastic modulus, short bar shear strength, and bar/concrete bond strength following conditioning (Al-salloum et al. 2013; Khatibmasjedi et al. 2020; Wang et al. 2017). The strength loss of GFRP bars has also been shown to be higher in alkaline solutions than in water (Al-salloum et al. 2013). Kamal and Boulfiza (2011) investigated the effect of simulated pore water solution of concrete on GFRP bars. Because the diffusion of moisture into the fiber-matrix interphase in a composite could cause fiber-matrix debonding and the presence of alkalis at the locations of the glass surface would lead to fiber degradation, attention was devoted to investigating whether GFRP bars allow both species to penetrate or allow only water while blocking the alkalis. Their GFRP bars were immersed in five types of simulated concrete pore solutions, including NaOH, KOH, $Ca(OH)_2$, NaOH+KOH, NaOH+$Ca(OH)_2$, at elevated temperature. X-ray mapping was used to assess the alkalis penetration. The results showed that fiber-matrix debonding occurs in some specimens. However, the glass fibers

and matrix remained intact and there was no penetration of alkalis into the matrix. The debonding, which occurred only in specimens subjected to 75° C (167° F), was believed to due to hydrolysis of fiber sizing at high temperature.

Research also has been performed to create accelerated aging procedures and predictive models for the long-term strength of GFRP bars in concrete. Different models have been developed for accelerated aging tests of GFRP bars such as the diffusion model (Tannous and Saadatmanesh 1999) and the Arrhenius model (Porter and Barnes 1998; Chen et al. 2006). In general, these models suggest that higher temperatures, higher alkaline ion concentrations, and longer times are more detrimental to strength. Material constants used in these models necessarily depend on the exact constituents of the bar, such as type of glass in the fiber, type of coupling agent on the fiber, type of resin, and type of filler in the resin (Khatibmasjedi et al. 2020)(; Gremel et al. 2005). Additionally, the degree of access of the aggressive agents to the bar, for example through concrete cracks, has a notable influence on the rate of bar degradation as well (Yang et al. 2016).

There has been very little research conducted on-field exposure cases. Bakis et al. (2005) showed that strength loss in GFRP bars extracted from loaded concrete beams stored in natural (non-accelerated) indoor and outdoor environments for up to three years was negligible. Trejo et al. (2011) observed 12–26% strength loss in GFRP bars extracted from unloaded concrete specimen stored in an outdoor environment for 7 years. Benmokrane et al. (2018) investigated the physico-chemical attributes of GFRP bars extracted from bridge barrier walls after 11 years of service and found no changes. Additional information on the durability of GFRP bars following field service needs to be

collected to improve our understanding of the long-term service potential of GFRP bars in realistic situations and to assist the development of appropriate strength retention factors for design purposes (Micelli and Nanni 2004).

In the investigation described in this paper, mechanical and physico-chemical tests were carried out on GFRP bars extracted from 11 existing bridges located in various US states to assess the condition and strength of the bars after 15 to 20 years of service. The types of tests performed include fiber content, water absorption, moisture content, scanning electron microscopy (SEM), energy dispersive spectroscopy (EDS), glass transition temperature ($T_g$), short bar shear (SBS) strength, tensile strength, and constituent volume contents by image analysis. These tests were performed to enrich the durability database for GFRP bars subjected to long-term service conditions. Investigations of this type have been identified as high priority in a recent workshop sponsored by the US Department of Transportation (Gangarao et al. 2014) and address a critical need to document and disseminate information that overcomes barriers for the wider adoption of FRP composites in infrastructure (Sheridan et al. 2017).

## 2. BAR TESTING PROGRAM

In the first part of this two-paper series (Benzecry et al. 2020), information on the bridges from which the bars were extracted, bars extraction methods, and the specimen labeling scheme are detailed. Figure 1 shows photographs of bars from all the bridges investigated in this project. The list of states in which the bridges are located is shown in

the first column of Table 1. Prior to testing, the bars were brushed and gently scraped to remove obvious contaminants such as residual cementitious paste.

Table 1. Average fiber mass content for each bridge

| Bridge (State) | No. of Specimens | Fiber Mass Content (%) | Standard Deviation (%) |
|---|---|---|---|
| Gills Creek* (Virginia) | 6 | 72.1 | 1.78 |
| O'Fallon Park (Colorado) | 6 | 72.9 | 1.93 |
| Salem Ave. (Ohio) | 3 | 72.5 | 0.06 |
| Bettendorf (Iowa) | 3 | 73.3 | 1.29 |
| Cuyahoga County* (Ohio) | 15 | 76.4 | 2.41 |
| McKinleyville (West Virginia) | 6 | 73.5 | 2.82 |
| Thayer Road (Indiana) | 3 | 76.5 | 0.078 |
| Roger's Creek (Kentucky) | 5 | 69.2 | 1.08 |
| Sierrita de la Cruz Creek (Texas) | 9 | 76.4 | N/A |
| Walker Box Culvert (Missouri) | 4 | 82.8 | N/A |
| Southview (Missouri) | 4 | 73.4 | N/A |

## 2.1. FIBER MASS CONTENT

A burn-off procedure based on ASTM D2584 (ASTM 2011) was implemented to evaluate fiber mass content. Bar specimens weighed approximately 5 g (0.011 lb). The burn-off temperature of 575°C (1067°F) eliminated the matrix material but not the sand particles and helical fiber wrap on some of the bars, the filler particles in the matrix, and the fibers. The sand particles and helical wrap were excluded from the mass of the longitudinal fibers and residual filler remaining after burn-off.

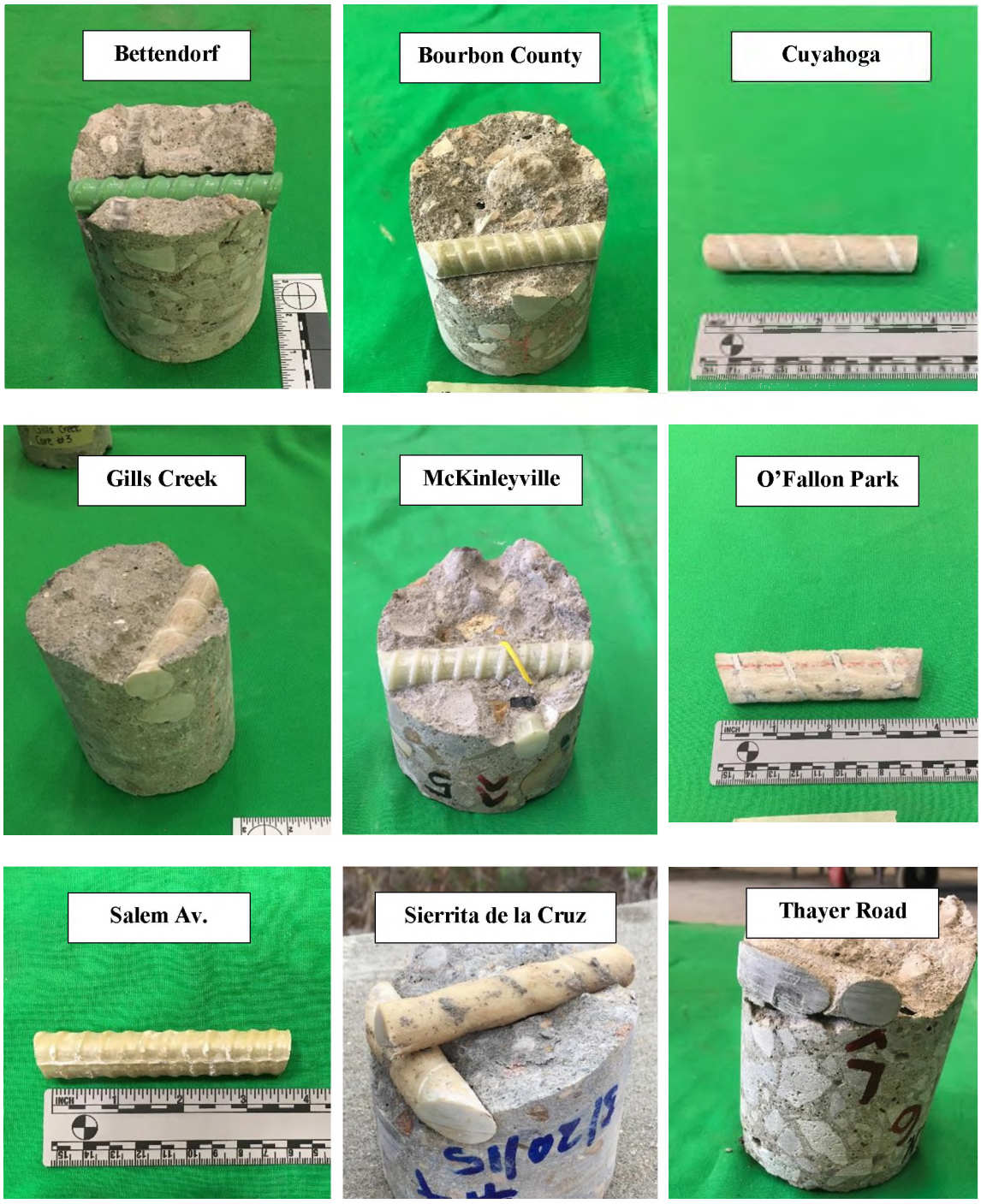


Figure 1. Bars from each of the 11 bridges

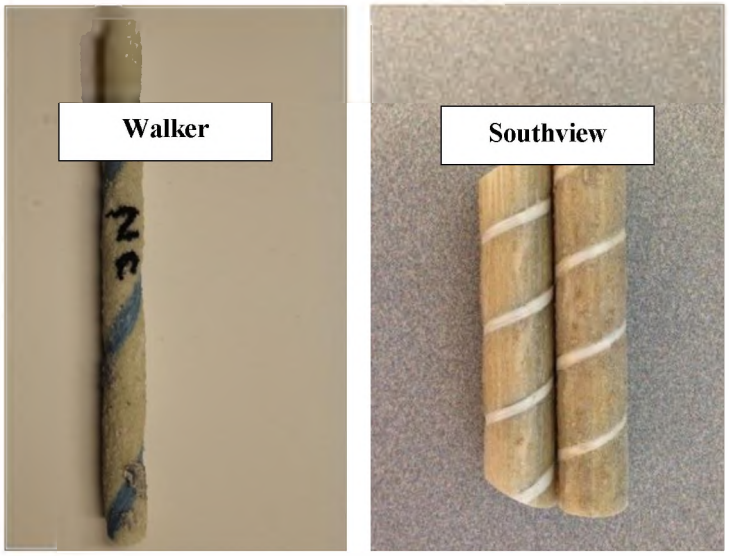


Figure 1. Bars from each of the 11 bridges (Cont.)

Following the fiber mass fraction calculation method in the ASTM D7957 (ASTM 2017) GFRP bar specification, the mass fraction of fiber was determined by dividing the mass of the fibers and residual filler divided by the mass of these same materials plus the mass of the burned off resin.

## 2.2. WATER ABSORPTION

Water absorption to equilibrium in 50° C (122° F) distilled water was measured using ASTM D570 (ASTM 2014). Specimens of approximately 25-mm (1.0 in.) length were preconditioned in an oven at 40°C (104°F) for 48 hours to minimize variances in near-surface moisture that might have accrued due to storage in different laboratory environments prior to absorption testing. Using the preconditioned weight as the reference weight, the weight gain and time to equilibrium weight were then obtained by

repeated measurements until the increase in weight per two-week period, as shown by three consecutive weighings, averaged less than 1% of the total increase in weight or 5 mg (US units) whichever is greater. The 5 mg (US units) criterion controlled in these experiments.

## 2.3. MOISTURE CONTENT

The moisture content of the as-received (without preconditioning) bars was measured by drying 13-mm-long (0.5 in.) specimens to equilibrium in a forced-air oven set to 80°C (176°F), as described in Procedure D of ASTM D5229 (ASTM 2014). Once the test was underway, specimens were weighted every day for 10 days and every week thereafter. The dry-out test was terminated when the weight changes of all of the specimens were less than 0.02% for two consecutive 7-day periods and examination of the moisture content versus square root of time plot supports the percent change criteria that effective equilibrium is reached. No preconditioning was conducted on the moisture content specimens. Data from the moisture content tests reflect field exposure as well as laboratory exposure after extraction.

## 2.4. SCANNING ELECTRON MICROSCOPY

Scanning electron microscopy (SEM) of polished cross-sections of bars was performed to visually identify signs of microstructural degradation, such as cracks in the fibers and matrix, voids, and fiber/matrix debonding.

The inspected surfaces were sanded with 1200 grit abrasive paper, polished with a 0.2 μm (US units) abrasive paste, and then plated with gold.

## 2.5. ENERGY DISPERSIVE SPECTROSCOPY

Energy dispersive spectroscopy (EDS) was used to evaluate the chemical composition of the surface of the SEM specimens. As wet concrete is highly alkaline, the possibility of degradation of the fibers and matrix due to excessive amounts of Na, K, and Ca penetrating into the bar must be investigated (Mufti et al. 2007[a]). Moreover, if the fibers are shown to contain Zr, then it can be concluded that the bars are alkali-resistant glass rather than traditional E-glass (Nkurunziza et al. 2005). EDS can detect elements Na, K, and Ca. A 10-20 kV electron beam was used for the EDS testing. The size of the region of evaluation is approximately 1 μm (US units) or less, which allows for the separate evaluation of fibers and matrix (but not necessarily resin and filler).

## 2.6. GLASS TRANSITION TEMPERATURE

The glass transition temperature, $T_g$, can be defined as the temperature range where the polymer substrate changes from a solid glassy material to a rubbery material (Becker and Locascio 2002). In this investigation, differential scanning calorimetry (DSC) according to ASTM E1356 (ASTM 2014) was used to characterize the glass transition temperature of bars from 10 of the 11 bridges and dynamic mechanical analysis according to ASTM E1640 (ASTM 2018) was used for one bridge. For DSC testing, small pieces of material weighing 10–15 mg were cut from a bar and preconditioned in

an oven for 48 hours at 48°C (118°F) to remove surface moisture. During the DSC test, the temperature was ramped upward only one time at 5–10°C/min (41-50°F/min). The mid-point method was used to determine the $T_g$.

## 2.7. SHORT BAR SHEAR

Short bar shear (SBS) tests for evaluating the longitudinal shear strength of bars were carried out following ASTM D4475 (ASTM 2016). The span to depth ratio ranged from 3 to 6 based on the specimen length. The loading rate was 1.27 mm/min (0.05 in./min). Due to the limited number of bars of suitable length taken from the 102-mm-dia. (4 in.) concrete cores, a minimum of three test repetitions per bridge could not be achieved for all the bridges and only eight bridges could be tested for shear strength.

## 2.8. TENSILE TEST

Although even the longest witness bars from the Sierrita de la Cruz Creek Bridge were too short to test according to ASTM D7205 (ASTM 2016), they were of sufficient length to evaluate using a modified tensile test method developed in this investigation. The modified tensile strength test method entailed slicing a bar longitudinally into flat coupons that could be tested with short lengths using ASTM D3039 (ASTM 2014). The three 16-mm-dia (0.63 in.). witness bars extracted from the Sierrita de la Cruz Creek Bridge were cut into nine thin rectangular coupons utilizing a computer numerical control (CNC) wet saw with a diamond abrasive blade, as shown in Figure 2(a). The 3 × 11 × 254 mm (0.11×0.43×10 in.) (thickness × width × length) coupons were fitted with 57-

mm-long (2.24 in.) composite tabs, resulting in a gauge length of approximately 140 mm (5.5 in.). Pristine current-production bars similar in shape, size (16 mm dia.), and manufacturer to the bars extracted from the Sierrita de la Cruz Creek Bridge were obtained and tested as-is (ASTM D7205, 2016) and as flat coupons. The specific fiber and matrix materials in the current-production bars differ from those used in the bars installed in the bridge in year 2000. The tests from current-production bars enabled calculation of a ratio of full bar strength to flat coupon strength. This ratio, assumed to apply to environmentally exposed bars from year 2000 as well, was then used to estimate the full-bar strength of extracted bars based on their measured coupon strength.

Finally, the estimated full-bar strength of the extracted bars is compared to published strength data for pristine 16-mm (0.63 in.) bars installed in the bridge in year 2000. Photographs of the extracted and current-production coupons with tabs are shown in Figures 2(b) and 2(c).

All coupons were tested using a 100 kN (22.5 kips) servo-hydraulic load frame and a 50-mm (2.0 in.) extensometer for measuring strain. The full-size bars were tested in the 890 kN (200 kips) Baldwin screw-driven universal test frame and a 100-mm (4.0 in.) extensometer was used to record strain. Both tests were performed at a rate of 2 mm/min (0.08 in./min.). Young's modulus of the coupons and bars was measured by the chord method between strains of 1,000 and 3,000 με.

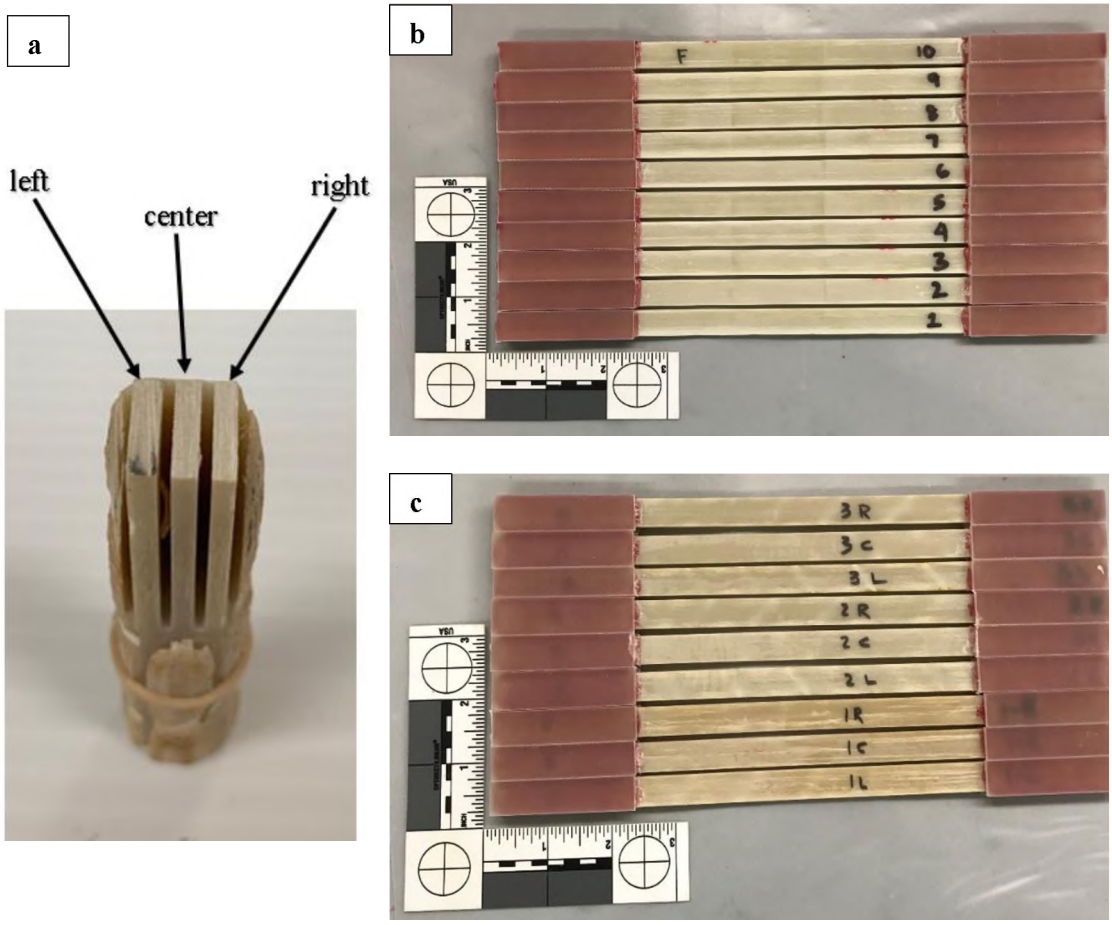


Figure 2. (a) Method of cutting flat coupons for tensile testing; (b) Current-production tensile coupons; (c) Extracted tensile coupons

## 2.9. CONSTITUENT VOLUME CONTENTS BY IMAGE ANALYSIS

Fiber, matrix, and void volume contents were measured by analyzing area fractions in polished transverse cross-sections of bars. The test is based on the assumption that all features observed on a transverse cross-section extend through the entire length of the bar (Little et al. 2012). To minimize section bias in computing void volume fractions (Ghiorse 1991; Little et al. 2012), statistics on the constituent volume contents were

obtained based on the analysis of 30 individual micrographs for each bar. The micrographs were attained at evenly spaced intervals along a radial path emanating from the center of the bar in the case of fiber content and along the full diameter in the case of void content. Due to the similarity in brightness of the glass fibers and the polymer part of the matrix, a MATLAB script was employed to collect manually-selected fiber/matrix boundaries and to use these boundaries to automatically calculate fiber area in a given micrograph. The fibers were assumed to be circular in the cross-section, and the user selected three observable points on the circumference of the fiber-matrix boundary, which defines each fiber in the micrograph. While initial attempts involving thresholding and shape-detection techniques were unsuccessful, the boundary between the fiber and matrix was readily identifiable as a thin, relatively dark circle for the vast majority of fibers. The relatively low brightness of voids allowed void area to be calculated simply based on the proportion of image pixels darker than a judiciously selected threshold. The matrix volume content, consisting of polymer and filler, was found by subtraction of the fiber and void volume percentages from 100%. Due to the time-intensive nature of this image analysis approach, only three bars from the O'Fallon Bridge were analyzed for constituent volume content.

# 3. GFRP TEST RESULTS AND DISCUSSION

## 3.1. FIBER MASS CONTENT

Table 1 shows the fiber mass contents for bars from each bridge. In all bridges except one, the fiber mass content, including resin filler particles but excluding larger sand particles and helical fiber wraps added to some bars for bond enhancement, exceeded 70%—the current requirement for GFRP bars satisfying ASTM D7957 (ASTM 2017). Bars from Roger's Creek Bridge had fiber mass content only fractionally less than the current standard—69.2%.

## 3.2. WATER ABSORPTION

Water absorption at 50°C (US units) was evaluated on bars from eight of the 11 bridges. Several observations were noted that can affect the weight of bar specimens. A loss in helical wrap was noticed when Cuyahoga Bridge specimens were soaked in water, as shown in Figure 4. For continuity in the data, the weights of such large pieces of material were recorded along with the remainder of the specimens. Smaller particles on the surface of the bars, such as sand and residual cementitious material, were also observed to fall off during conditioning, but the mass of such particles could not be tracked.

Figure 3 shows the weight change at equilibrium versus time to reach equilibrium for each specimen. The current ASTM GFRP bar specification, ASTM D7957 (ASTM 2017), stipulates a qualification limit of 1% water absorption in pristine bars as an

indication of bar durability. Bars from five of the eight bridges had equilibrium water absorption values of less than 1%, with the exceptions being those from Gills Creek Bridge (1.5%), Bettendorf Bridge (2.1%), and Cuyahoga Bridge (1.5%). The times to equilibrium in the latter three bridges were considerably over 150 days, while the others were around 80 days.

Table 2 shows the average weight change measured at 24 hours and at equilibrium as well as the average time required to reach equilibrium for each bridge. It is emphasized that the water uptake measurements are relative to the existing water content of the bars following the superficial 48 hr., 40°C (104°F) preconditioning regimen. In the cases of O'Fallon and Cuyahoga bars, the water content at the beginning of the uptake test (i.e., after preconditioning) was found to be approximately 0.36%, according to dry-out tests performed at 80°C using ASTM D5229 (ASTM, 2014). Thus, actual moisture contents in the bars at equilibrium can be expected to be approximately 0.36% more than the values listed in Table 2. While some of the extracted bars clearly have the capacity to exceed the 1% absorption limit of ASTM D7957, it should be noted that the bars evaluated in this investigation were manufactured before the existence of contemporary standards. Also, as shown in the following section, the water content of the bars after 15–20 years of service was well below 1%.

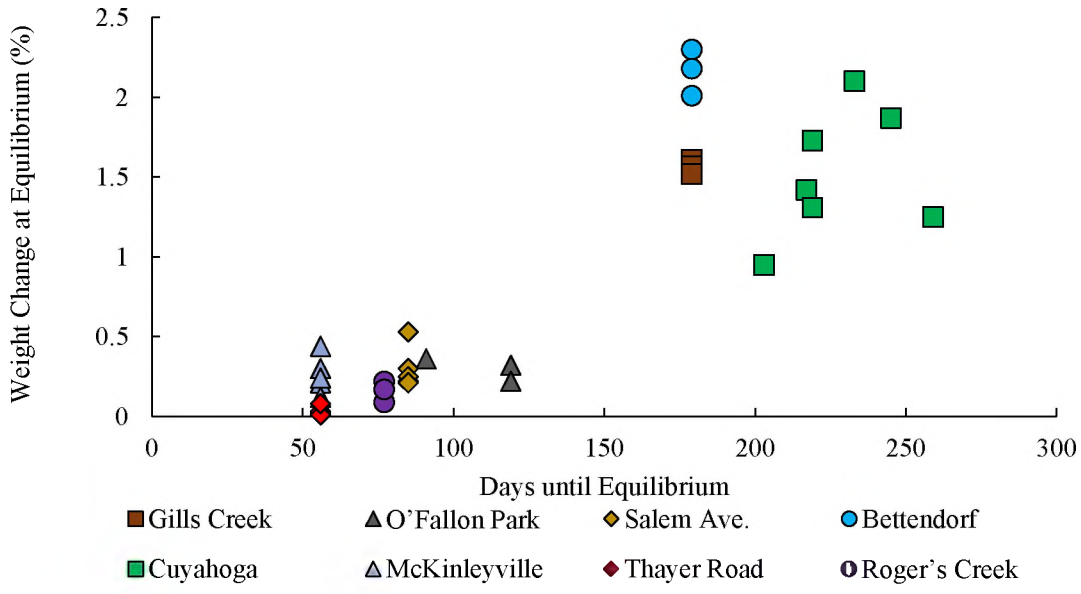


Figure 3. Equilibrium weight change and time to reach equilibrium for bars immersed in 50°C water

### 3.3. MOISTURE CONTENT

As-received (without preconditioning) moisture content was evaluated by drying out bars from two bridges, O'Fallon Park and Cuyahoga, at 80°C (176°F) (Table 3). Figure 5 shows the weight change at equilibrium versus the time required for individual specimens to reach equilibrium. All of the specimens reached equilibrium after 49 days. Weight loss was observed to be non-monotonic, possibly due to the variations in the humidity level in the laboratory. The O'Fallon Bridge bars had less as-received moisture (0.32% on average) than the Cuyahoga Bridge bars (0.44% on average).

Figure 4. Part of the helical wrap fell off of a bar from the Cuyahoga Bridge during 50° C (122° F) water absorption testing

Table 2. Results of the 50° C (122° F) water uptake tests

| Bridge | Number of Specimens | Avg. 24-hr Weight Change (%) | Avg. Weight Change at Equilibrium (%) | Avg. Days until Equilibrium |
|---|---|---|---|---|
| Gills Creek | 3 | 0.58 | 1.57 | 179 |
| O'Fallon Park | 3 | 0.01 | 0.30 | 110 |
| Salem Ave. | 5 | 0.10 | 0.30 | 85 |
| Bettendorf | 3 | 0.54 | 2.16 | 179 |
| Cuyahoga | 7 | 0. 28* | 1.52 | 228 |
| McKinleyville | 6 | 0.10 | 0.23 | 56 |
| Thayer Road | 5 | 0.02 | 0.02 | 56 |
| Roger's Creek | 3 | 0.05 | 0.16 | 77 |

*This average reflects only five specimens because two of the specimens showed erroneous results for this measurement.

For reference, both of these values are well less than 1% equilibrium value allowed by ASTM D7957 for 50°C (176°F) water immersion, although the bars were not necessarily expected to be saturated to such a high degree by field conditioning.

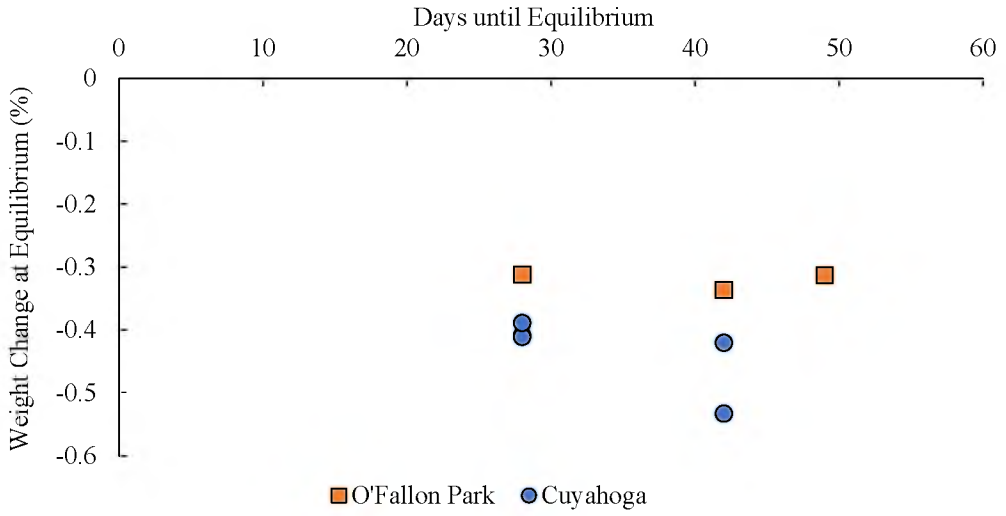


Figure 5. As-received moisture content of bars as determined by drying at 80° C (176° F), along with time required to reach equilibrium

Table 3. Results of 80° C (176° F) dry-out tests

| Bridge | Number of Specimens | Avg. 24-hr Weight Change (%) | Weight Change at Equilibrium (%) | Avg. Days until Equilibrium |
|---|---|---|---|---|
| O'Fallon Park | 3 | -0.150 | -0.320 | 40 |
| Cuyahoga | 5 | -0.218 | -0.436 | 34 |

### 3.4. SCANNING ELECTRON MICROSCOPY

SEM was performed on bars from all 11 bridges. In general, minimal evidence of environmental damage to the fibers, matrix, or fiber/matrix interface was seen. For example, in the Gill's Creek Bridge, a few matrix and interfacial cracks were seen near voids which were located near the outer radius of the bar. Moreover, the number of fibers showing signs of environmental degradation was about 192 out of 352,000 fibers

(0.05%), estimated by counting fibers with and without signs of environmental damage in one quadrant and then multiplying by four. Figure 6 shows an SEM image of a bar from the Gill's Creek Bridge. The Cuyahoga Bridge bars also displayed a small percentage of environmentally damaged fibers (Figure 7). In these quantitative analyses of environmental damage in the fibers, damage attributed to specimen preparation, such as chipped or cracked fibers having weak matrix support (e.g., located near a void), was omitted from consideration.

In bars from Roger's Creek and McKinleyville Bridges, the incidence of environmentally damaged fibers, matrix and interfaces was similar to or less than that seen in the Cuyahoga and Gills Creek bars. Figure 8 illustrates representative SEM images from Roger's Creek Bridge. Damage attributed to environmental effects was confined to regions near the outer radius of the bar.

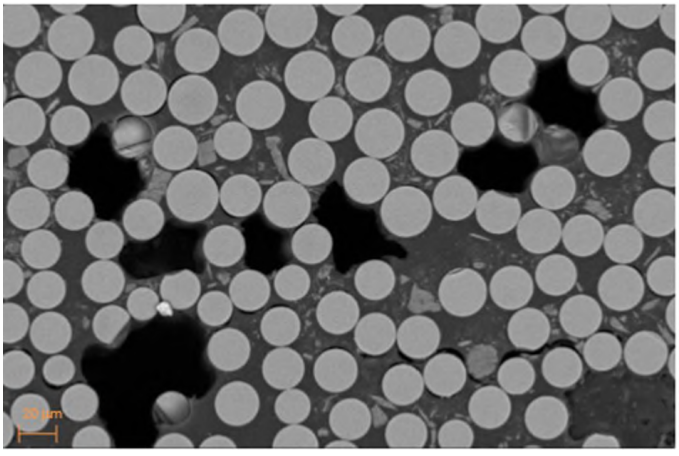


Figure 6. SEM image of a bar from Gill's Creek Bridge (Reference dimension = 20 µm)

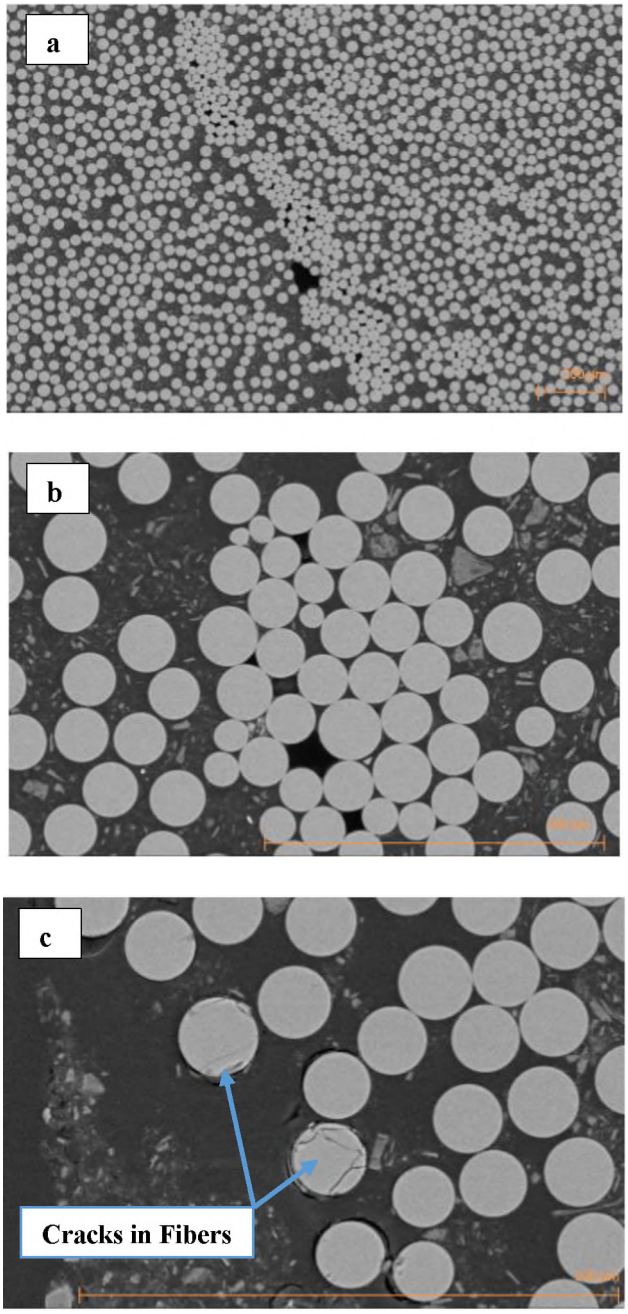


Figure 7. SEM images of a bar from the Cuyahoga Bridge: (a) ×100 magnification; (b) ×750 magnification; (c) ×1000 magnification (Reference dimension = 200 μm for all)

In the Thayer Road Bridge, fiber damage was found in some bars, but it is believed to be caused by the particular manufacturing procedure used to make the bars. While the interior region of the bar showed negligible fiber damage, numerous fibers at the outside radius appeared to be partially removed, as if they were abraded during manufacture (Figure 9).

### 3.5. ENERGY DISPERSIVE SPECTROSCOPY

Bars from all bridges were evaluated by EDS. The EDS results are presented as histograms of counts detected versus the energy level of the X-rays emitted by the surface, where the energy level depends on the element emitting the X-rays. In all bars, there were no signs of zirconium (Zr), which confirms that the fibers used to make the bars were not alkaline-resistant (AR) fibers (Kamal and Boulfiza 2011). Magnesium (Mg) was found in some bars, which indicates conventional E-glass, while those without Mg indicate acid- resistant (ECR) E-glass. In the fiber regions of all bars, the main elements were Si, Al, and Ca. Some of the bars showed Na in their analysis. Reference bars without environmental exposure would be required to discern changes in Na over time. The presence of Au in the EDS results is simply an artifact of the gold coating used to make the specimens electrically conductive for SEM. Regarding the resin, the main element, C, was found in abundance.

Representative EDS results for the Bettendorf and O'Fallon bars (Figure 10) do not show evidence of environmental attack, which would be manifested as Na, K, and Ca present in the resin. On the other hand, for the Southview Bridge (Figure 11), Na was

found in the resin but not in the fiber. Na in the resin indicates that the GFRP bar was under environmental attack, especially considering that the concrete tests showed a high pH and no signs of carbonation (Benzecry et al. 2020). Additionally, the lack of Na in the fiber confirms that the Na in the resin came from the environment rather than the fiber.

In the bar extracted from the Sierrita de la Cruz Creek Bridge, Na was found in the resin as well as the fiber (Figure 12a). EDS was also done on pristine new-generation bars similar to the bars extracted from the Sierrita de la Cruz Creek Bridge (Figure 12b). The Na emittances were similar in both tests, providing no evidence of chemical attack (leaching and/or alkali-hydrolysis) of the fibers in the bars of the Sierrita de la Cruz Creek Bridge.

### 3.6. GLASS TRANSITION TEMPERATURE

Extracted bars from all bridges had $T_g$ values between 80°C (176°F) and 115°C (239°F), as shown in Table 4. For reference, ASTM D7957 (ASTM 2017) requires a $T_g$ of no less than 100°C.

Thus, bars from several of the bridges showed $T_g$ values less than the ASTM D7957 lower limit. Without $T_g$ data from bars as produced about two decades ago, the cause for low $T_g$ values in some bars can only be conjectured in the current investigation. For example, certain types of bar could have been made with a low-$T_g$ resin system, before contemporary standards were developed. Incomplete cure would also be manifested by a $T_g$ less than the potential that is inherent in the polymer chemistry.

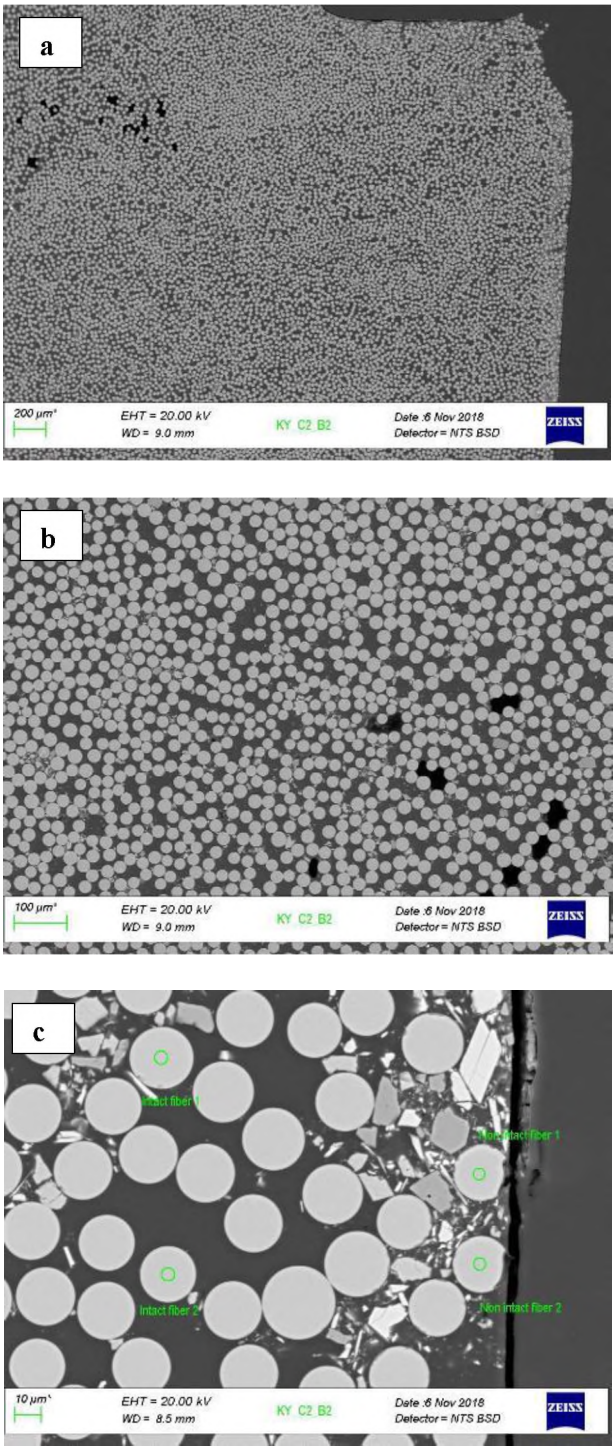


Figure 8. SEM images of a bar from the Roger's Creek Bridge: (a) ×50 magnification; (b) ×100 magnification; (c) ×800 magnification

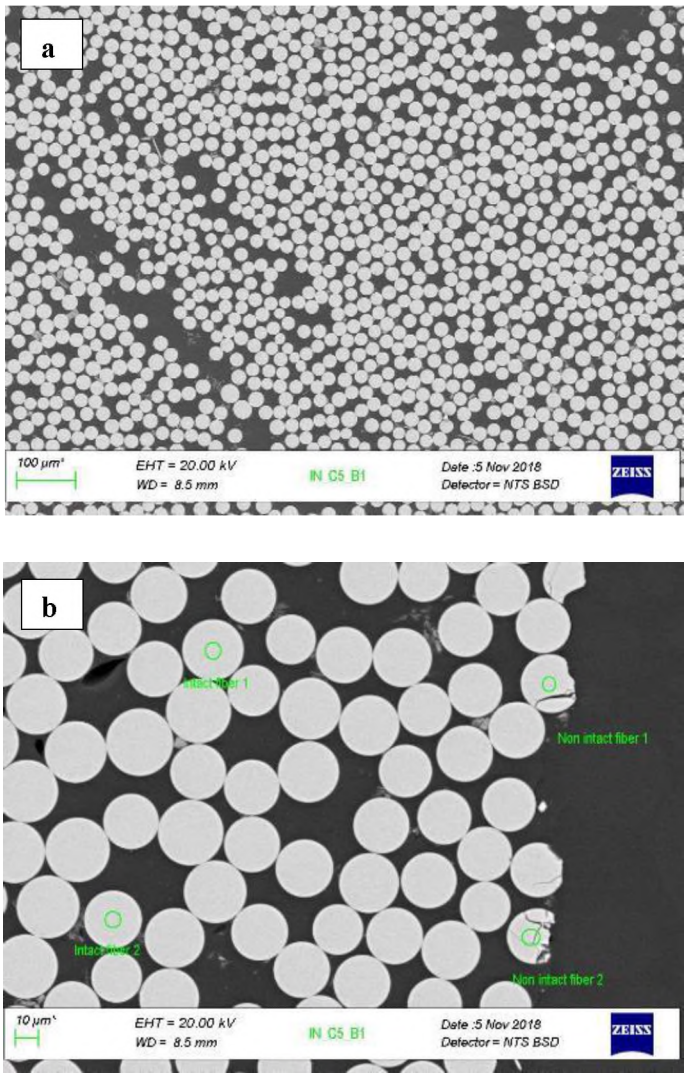


Figure 9. SEM images of a bar with manufacturing issues from the Thayer Road Bridge: (a) ×100 magnification; (b) ×800 magnification

### 3.7. SHORT BAR SHEAR

Table 5 lists the apparent shear strengths and nominal diameters of the bars tested, along with the strengths of control bars and dowel bars. The control bars refer to pristine bars tested when the bridges were built (Gooranorimi et al. 2006). Only the Cuyahoga

and Sierrita de la Cruz Creek Bridges have control bars. Dowel bars refer to smooth, round E-glass/vinyl ester rods currently manufactured by the same manufacturer that made the bars in the bridges listed in Table 5 (Owens Corning, 2018). The dowel bars also have the same diameter as the bars in the bridges. Dowel bar strengths are provided as a rough measure of comparison with SBS strengths, particularly for bridges lacking control bars.

The SBS strength of extracted bars ranged from 30 MPa (4316 psi) to 47 MPa (6809 psi). For the three bridges with control bars, it can be seen that the extracted bars retained between 72 and 92% of their initial strength. The Cuyahoga and Sierrita de la Cruz Creek (19 mm) bars, which were at the lower end of the strength retention spectrum (72 and 76%, respectively), were noted to also have uniquely low span-to-diameter ratios in relation to the 3-6 range recommended in ASTM D4475 (ASTM 2016), which may have contributed to their relatively low strengths. Multiple specimens, ideally of greater span-to-diameter ratio, would be needed to confirm this hypothesis.

In relation to the dowel bar strengths, three of the extracted bars (O'Fallon Park, Cuyahoga, and Sierrita de la Cruz Creek 19 mm) were markedly (20-40%) weaker and the remainder were within roughly ±10%. It is noteworthy that the O'Fallon Park and Cuyahoga bars also had the two lowest $T_g$ values, which together with low shear strengths could be consistent with improper curing or chemical degradation of the resin that could not be detected by the other test methods.

### 3.8. TENSILE TEST

The tensile test results for flat coupons cut from Sierrita de la Cruz Creek Bridge 16-mm witness bars indicate an ultimate strength of 622 MPa (90.2 ksi) and an elastic modulus of 47.1 GPa (6,931 ksi), as shown in Table 6. The stress strain curves for the extracted coupons were nearly linear (Figure 13), as is commonly seen in a test of a typical full-size GFRP bar. Tables 7, and 8 show the strength and moduli of current-production 16-mm bars tested as flat coupons and full bars, respectively. To calculate the correlation factor between flat coupons and full-size bars, the strength of the current-production full bars (823 MPa (119.3 ksi)) was divided by the strength of the current-production flat coupons (670 MPa (97.2 ksi)), which resulted in a conversion rate of 1.23. The 23% difference in strength of the full bars versus flat coupons can be attributed to factors including fiber damage caused by the machining. Applying the 1.23 strength conversion ratio to the extracted flat coupons provides a 765 MPa (111 ksi) estimated strength for full extracted bars. The strength and modulus of full bars manufactured and tested in year 2000 are 785 MPa (113.8 ksi) and 40.8 GPa (5,920 ksi), shown in Table 9. Therefore, the estimated strength reduction of the full bars extracted from the bridge after 17 years of service, found by comparing the 765 MPa (111 ksi) estimated extracted bar strength to the 785 MPa (113.8 ksi) published strength of bars used to construct the bridge, is 2.5%.

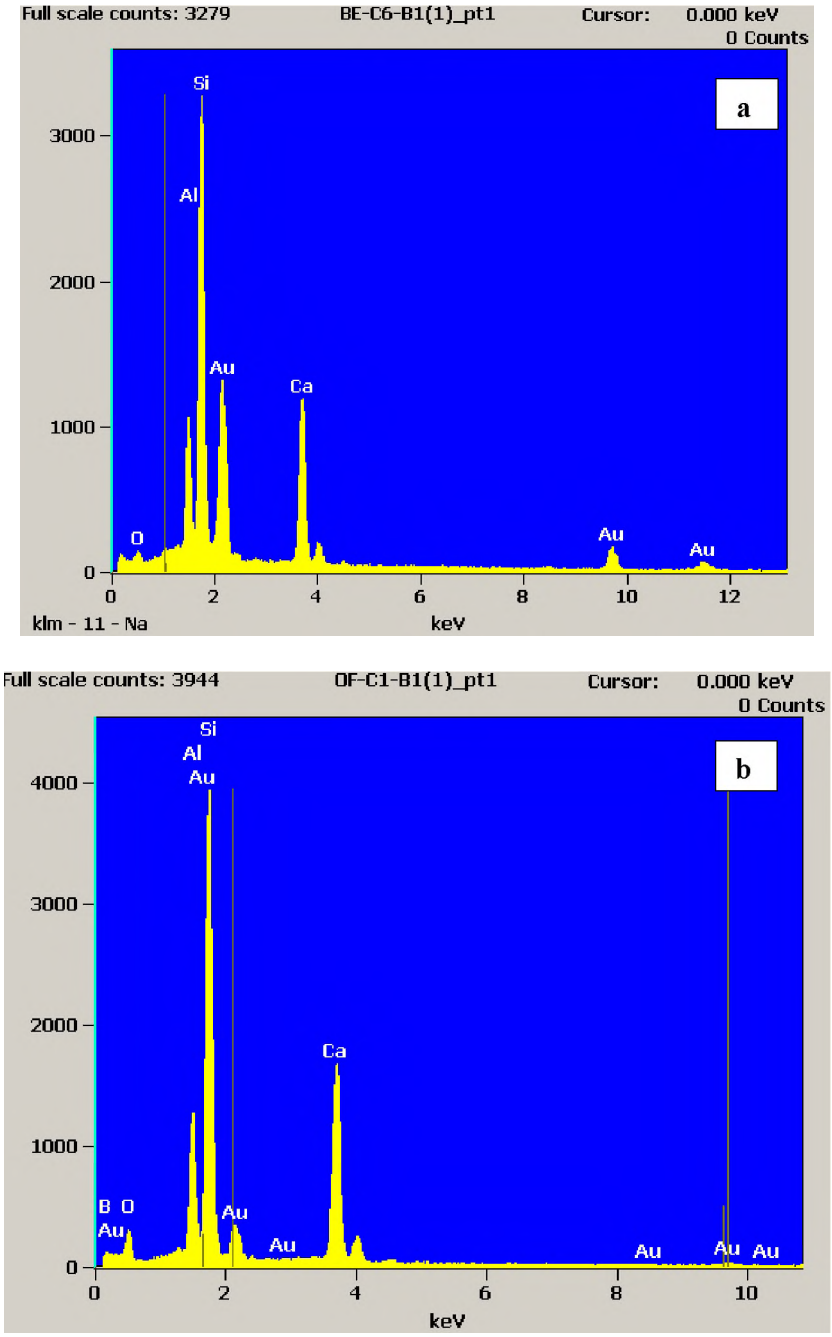


Figure 10. EDS test results for bars from (a) Bettendorf Bridge and (b) O'Fallon Bridge

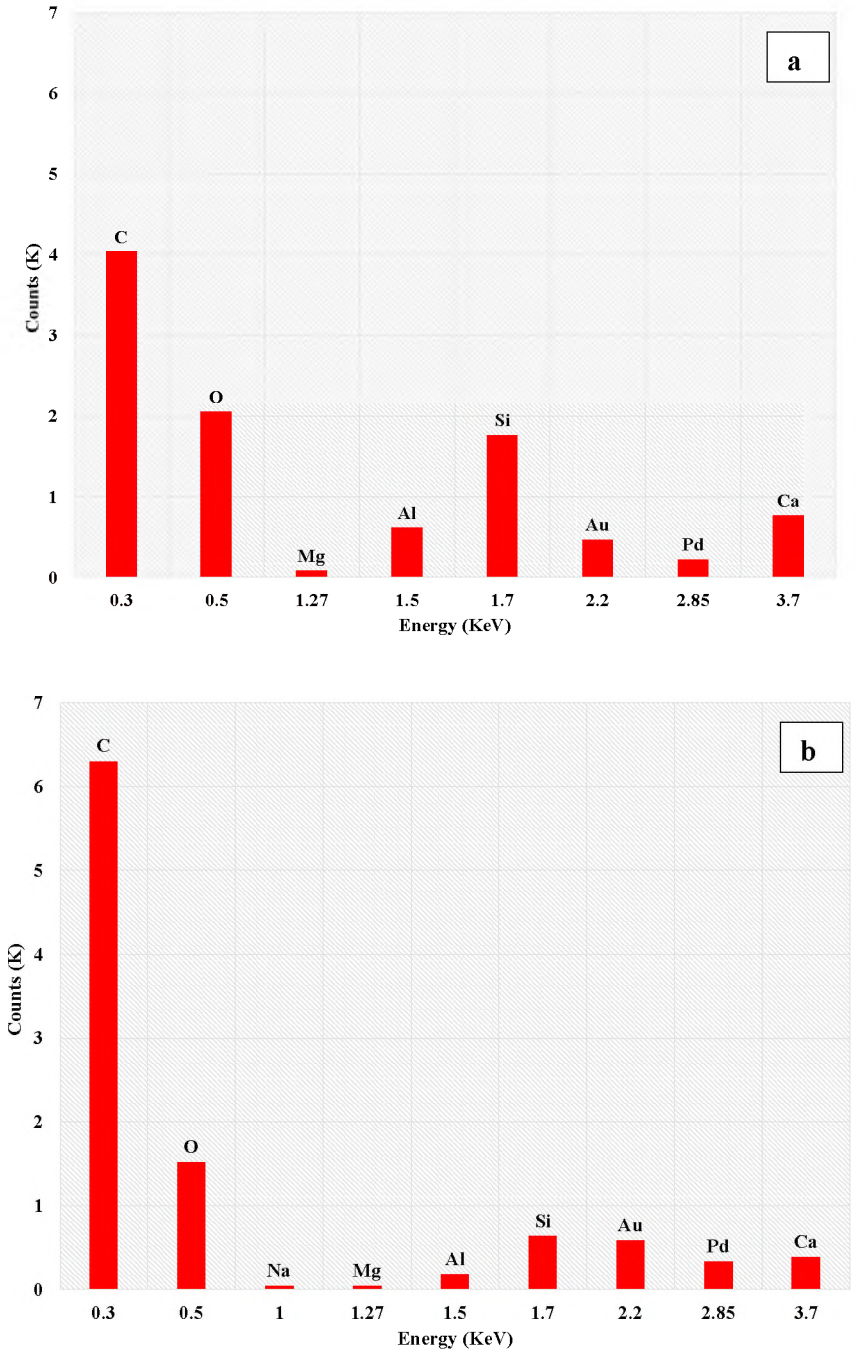


Figure 11. EDS test results for a bar from the Southview Bridge: (a) fiber and (b) resin

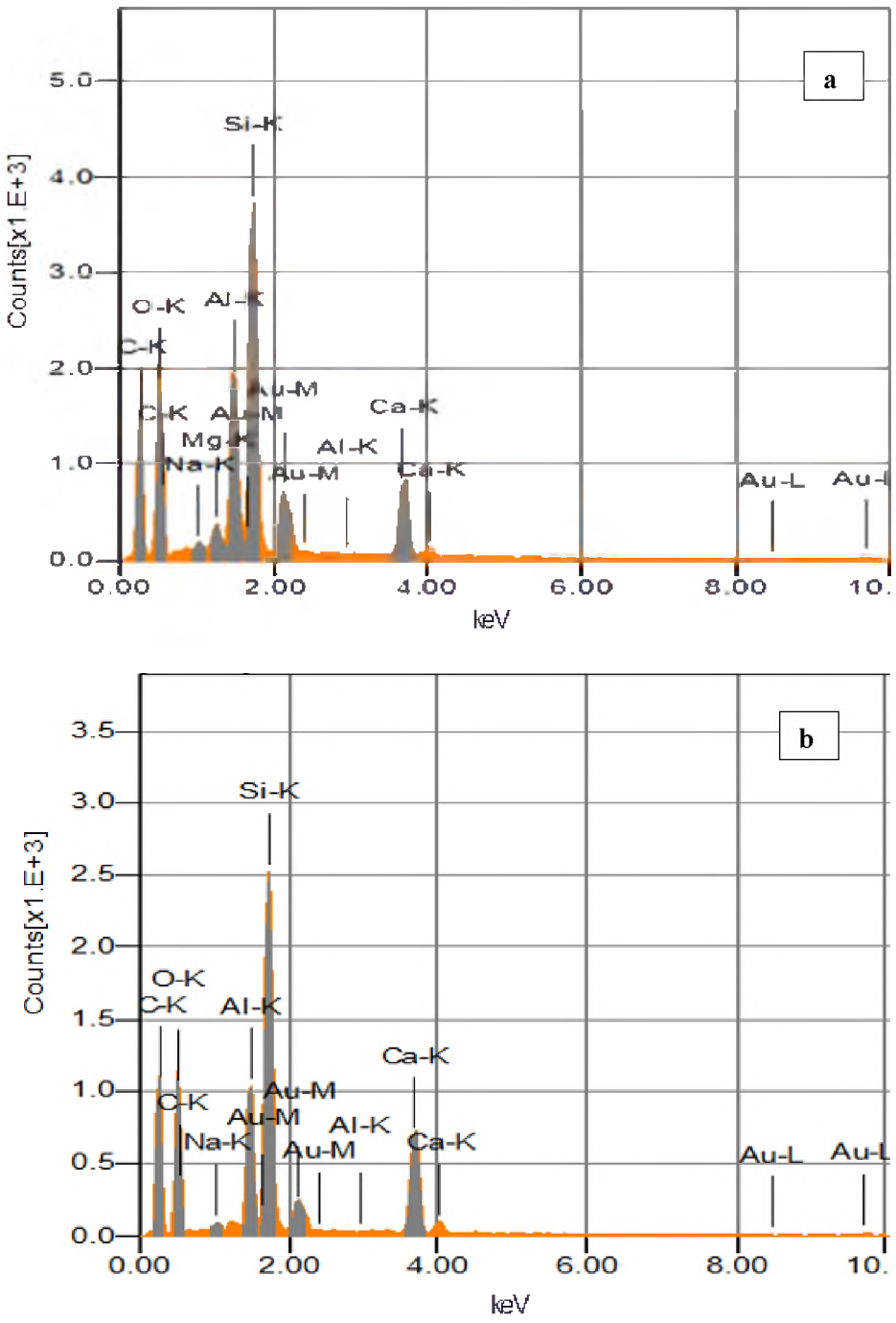


Figure 12. EDS test results for bars from the Sierrita de la Cruz Creek Bridge: (a) extracted bars; (b) pristine new-generation bars

Table 4. Average $T_g$ results for all bars

| Bridge | Average $T_g$, °F (°C) |
|---|---|
| Bettendorf | 228 (109) |
| Cuyahoga | 198 (92) |
| Gills Creek | 202 (95) |
| O'Fallon Park | 176 (80) |
| Salem Ave. | 226 (108) |
| Roger's Creek | 203 (95) |
| Sierrita de la Cruz Creek* | 239 (115) |
| Walker Box Culvert* | 233 (112) |
| Southview* | 213 (101) |
| McKinleyville** | 202 (95) |
| Thayer Road** | 189 (87) |

Notes:
*$T_g$ obtained with dynamic mechanical analysis rather than DSC.
**The lower of two transition temperature is reported.

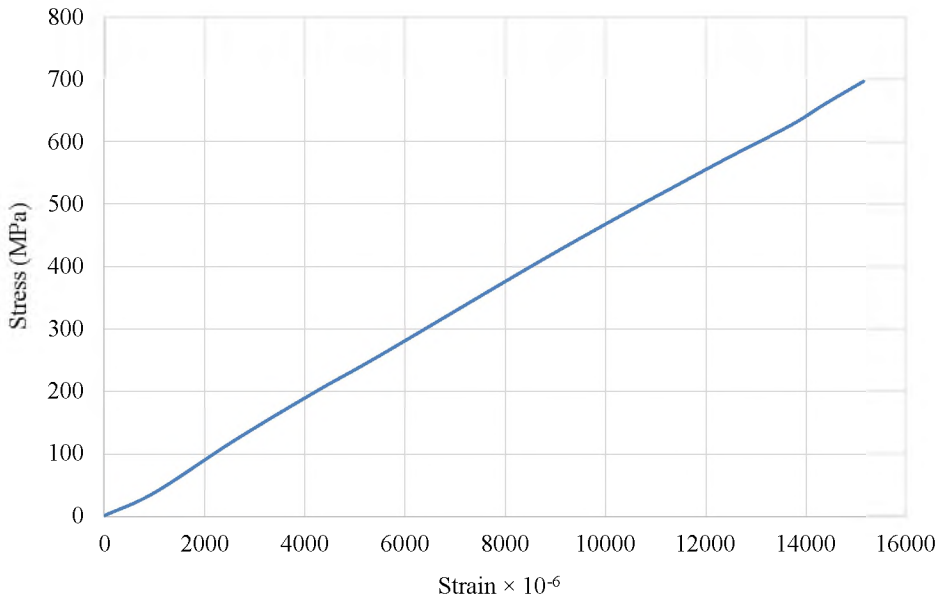


Figure 13. Tensile stress-strain curve of flat coupon 2C taken from a 16-mm bar extracted from the Sierrita de la Cruz Creek Bridge

Table 5. Average apparent shear strength from short beam shear tests

| Bridge | Nominal Diameter, mm (in.) | Extracted Bar Strength, MPa (psi) | Control Bar Strength, MPa (psi) | Dowel Strength, MPa (psi)‡ |
|---|---|---|---|---|
| O'Fallon Park | 22 (0.88) | 42 (6115) | - | 53 (7687) |
| Salem Ave. | 19 (0.75) | 45 (6459) | - | 47 (6800) |
| Cuyahoga | 19 (0.75) | 30 (4316) | 41† (5956) | 47 (6800) |
| McKinleyville | 10 (0.38) | 36 (5214) | - | 36 (5220) |
| Thayer Road | 16 (0.63) | 47 (6809) | - | 42 (6092) |
| Sierrita de la Cruz Creek | 16 (0.63) | 42 (6047) | 45* (6540) | 42 (6092) |
| Sierrita de la Cruz Creek | 19 (0.75) | 37 (5361) | 49* (7040) | 47 (6800) |
| Southview | 19 (0.75) | 44 (6340) | - | 47 (6800) |
| Southview | 13 (0.50) | 38 (5558) | - | 38 (5511) |
| Walker | 6.4 (0.25) | 33 (4828) | - | 35 (5000) |

†Measured by bar manufacturer in year 2000.
*Measured by bar manufacturer in year 2000, as reported in Gooranorimi et al. (2006)
‡Dowel bars currently produced by same manufacturer that made the bars installed in the bridges (Owens Corning, 2018).

It is noted that the elastic modulus of the extracted bars was around 20% higher than the original ones. This apparent increase over time is due to the unjustified low elastic modulus obtained in the year 2000 test. First, only one value is provided and second, and most important, this value is significantly lower than the average value (48.6 GPa) obtained by the manufacturer in those years during the routine Quality Control tests (D. Gremel - Private Communications 2017). If the degradation rate of the bars is hypothesized to be linear with time, tensile strength would be reduced 15% over a period of 100 years. On the other hand, considering the evidence that creep rupture strength of

GFRP varies with log-time rather than time itself (Green wood 2002); (Bakis et al. 2005), the 100-year strength reduction would be 3.6%. In any case, it should be kept in mind that the rate of change strength over time can be expected to vary depending on the sustained stress carried by the bars, the diameter of the bars, the materials used to manufacture the bars, and local environmental details such as temperature, chemical exposure, and condition of the concrete (Nkurunziza et al. 2002). In the case of the Sierrita de la Cruz Creek Bridge, the bars were made of E-glass fiber and vinyl-ester resin and had 15.9 mm of concrete cover. In addition, the concrete near the bars had a high pH of 11.5, although carbonation was suspected to have reached the level of the bars (Benzecry et al. 2020).

## 3.9. CONSTITUENT VOLUME CONTENTS BY IMAGE ANALYSIS

Table 10 shows the fiber, matrix, and void volume contents of O'Fallon bars based on image analysis. The fiber volume contents range between 52.3 and 53.5% while the void volume contents range from 0.5to 0.7%. Void contents less than 1% are generally considered to represent well-consolidated composites.

Table 6. Tensile test results for flat coupons extracted from the 16-mm bars in the Sierrita de la Cruz Creek Bridge.

| Specimen ID | Ult. Strength, MPa (ksi) | Elastic Modulus, GPa (ksi) |
|---|---|---|
| 1L | N/A | N/A |
| 2L | 625 (90.7) | 47.8 (6926) |
| 3L | 513 (74.4) | N/A |
| 1R | 660 (95.7) | N/A |
| 2R | 601 (87.1) | 49.7 (7214) |
| 3R | 560 (81.2) | 44.7 (6489) |
| 1C | 642 (93.1) | 44.8 (6498) |
| 2C | 691(100.2) | 48.5 (7036) |
| 3C | 686 (99.4) | N/A |
| **average** | **622 (90.2)** | **47.1 (6831)** |
| **std. deviation** | **62 (9.0)** | **2.2 (319)** |

Table 7. Tensile test results for flat coupons from pristine current-production 16-mm. bars similar to those extracted from the Sierrita de la Cruz Creek Bridge (same manufacturer)

| Specimen ID | Ult. Strength, MPa (ksi) | Elastic Modulus, GPa (ksi) |
|---|---|---|
| 1F | 656 (95.2) | 45.3 (6575) |
| 2F | 635 (92.1) | N/A |
| 3F | 608 (88.1) | 43.3 (6287) |
| 4F | 709 (102.7) | 44.5 (6456) |
| 5F | 787 (114.1) | 43.9 (6363) |
| 6F | 618 (89.6) | 45.8 (6637) |
| 7F | 646 (93.7) | 43.3 (6287) |
| 8F | 675 (97.9) | 44.8 (6493) |
| 9F | 689 (99.9) | 45.3 (6577) |
| 10F | 678 (98.3) | 43.3 (6278) |
| **average** | **670 (97.2)** | **44.4 (6439)** |
| **std. deviation** | **52 (7.5)** | **1.0 (140)** |

Table 8. Tensile test results for pristine current-production 16-mm bars similar to bars extracted from the Sierrita de la Cruz Creek Bridge (same manufacturer). The nominal bar area used in the calculations is 0.31 $in^2$ (200 $mm^2$).

| Specimen ID | Ult. Strength, MPa (ksi) | Elastic Modulus, GPa (ksi) |
|---|---|---|
| 1 | 830 (120.4) | 49.7 (7215) |
| 2 | 845 (122.6) | 51.7 (7490) |
| 3 | 792 (114.9) | 51.6 (7476) |
| 4 | 829 (120.2) | 50.8 (7367) |
| 5 | 849 (123.2) | 51.4 (7451) |
| 6 | 784 (113.8) | 51.6 (7488) |
| 7 | 834 (120.9) | N/A |
| 8 | 828 (120.0) | 50.4 (7302) |
| 9 | 813 (118.0) | 52.5 (7614) |
| 10 | 822 (119.3) | 52.8 (7658) |
| **Average** | **823 (119.3)** | **51.4 (7451)** |
| **Std. Deviation** | **21 (3.0)** | **1.0 (140)** |

Table 9. Tensile test results for pristine 16-mm bars identical to those in the Sierrita de la Cruz Creek Bridge, tested in year 2000. The nominal bar area used in the calculations is 0.31 $in^2$ (200 $mm^2$).

| Specimen ID | Ult. Strength, MPa (ksi) | Elastic Modulus, GPa (ksi)* |
|---|---|---|
| 1 | 801 (116.2) | |
| 2 | 843 (122.3) | |
| 3 | 735 (106.6) | |
| 4 | 760 (110.3) | |
| **Average** | **785 (113.8)** | **40.8 (5920)** |
| **Std. Deviation** | **48 (6.9)** | |

*Data from Phelan et al. (2003).

Table 10. Bar constituent contents, in percent by volume, according to image analysis (mean +/- standard deviation)

| Specimen ID | Fiber Volume Content (%) | Matrix Volume Content (%) | Void Volume Content (%) |
|---|---|---|---|
| CO_C2B_B2 | 53.3±6.6 | 46.1±6.8 | 0.5±0.8 |
| CO_C3_B2 | 52.3±5.3 | 47.0±5.1 | 0.7±0.6 |
| CO_C5_B2 | 53.5±9.6 | 45.9±9.7 | 0.6±0.9 |

# 4. CONCLUSIONS AND RECOMMENDATIONS

To help overcome barriers to the deployment of GFRP bars in the construction industry, an extensive investigation of the durability of GFRP reinforcement bars extracted from bridges built 15-20 years ago was undertaken. Several mechanical and physical tests were conducted on these bars. In addition to the bar tests, concrete tests were performed to evaluate the surrounding environment of those bars (Benzecry et al. 2020). Overall, the test results suggest that GFRP bars can be considered a promising replacement for steel reinforcement in bridge decks subjected to de-icing salts. The following list summarizes the outcomes of the individual tests on the bars and provides recommendations for future investigations.

1. **Fiber mass content:** Burn off tests of bars from all 11 bridges determined that the fiber mass content of the bars, which includes filler particles as allowed in ASTM D7957 (ASTM 2017), met or exceeded the 70% requirement of ASTM D7957 (ASTM 2017) with only one exception. The single exception was 69.2%. It is recommended that improved experimental procedures be developed for accounting for residual filler stuck to the fibers.

2. **Water absorption:** Water uptake to equilibrium at 50°C (122°F), relative to a superficially dried initial condition, was less than 1% in bars from five of the eight tested bridges and between 1.5 and 2.1% for the other three. While some bars exceeded the contemporary 1% limit for bar qualification in ASTM D7957 (ASTM 2017), it should be kept in mind that these bars were manufactured before any bar material standards existed. Additionally, it is recommended that methods for quantifying moisture uptake be developed to overcome difficulties caused by the water-induced loss of surface materials applied to the bars for bond enhancement, such as sand particles.
3. **Moisture content:** Based on dry-out tests, moisture content in as-received bars from two bridges ranged between 0.32 and 0.44%. While the as-received moisture content of the bars was not expected to be saturated due to field exposure, the measured moisture contents are noted to be well below the 1% equilibrium value stipulated in ASTM D7957 (ASTM 2017) as a limit for durable GFRP bars.
4. **Scanning electron microscopy:** A minimal amount of micro-cracking was observed in the matrix and fibers of the bars from all 11 bridges. Some of the observed damage was attributed to specimen polishing, while other damage was attributed to environmental degradation due to its concentration near the outer radius of the bars.
5. **Energy dispersive spectroscopy:** Zirconium (Zr) was not seen in the fibers of bars in any of the 11 bridges, which indicates that the bars were not alkali-resistant. No chemical evidence of leaching of fiber material into the matrix was

seen. In one bridge, sodium found in the matrix of the bar was attributed to ingress from the environment because it was not found in the fibers of the same bar. The availability of EDS results on similar bars tested at the time of installation would have enabled more certain evaluations in changes of atomic species over the service life.

6. **Glass transition temperature:** Extracted bars from all bridges had $T_g$ values between 80 and 115°C (US units), with roughly half above the 100°C limit stipulated in ASTM D7957 and half below that limit. Data on $T_g$ at the time of installation of the bars would be required to determine if the $T_g$ decreased due to service conditions or if it was low from the outset due to resin choice or incomplete cure.
7. **Short bar shear:** The SBS strength of bars extracted from eight bridges ranged from 30 to 47 MPa (4,316 to 6,809 psi), which implies a strength retention of 72-92% in the three cases where identical bars were tested at the time of bridge construction. Bars at the weaker end of the spectrum were noted to be at the shorter end of the standardized span-to-diameter ratio limit.
8. **Tensile test:** Based on a special method developed for evaluating the strength of flat tensile coupons extracted from bars and relating the flat coupon strength to the strength of full-size bars, it is concluded that extracted bars from one bridge had a reduction in tensile strength of 2.5% after 17 years of service. Extrapolating this result to 100 years, the predicted tensile strength would be reduced by 15% if the extrapolation was linear in time and 3.6% if it was linear in log-time. In the

future, additional tensile test data from extracted bars should be obtained to improve our confidence in these conclusions.

9. **Constituent volume contents by image analysis:** Image analysis has certain advantages over burn-off testing in that it provides a measure of void volume content as well as fiber volume content uncontaminated by filler material. Bar specimens from one bridge had void volume contents between 0.5 and 0.7% and fiber volume contents between 52.3 and 53.5%.

## ACKNOWLEDGMENTS

The authors gratefully acknowledge support from the American Concrete Institute's Strategic Development Council (SDC), the ReCAST Tier 1 University Transportation Center at the Missouri University of Science and Technology, The United States Department of Education GAANN Program, and NSF I/UCRC CICI (Grant # NSF-1916342). Deeply appreciated is also technical assistance from staff at Owens Corning (Mr. Ryan Koch and Mrs. Mala Nagarajan), University of Miami (Ms. Janna Brown and Mr. Jorge Alvarez), Missouri S&T (Dr. Clarissa Wisner and Mr. Eric Bohannan), and Pennsylvania State University (Mr. Jeffrey Kim and Mr. Jinhoo Kim. The opinions expressed in this material are those of the authors and do not necessarily reflect the views of sponsoring agencies.

# REFERENCES

ACI 440.1R. (2015). "Guide for the Design and Construction of Structural Concrete Reinforced with Fiber-Reinforced Polymer Bars." *ACI*.

Al-salloum, Y. A., El-gamal, S., Almusallam, T. H., Alsayed, S. H., and Aqel, M. (2013). "Composites : Part B Effect of harsh environmental conditions on the tensile properties of GFRP bars." *Composites Part B*, Elsevier Ltd, 45(1), 835–844.

ASTM-D3039. (2014). "Astm D3039/D3039M." *Annual Book of ASTM Standards*, 1–13.

ASTM-D4475. (2016). "Standard Test Method for Apparent Horizontal Shear Strength of Pultruded Reinforced Plastic Rods By the Short-Beam Method 1." *ASTM Standard*, 14(Reapproved 2008), 3–5.

ASTM-D5227. (2014). "Water Absorption of Plastics 1." *ASTM*, 98(Reapproved 2010), 25–28.

ASTM-D5229. (2010). "ASTM-D5229 Standard Test Method for Moisture Absorption Properties and Equilibrium Conditioning of Polymer Matrix Composite Materials." *Annual Book of ASTM Standards*, 92(Reapproved), 1–13.

ASTM-D570. (2017). "Water Absorption of Plastics 1." *ASTM Standards*, 98(Reapproved 2010), 25–28.

ASTM-D7205. (2011). "Standard Test Method for Tensile Properties of Fiber Reinforced Polymer Matrix." *ASTM*, i(Reapproved 2011), 1–13.

ASTM-D7957. (2017). "ASTM D7957 - Standard Specification for Solid Round Glass Fiber Reinforced Polymer Bars for Concrete Reinforcement." *ASTM*.

ASTM-E1356. (2014). "ASTM E1356-08 Standard Test Method for Assignment of the Glass Transition Temperatures by Differential Scanning Calorimetry." *ASTM International*, 08(Reapproved), 1–4.

Becker, H., and Locascio, L. E. (2002). "Polymer microfluidic devices." *Talanta*, 56(2), 267–287.

Benmokrane, B., Nazair, C., Loranger, M. A., and Manalo, A. (2018). "Field Durability Study of Vinyl-Ester-Based GFRP Rebars in Concrete Bridge Barriers." *Journal of Bridge Engineering*, 23(12), 1–13.

Benmokrane, B., Wang, P., Ton-That, T. M., Rahman, H., and Robert, J. F. (2002). "Durability of glass fiber-reinforced polymer reinforcing bars in concrete environment." *Journal of Composites for Construction*, 6(3), 143–153.

Benzecry, V., Al-Khafaji, A. F., Haluza, R. T., Bakis, C. E., Myers, J. J., and Nanni, A. (2020). "Durability Assessment of 15-20 Years Old GFRP Bars Extracted from Bridges in the USA: Part I – Selected Bridges, Bar Extraction, and Concrete Assessment." *ASCE J. Compos. Constr.*

C.E. Bakis R.A. Schaut, and C.G. Pantano, T. E. B. (2005). "Tensile Strength of GFRP Bars Under Sustained Loading in Concrete Beams." *ACI Symposium Publication*, 230, 1429–1446.

Diamond, S. (1981). "Effects of two Danish flyashes on alkali contents ofpore solutions of cement fly ash pastes." *Cement and Concrete Research*, 11, 383–394.

Ghiorse, S. R. (1991). *A Comparison of Void Measurement Methods for Carbon/Epoxy Composites*. Watertown, MA, USA.

Gooranorimi, O., Myers, J., and Nanni, A. (2017). "GFRP Reinforcements in Box Culvert Bridge: A Case Study After Two Decades of Service BT - GFRP Reinforcements in Box Culvert Bridge: A Case Study After Two Decades of Service." ASTM.

Green wood, M. (2002). "Creep-rupture testing to predict long-term performance, durability of fiber reinforced polymer (FRP) composites for construction." *2nd International Conference Durability of Fiber Reinforced Polymer for Construction (CDCC'02)*, Montreal, Quebec, 203–212.

Gremel, D. (2017). "Private Communications." *Hughes Brother*, Seaward, Nebraska.

Kamal, A. S. M., and Boulfiza, M. (2011). "Durability of GFRP rebars in simulated concrete solutions under accelerated aging conditions." *Journal of Composites for Construction*, 15(4), 473–481.

Khatibmasjedi, M., Ramanathan, Sivakumar Suraneni, P., and Nanni, A. (2020). "Durability of Commercially Available GFRP Reinforcement in Seawater-Mixed Concrete under Accelerated Aging Conditions." 24(4), 1–10.

Koch, G., Varney, J., Thopson, N., Moghissi, O., Gould, M., and Payer, J. (2016). "International Measures of Prevention , Application , and Economics of Corrosion Technologies Study." *NACE International*, 1–216.

Little, J. E., Yuan, X., A., and Jones, M. I. (2012). "Characterisation of Voids in Fibre Reinforced Composite Materials." *NDT&E Intl.*, 122–127.

Materials, E. I. (2010). "Standard Guide for Identification of Fiber-Reinforced Polymer-Matrix Composite Materials in Databases 1." *Order A Journal On The Theory Of Ordered Sets And Its Applications*, 00(Reapproved 2005), 1–15.

Micelli, F., and Nanni, A. (2004). "Durability of FRP rods for concrete structures." *Construction and Building Materials*, 18(7), 491–503.

Mufti, A., Onofrei, M., Benmokrane, B., Banthia, N., Boulfiza, M., Newhook, J., Bakht, B., Tadros, G., and Brett, P. (2007). "Durability of GFRP reinforced concrete in field structures." *Proceedings of the 7th International Symposium on Fiber Reinforced Polymer Reinforcement for Concrete Structures - FRPRCS-7*, 889–895.

Murphy, K., Zhang, S., and Karbhari, V. M. (1999). "Effect of concretebased alkaline solutions on short term response of composites." *44th. SAMPE Symposium and Exhibition, L. J. Cohen, J. L. Bauer,and W. E. Davis, eds., Society for the Advancement of Material andProcess Engineering*, Long Beach, CA, 2222–2230.

Nanni, A., De Luca, A., and Zadeh, H. (2014). *Reinforced Concrete with FRP Bars*. CRC Press.

Nkurunziza, G., Debaiky, A., Cousin, P., and Benmokrane, B. (2005). "Durability of GFRP Bars: A Critical Review of the Literature." *Progress in Structural Engineering and Materials*, 7(4), 194–209.

Nkurunziza, G., Masmoudi, R., and Benmokrane, B. (2002). "Effect of sustained tensile stress and temperature on residual strength of GFRP composites." *2nd International Conference Durability of Fiber Reinforced Polymer for Construction (CDCC'02)*, Montreal, Quebec, 347–358.

Owens Corning. (2018). *Aslan 600 FIBERGLASS*.

Taylor, H. (1987). "A method for predicting alkali ion concentra-tion in cement pore water solutions." *Advance Cement Research*, 1(1), 5–16.

Trejo, D., Gardoni, P., and Kim, J. J. (2011). "Long-Term Performance of Glass Fiber-Reinforced Polymer Reinforcement Embedded in Concrete." *ACI Materials Journal*, American Concrete Institute, Farmington Hills, 108(6), 605–613.

Wang, Z., Zhao, X., Xian, G., Wu, G., Raman, R. K. S., and Al-saadi, S. (2017). "Long-term durability of basalt- and glass-fibre reinforced polymer ( BFRP / GFRP ) bars in seawater and sea sand concrete environment." *Construction and Building Materials*, Elsevier Ltd, 139, 467–489.

Yang, W.-R., Xiong-Jun He, ;, Dai, ; Li, Zhao, X., and Shen, F. (2016). "Fracture Performance of GFRP Bars Embedded in Concrete Beams with Cracks in an Alkaline Environment." *ASCE J. Compos. Constr.*, 20(6).

# SECTION

# 2. SUMMARY, CONCLUSIONS, AND RECOMMENDATIONS

## 2.1. SUMMARY

The first purpose of this research was to evaluate the durability performance of GFRP bars extracted from several bridges in the United States after being in service for almost two decades. Several tests were conducted on the extracted GFRP bars and the surrounding concrete to make the assessment.

The second purpose of this research was to assess the bond performance of GFRP bar installed in high-volume fly ash concrete. In this investigation, two levels of fly ash class- C were used, 50% and 70%. In addition, two bar diameters and two embedment length were implemented to make the bond-slip assessment. The GFRP bars used in the test were also examined microstructurally and chemically before and after pullout tests were carried out to see if the fly ash affected the bars, even though the time was limited solely to the curing time of specimens.

This section contains conclusions from the studies.

## 2.2. CONCLUSIONS

The following section summarizes the conclusions from both the durability and bond studies of GFRP bars.

**2.2.1. Durability of GFRP Bars from Two Bridges.** Glass fiber-reinforced polymer (GFRP) bar is an effective alternative to replace conventional steel

reinforcement in concrete and hence avoid corrosions issues. However, the on-site long-term performance has not been investigated enough. Therefore, a thorough durability study was carried out on bars extracted from bridges across the United States. Several tests were conducted on the bars and surrounding concrete to make the evaluation.

- The chlorides content tests yielded insignificant level of chlorides in concrete. Carbonation was found in one bridge and pH levels in that bridge was within the normal 11 to 12 (normal range for such concrete). While on the other bridge, pH was found a little high for such concrete (around 13).
- SEM test did not show any obvious sings of microstructural degradations. FTIR test showed that OH group in one of the two bridges was higher than the normal range (the same bridge with high pH of concrete). In EDS test, signs for alkalis hydrolysis attack was found only in one bridges of the two bridges examined.
- Glass transition temperature (Tg) of both bridges was less than those resulted from control bars. The reduction in Tg could be due to the hygrothermal environment that surrounded the bridges. Fiber content tests of both bridges showed that the fiber percentages were above the standard limits (ASTM D7957) for both bridges (more than 70%).

#### 2.2.2. Bond-Slip of GFRP Bar Embedded in High-Volume Fly Ash Concrete.

A pullout test was conducted to assess the bond performance between high-volume fly ash concrete and GFRP bars. GFRP bar is a solid candidate to replace conventional steel reinforcement owing to its noncorrosive and high-strength-to-weight ratio features. High-volume fly ash is considered a type of eco-friendly concrete as it

lowers the use of Portland cement and thus lowers the emissions of $CO_2$. In addition, fly ash reduces the alkalis of concrete and that can be considered a great advantage when GFRP bars are used as reinforcement because they are sensitive (easily affected) to alkalis. The following was found form the study:

- GFRP bars showed less peak bond strength. All the specimens failed in slippage with no splitting failure cases. It was found that the higher the bar diameter was, the higher the bond strength. In addition, the higher the compressive strength, the higher the bond was found to be. Steel bar's deformation was the reason behind the higher bond strength, because GFRP bars were sand-coated only with no deformations. However, the bar deformations were the reason behind the sharp post-peak bond strength drop. While, in GFRP bars, a steady loss of bond strength was noticed after peak bond strength was reached. The sand-coating of the GFRP bar was the main reason behind the steady loss of the bond strength. Conventional concrete (CC) had a higher bond strength than 50% and 70% HVFA concrete owing to the higher compressive strength of CC.
- The microstructural and chemical tests conducted on the GFRP bar after pullout tests were carried out showed that there were no obvious sings of microstructural or chemical deteriorations.
- Statistical-based models were built using multiple regression analysis to predict the bond strength, peak toughness, and post-peak toughness. The predictive models of bond strength, toughness, and peak-toughness were in match with the experimental results. In addition, compressive strength of concrete and bar

diameter to embedment length ratio were the most influential factors on bond and toughness.

- Comparisons with former studies yielded that compressive strength and bar diameter increase the bond strength while the embedment length lowers it. In addition, the hypothesis test results conducted between current and former bond equations exhibited non-significance.

**2.2.3. Durability of GFRP Bars from Eleven Bridges.** In order to increase the acceptability of GFRP bars as an effective construction material in the industry, a massive durability study was carried on GFRP bars extracted from 11 bridges across the United States with on-site service life of around two decades. The following is the conclusion:

- Fiber content tests results (also called burn-off) showed that the bars met or exceeded the 70% requirement of ASTM D7957. Only one bridge yielded a result less than 70% (specifically 69.2%). In water absorption examination, the water absorption to equilibrium was less than 1% in bars from 8 bridges, and it was between 1.5% to 2.1% for the other 3 bridges. In moisture content test, the results were between 0.32% and 0.44%. The as-received moisture content of the bars was not expected to be saturated owing to on-site exposure. However, the measured moisture contents were seen to be below the 1% equilibrium value.
- In SEM test, a minimal amount of micro-cracking was observed in the matrix and fibers of the bars from all 11 bridges. Some of he observed deteriorations were attributed to the improper sample preparations. In EDS test, Zr was not seen in the

fibers of all bridges and that indicates that the bars were not alkali-resistant. Also, no chemical sings of leaching of fiber material into the matrix was seen. In one bridge, Na was found in the resin of the bar and was attributed to the ingress from the environment because it was not found in the fiber. In $T_g$ test, $T_g$ was found to be between $80^o$ C and $115^o$ C. The short bar shear (SBS) test results were between 30 to 47 MPa (4316 to 6809 psi), which implied strength retention of 72% to 92% in the 3 cases where identical bars were tested at the time of bridge construction. In tensile test, based on a special way developed to assess the strength of flat tensile coupons taken out from bars and relating the flat coupon strength to the strength of full-size bars, it was concluded that extracted bars from one bridge had a tensile strength reduction of 2.5% after 17 years of service. Lastly, in the constituent volume contents by image analysis, image analyses had some advantages over fiber content test (burn-off), as it gives a measure of void volume content as well fiber volume content undistorted.

# APPENDIX A

# DURABILITY ASSESSMENT OF 15-20 YEARS OLD GFRP BARS EXTRACTED FROM BRIDGES IN THE USA: PART I – SELECTED BRIDGES, BAR EXTRACTION, AND CONCRETE ASSESSMENT

## ABSTRACT

Glass fiber-reinforced polymer (GFRP) bars have been used in concrete structures as an alternative to steel bars due to their non-corrosive behavior. However, due to the lack of full understanding of long-term performance, their use as internal reinforcement is still limited. To evaluate the durability of in-service GFRP bars under natural exposure, a collaborative project including four organizations investigated the conditions of GFRP bars and their surrounding concrete from bridges with 15 to 20 years of service. The aim of Part I of a two-paper series is to describe the bridge structures, methods of extraction and the results of concrete testing, while Part II focuses on GFRP bar performance.

The extracted bars were tested for physical, mechanical and chemical properties and the surrounding concrete was evaluated for chloride penetration, pH, and carbonation depth at the level of reinforcement. Results showed that carbonation and chloride may have reached the depth of the GFRP bars. This paper discusses the process of extraction of the bars, including the location and type of the selected bridges, and the concrete tests performed in terms of procedure, results, and observations.

## 1. INTRODUCTION

The use of fiber-reinforced polymer (FRP) bars in civil infrastructure has emerged due to their high strength, corrosion resistance, and low density of the material (Van Den Einde et al., 2003). The first use of FRP bars in a vehicular bridge in the United States

occurred in 1996, where glass FRP (GFRP) bars were used in the concrete deck of McKinleyville Bridge in West Virginia (Kumar et al. 1996). In the early 2000s, influenced by infrastructure degradation, research and government agencies implemented GFRP bars in the deck of several bridges with the objective to eliminate corrosion and increase durability.

In addition to traffic loads, bridge decks are commonly exposed to thermal effects (e.g., high temperatures, freeze-thaw cycles), which are known to influence the durability of concrete and steel reinforcement. The main cause of deterioration in reinforced concrete (RC) bridges is corrosion of steel reinforcement (Zhou et al. 2014) induced by carbonation and chlorides that are derived from the application of deicing salts (Cady and Weyers 1983). Carbonation reduces the pH of concrete and as a result it weakens the passivity of embedded steel bars (Chen et al. 2018). Chloride penetration can cause chemical reactions with components of the cement paste and trigger corrosion of steel reinforcement when ions reach the bars level (Xi et al. 2018). Consequently, due to their non-corrosive properties, GFRP bars have emerged as an alternative to steel reinforcement.

Although proven to be non-corrosive, GFRP bars may be susceptible to degradation by a variety of factors, including high temperature, moisture absorption and alkaline environments (Al-Salloum et al. 2013). A variety of studies in the literature focuses on the durability of GFRP bars, and some studies suggest that GFRP bars are negatively affected by concrete due to the high alkalinity of its pore solution (Dejke and Tepfers 2001, Chen et al. 2006). The alkaline solution can chemically attack the glass

fibers and damage the fiber-resin interface due to the growth of hydration products (Micelli et al. 2001, Robert et al. 2009). To determine the durability conditions of the GFRP bars, laboratory tests to evaluate the physical, chemical and mechanical properties of the bars are generally performed. These tests are discussed in detail in Part II of this two-paper series.

Many researchers have recorded a loss in the properties of the bars when exposed to alkaline environment. For instance, Davalos et al. (2012) recorded tensile strength reduction of 40% for GFRP bars embedded into concrete after 120 days exposure to water at 60°C and Benmokrane et al. (2017) recorded between 13 and 21% of reduction in interlaminar shear strength for GFRP bars after 5,000 hours exposed to a simulated concrete alkaline solution at 60°C. Most of the available literature on the durability of GFRP bars, however, is based on accelerated laboratory tests and analytical models that may present conditions hasher than field exposure (Benmokrane et al. 2002, Chen et al. 2007, Robert et al. 2009). As an exception, Mufti et al. (2007) analyzed the chemical composition of GFRP bars removed from bridges in Canada using laboratory techniques such scanning electron microscopy and energy dispersive x-ray, optical microscopy, differential scanning calorimetry, and infrared spectroscopy. It was concluded that the GFRP bars suffered no chemical changes during 5-8 years of field exposure. Consequently, additional field investigation of the long-term durability of GFRP bars is needed for the widespread use of this material.

To provide new information on the durability of in-service GFRP bars with field exposures, a collaborative project including the University of Miami (UM), Penn State

University (PSU), Missouri University of Science &Technology (M S&T), and Owens Corning Composites (OC) investigated in 2017-18 the conditions of concrete and GFRP bars extracted from eleven bridges with 15 to 20 years of service in several regions of the United States. The bridges were exposed to aggressive environmental conditions including deicing salts, wet and dry cycles and freeze-thaw cycles. Concrete cores of 102-mm diameter, most containing pieces of GFRP bar, were extracted from the bridges.

As the long-term durability of the GFRP bars is related to the bar environment (Nkurunziza et al. 2005), evaluating the condition of the concrete is essential. Thus, in the current investigation, chloride penetration, pH, and carbonation depth were evaluated to describe and further detail the environment surrounding the bars. The GFRP bars were evaluated for fiber content, moisture content, water absorption, scanning electron microscopy (SEM), energy dispersive spectroscopy (EDS), glass transition temperature (TA), short bar shear (SBS), modified tensile test, and constituent volume contents by image analysis (CVC). Part I of this two-part series describes the 11 bridges selected for evaluation, the core locations, the procedure for acquiring specimens for testing, and the results from the concrete tests. Part II contains the test procedures and results from the bar tests.

## 2. SELECTED BRIDGES

Eleven bridges with 15 to 20 years of service are included in the investigation from geographically dispersed and environmentally varying locations across the United

States. Nine of the investigated bridges contain GFRP bars in the deck, while two bridges contain GFRP at other locations. Descriptions of the bridges and locations of the extracted cores are given in this section. Table 1 presents a summary of the most relevant information from the bridges to assist in the interpretation of the test results.

Table 1. Information from the bridges

| **Bridge** | **Rain, mm (in.)** | **Snow, mm (in.)** | **Sunny days** | **Estimated Freeze-thaw cycle duration (days)** | **Year built** | **Bar type** | **Bar location** | **Concrete Cover, mm (in.)** |
|---|---|---|---|---|---|---|---|---|
| Bettendorf | 940 (37) | 711 (28) | 205 | 90 | 2003 | N/A | top | 63.5 (2.5) |
| Cuyahoga | 991 (39) | 1473 (58) | 163 | 90 | 2003 | E-glass fiber and vinyl-ester resin | Top and bottom | 63.5 (2.5) |
| Gills Creek | 1143 (45) | 279 (11) | 214 | 75 | 2003 | E-glass and vinyl-ester | top | 57 (2.2) |
| Mckinleyville | 991(39) | 584 (23) | 162 | 75 | 1996 | E-glass and polyester. Type 1: sand coated. Type 2: non-sand coated | Top and bottom | 44.5 (1.8) |
| O'Fallon | 432 (17) | 1524 (60) | 245 | 200 | 2003 | N/A | Top and bottom | 38 (1.5) |
| Roger's Creek | 1168 (46) | 203 (8) | 190 | 80 | 1997 | N/A | Top | 63.5 (2.5) |
| Salem Ave. | 1016 (40) | 432 (17) | 176 | 90 | 1999 | N/A | Top | 70 (2.8) |
| Sierrita de la Cruz Creek | 533 (21) | 381 (15) | 259 | 110 | 2000 | E-glass and vinyl-ester | Top | N/A |
| Southview | 1168 (46) | 330 (13) | 193 | 90 | 2004 | N/A | Top and bottom | N/A |
| Thayer Road | 991 (39) | 584 (23) | 184 | 95 | 2004 | E-glass and vinyl-ester | Top | 38 (1.5) |
| Walker Box | 1168 (46) | 330 (13) | 193 | 90 | 1999 | E-glass and polyester | N/A | N/A |

## 2.1. BETTENDORF BRIDGE (IA)

Bettendorf Bridge was completed in May 2003. It was built using funds provided through the Federal Highway Administration's (FHWA) Innovative Bridge Research and Construction (IBRC) program. The bridge extends 53rd Avenue over Crow Creek in Bettendorf, Iowa and is exposed to approximately 90 freeze-thaw cycles per year (Haley 2011). It is a 52.9-m (173.6 ft) three-span bridge as shown in Figure 1 (Wipf 2006).

Figure 1. Bettendorf Bridge

The bridge was the widest FRP reinforced concrete deck at the time of construction, measuring 30 m (98.7 ft) wide. It was also the first FRP bridge deck in the US to use composite action with prestressed concrete girders (Lee 2009).

The concrete deck system is made of three different material combinations. The west

span deck is constructed with cast-in-place (CIP) concrete reinforced with epoxy coated steel, the middle span deck is made of cast-in-place concrete reinforced with GFRP bars, and the east deck is made of pultruded FRP panels (Wipf 2006). The GFRP bars used in the middle span deck were placed on the top mat (Nanni and Faza 2002). Six concrete cores were extracted from the middle span bridge deck, as shown in Figure 2.

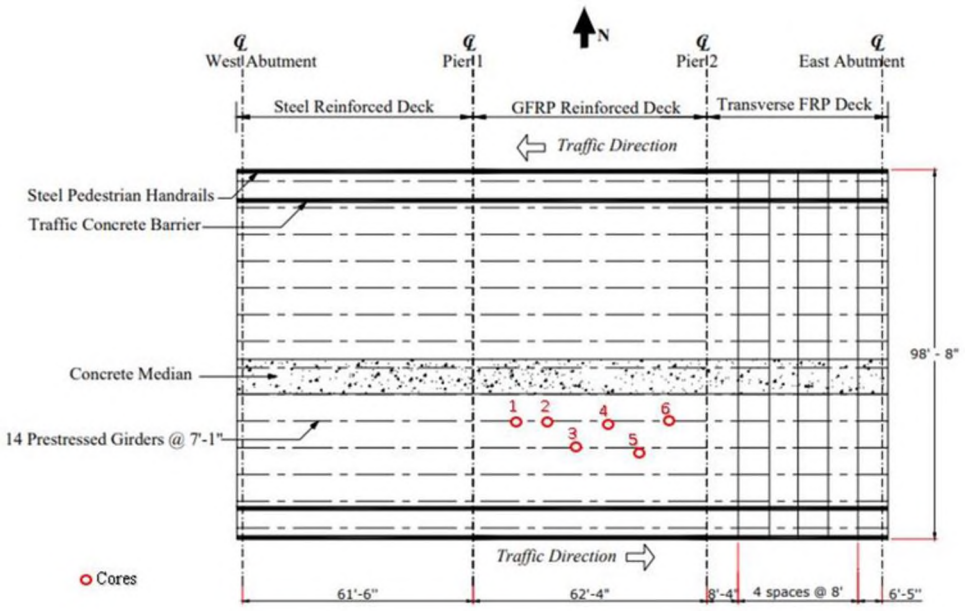


Figure 2. Bettendorf extracted core locations

## 2.2. CUYAHOGA COUNTY BRIDGE (OH2)

Miles Road Bridge No. 178, also known as Cuyahoga County Bridge, was a rehabilitation project completed in October 2003. This project was funded by the FHWA's Transportation Equity Act for the 21st Century - IBRC grant, administered

through the Ohio Department of Transportation. This rehabilitation project consisted of rebuilding the bridge deck with GFRP reinforced concrete and also implemented a monitoring system to collect strain, temperature and deflection data (Eitel 2005).

Cuyahoga County Bridge is located in the Southeastern Lake Erie snow belt in Ohio and is exposed to approximately 90 freeze-thaw cycles per year and heavy application of deicing salts. The bridge consists of two spans of 13.7 m (45 ft) long and an 11.6-m-wide (38-ft) deck. The original bridge was built in 1956 and consisted of five steel girders with a 229-mm-thick (9-in.) steel reinforced concrete deck with a 76-mm (3-in.) asphalt overlay. This bridge has the first deck on a multi-span vehicular bridge to be entirely reinforced with GFRP bars. The GFRP bars used in this bridge were made of E-glass fibers and vinyl-ester resin (Eitel 2005).

The Cuyahoga County Bridge is shown in Figure 3. The plan and section view are shown in Figure 4. Eight concrete cores were extracted from the Cuyahoga County Bridge deck, as shown in Figure 5.

Figure 3. Cuyahoga County Bridge

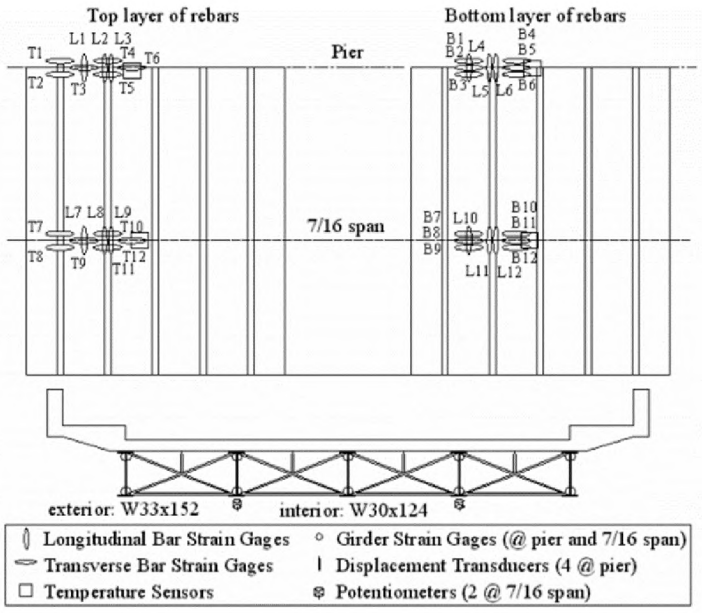


Figure 4. Cuyahoga County Bridge plan and section view

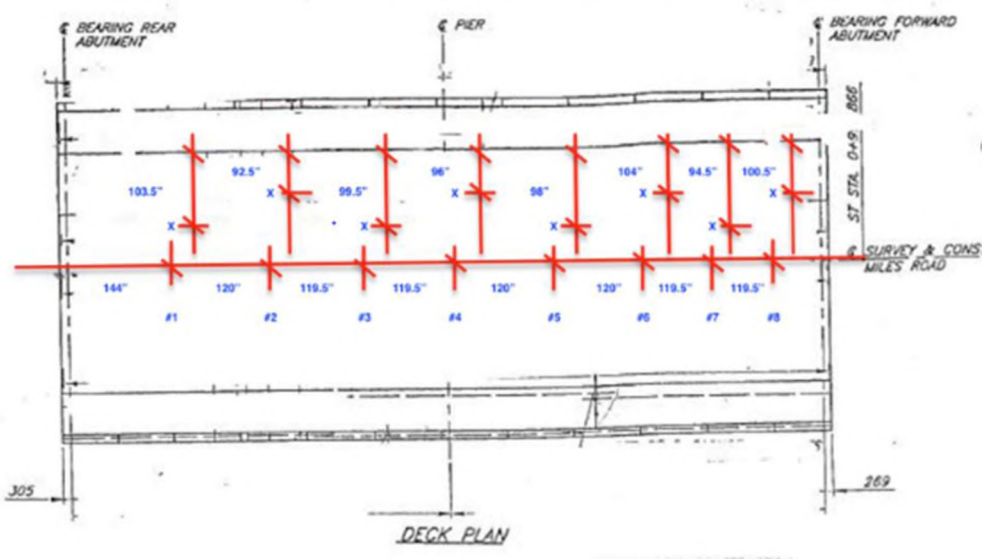


Figure 5. Cuyahoga Bridge location of extracted cores

## 2.3. GILLS CREEK BRIDGE (VA)

Gills Creek Route 668 Bridge was completed in July of 2003. This bridge was part of a project to investigate the durability and effectiveness of GFRP bar reinforcement in concrete decks. It was a project between the Virginia Department of Transportation, the Virginia Transportation Research Council and the Virginia Polytechnic Institute and State University, funded by the FHWA IBRC program (Phillips et al. 2005).

The bridge is located in Franklin County, Virginia and is exposed to approximately 75 freeze-thaw cycles per year (Haley 2011). It is a 52-m (170-ft) three-span steel girder bridge that cross over Gills Creek, as shown in Figure 6. The bridge has a width of 9.2 m (30.3 ft) and its spans A, B, and C measure 13.7 m (45 ft), 24.4 m (80 ft), and 13.7 m (45 ft), respectively.

Figure 6. Gills Creek Bridge

The reinforced concrete bridge deck has a minimum thickness of 20.3 cm (8 in.) between the girders and 22.9 cm (9 in.) at the overhang, as shown in Figure 7 (Phillips et al. 2005).

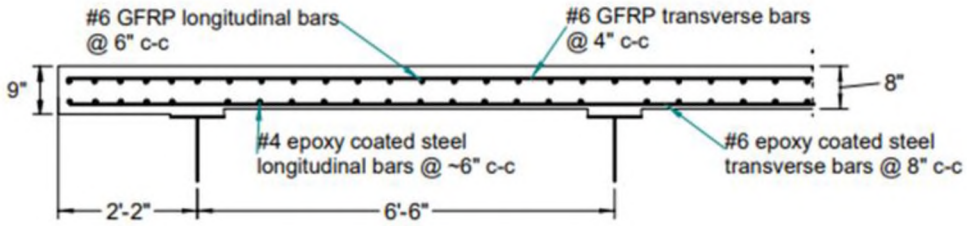


Figure 7. Gills Creek span A reinforcement cross section

The bridge deck span A was reinforced with M19 (#6) GFRP bars on the top mat and epoxy coated M13 and M19 (#4 and #6) steel bars on the bottom mat, as shown in Figure 7. The remaining two spans were reinforced with epoxy-coated steel bars (Phillips et al. 2005). The GFRP bars were made of E-glass fibers and vinyl-ester resin. Ten concrete cores were extracted from the Gills Creek Bridge deck span A, as shown in Figure 8.

## 2.4. MCKINLEYVILLE BRIDGE (WV)

McKinleyville Bridge was built in 1996. It was the first FRP reinforced concrete vehicular bridge in the U.S. (Kumar et al. 1996). The project was developed through the Constructed Facilities Center-West Virginia University in cooperation with FHWA and the West Virginia Department of Transportation-Division of Highways (Shekar et 2003).

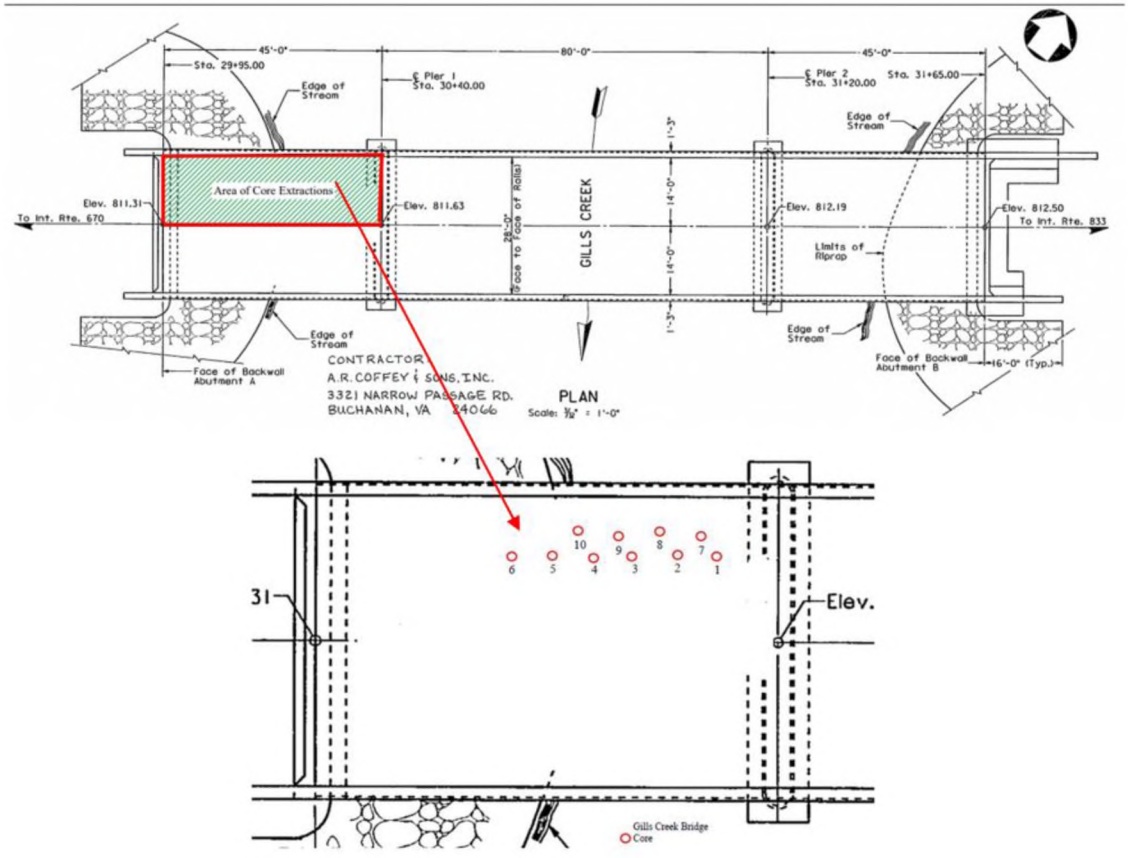


Figure 8. Gills Creek Bridge extracted core locations

The bridge crosses Buffalo Creek in Brooke County (District 6), West Virginia and is exposed to approximately 75 freeze-thaw cycles per year. It consists of three spans with a maximum span length of 22.3 m (73 ft), as shown in Figure 9, having a total length of 54.9 m (180 ft) and a deck width of 9 m (29.5 ft). The bridge was designed for HS-25 loading and it is estimated that 150 vehicles cross the bridge per day over the two lanes. The bridge deck is 229-mm (9-in.) cast-in-place concrete with two types of GFRP bars, one type was made of E-glass fibers with polyester resin and the other type was sand-coated made of E-glass fibers with isophthalic unsaturated polyester resin (Shekar et

al. 2003). The GFRP bars were used as top and bottom reinforcement. Six concrete cores were extracted from the McKinleyville Bridge deck as shown in Figure 10, however, only five concrete cores were received.

Figure 9. McKinleyville Bridge

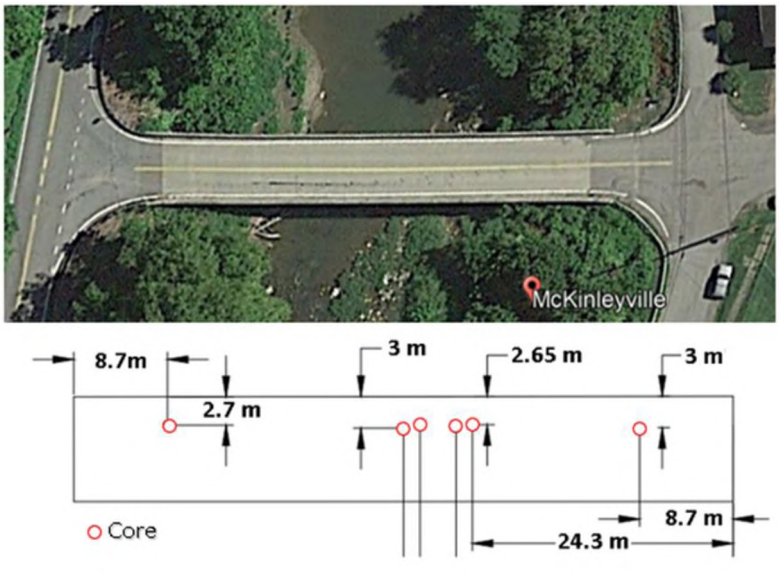


Figure 10. McKinleyville Bridge extracted core locations

## 2.5. O'FALLON PARK BRIDGE (CO)

O'Fallon Park Bridge, shown in Figure 11, was completed in 2003. This bridge was part of a project to investigate the feasibility of the use of FRP in highway bridge decks. The construction was developed through a collaboration between the City and County of Denver, the Colorado Department of Transportation (CDOT), and FHWA, and it was funded by the FHWA IBRC program (Camata and Shing 2005). This bridge is located west of the city of Denver and is exposed to approximately 200 freeze-thaw cycles per year (Haley 2011).

Figure 11. O'Fallon Park Bridge

O'Fallon Park Bridge has a total length of 13.34 m (43.75 ft) and a width of 4.95 m (16.25 ft). The bridge deck is a GFRP deck supported by five reinforced concrete risers built over an arch. The arch is made of concrete reinforced with GFRP bars, with M19

(#6) GFRP bars at the top mat and M22 (#7) GFRP bars at the bottom mat. The bridge is mainly used for pedestrian traffic and occasional small vehicles, but it was designed for H-25-44 loading for maintenance and/or emergency vehicles (Camata and Shing 2005). Six concrete cores were extracted from the bottom of the bridge arch, near the waterline, as shown in Figure 12. Some cores were broken and resulted in multiple pieces, and, therefore, ten cores were recorded in the inventory.

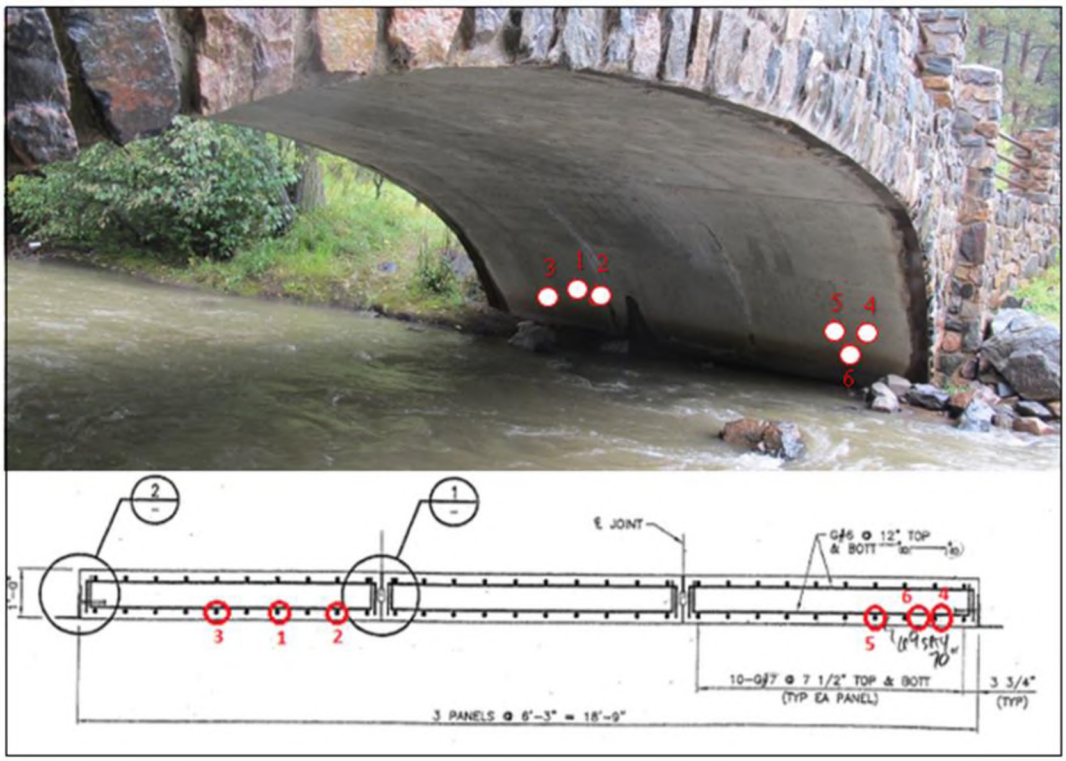


Figure 12. O'Fallon Bridge extracted core location

## 2.6. ROGER'S CREEK (US-460) (KY)

Roger's Creek Bridge was built in 1997. This bridge is the US-460 Bridge over Roger's Creek in Bourbon County, Kentucky and is exposed to approximately 80 freeze-thaw cycles per year. Its superstructure consists of a deck over simply supported prestressed concrete girders for a length of 11.1 m (36.5 ft) and a width of 11 m (36 ft), as shown in Figure 13. The bridge deck is partially reinforced with GFRP and steel bars. The GFRP reinforcing bars are placed as the top mat over an area that measures 2.7 m × 4.7 m (9 ft × 15.5 ft) and runs over three supporting girders (Harik et al. 2004). Six concrete cores were extracted from the Roger's Creek Bridge deck, as shown in Figure 14.

Figure 13. Roger's Creek Bridge

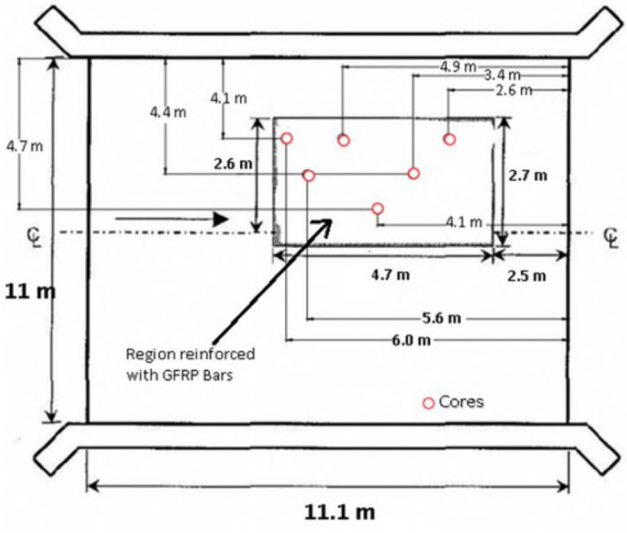


Figure 14. Roger's Creek Bridge extracted core locations

## 2.7. SALEM AVE. BRIDGE (OH1)

Salem Ave. Bridge was a retrofit project completed in 1999. This project was part of a study to understand the effectiveness of replacing concrete decks with FRP deck panels through the IBRC program (project OH-98-05) and the Ohio Department of Transportation (Mertz 2003). Salem Ave. Bridge consists of a pair of parallel bridges located on State Route 49 in Dayton, Ohio and exposed to approximately 90 freeze-thaw cycles per year (Haley 2011). The bridges are 207.3 m (680 ft) long and cross the Great Miami River, as shown in Figure 15. The bridges consist of built-up steel stringers with five spans of 39.6 m (130 ft), 41.8 m (137 ft), 44.2 m (145 ft), 41.8 m (137 ft), and 39.6 m (130 ft.). The deck of the original bridge, built in 1952, was retrofitted with four different FRP deck systems for one of the twin bridges, while the second bridge was retrofitted with only one deck system (FRP-4). (Reising et al. 2001).

Figure 15. Salem Ave. Bridge aerial view

The investigated bridge was retrofitted with FRP-4 deck system, which is a hybrid system that consists of a concrete deck poured over pultruded GFRP panels reinforced with GFRP tubular sections and additional GFRP reinforcing bars (Reising et al. 2001). The GFRP bars were placed at the top longitudinally and transversally. Six concrete cores were extracted from the bridge deck as shown in Figure 16; however, only five concrete cores were received.

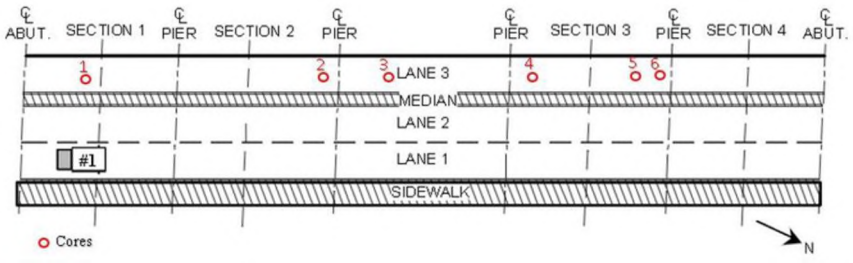


Figure 16. Salem Bridge extracted core locations

## 2.8. SIERRITA DE LA CRUZ CREEK BRIDGE (TX)

Sierrita de la Cruz Creek Bridge was a replacement project completed in 2000. The bridge, shown in Figure 17, is located on State Highway 1061, approximately 50 km (30 mi) northwest of Amarillo, Texas (Gooranorimi & Nanni 2017) and is exposed to approximately 110 freeze-thaw cycles per year (Haley 2011). The replacement was performed due to the bridge being structurally deteriorated and obsolete. The new design consists of seven spans, 24.1 m (79 ft) long and 14.3 m (45-ft) wide, supported by six prestressed concrete Texas type "C" I-beams (Phelan et al. 2003). The replacement project included M16 (#5) and M19 (#6) GFRP reinforcing bars made of E-glass fibers and vinyl-ester resin. The GFRP bars were placed in the top mat of the deck of the two southern-most spans (Spans 6 and 7). The other five spans used epoxy-coated steel bars, including Spans 1 and 2, which are symmetric with Spans 6 and 7, as shown in Figure 18. Witness bars were also embedded in the bridge overhang during construction, these were M16 (#5) GFRP bars with 15.9 mm of cover (0.63 in.) (Gooranorimi et al. 2016). Five concrete cores and three witness bars were extracted from the overhang of Sierrita de la Cruz Creek Bridge deck. The cores were extracted from locations near the bridge guardrail, as shown in Figure 19. Figure 20 shows the location of the extracted witness bars.

Figure 17. Sierrita de la Cruz Creek Bridge

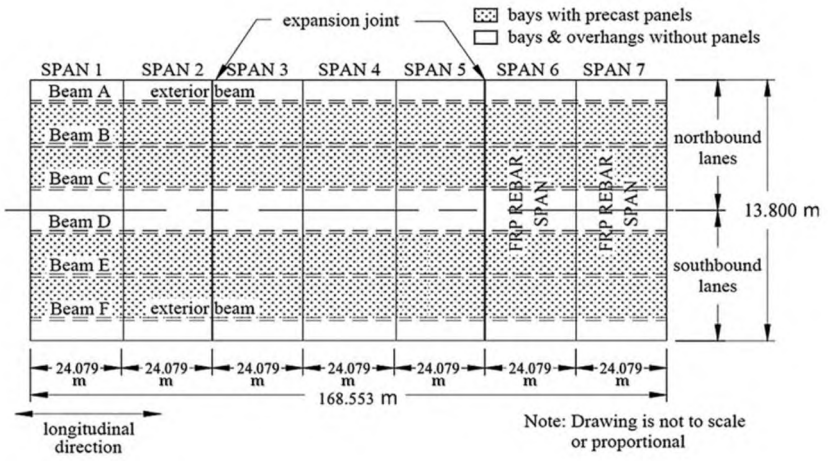


Figure 18. Sierrita de la Cruz Creek Bridge plan view

Figure 19. Sierrita de la Cruz Creek Bridge extracted core approximate location

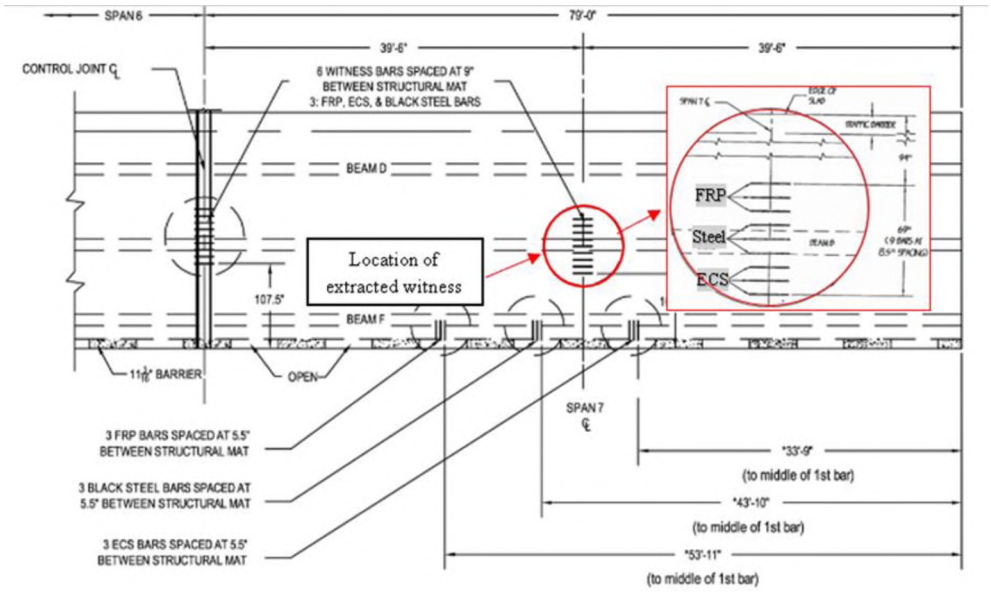


Figure 20. Sierrita de la Cruz Creek Bridge extracted witness bar locations

## 2.9 SOUTHVIEW BRIDGE (MO2)

Southview Bridge was an expansion project completed in 2004. The bridge is located in Rolla, Missouri over Carter Creek and is exposed to approximately 90 freeze-thaw cycles per year. The bridge has an overall length of 12 m (40 ft), as shown in Figure 21. It was originally a one-lane bridge using conventional four-cell steel RC box culverts. It went through a widening in 2004 which included the construction of an additional lane and a sidewalk (Holdener et al. 2008). As a demonstration project to apply the use of FRP bars and tendons, the new deck was made of FRP prestressed/reinforced concrete, including M19 (#6) GFRP bars at the top and bottom mat, M13 (#4) GFRP bars for temperature and shrinkage, and M10 (#3) CFRP bars as the prestressing tendons, as shown in Figure 22. The 254-mm-thick (10-in.) concrete deck is continuous on three conventional RC walls as for the existing structure (Fico et al. 2006). The extension of the deck plus a 2-m-wide (6.6-ft) conventional RC sidewalk on the opposite side extended the overall width of the bridge from 3.9 m (12.8 ft) to 11.9 m (39.0 ft). Ten concrete cores were extracted from the Southview Bridge deck but only two cores were available for this specific study. Figure 23 shows the location of the extracted cores.

Figure 21. Southview Bridge before extension

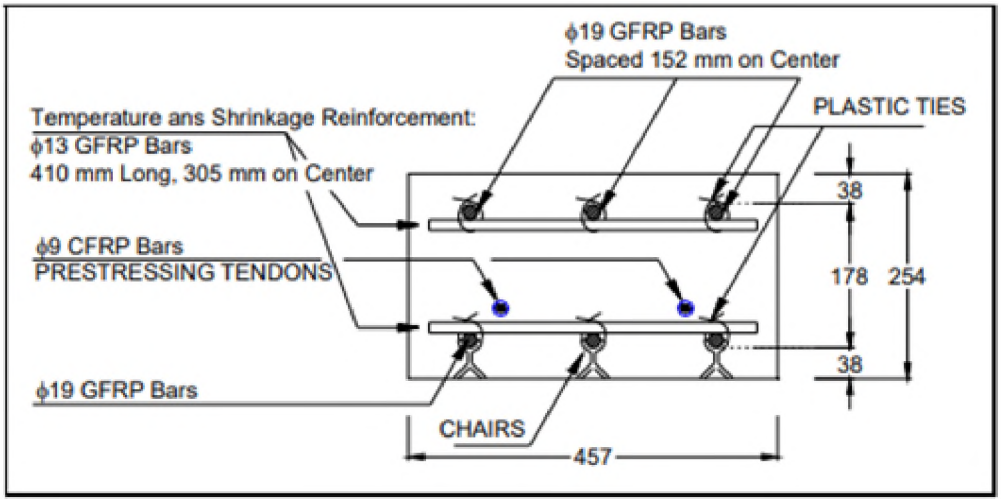


Figure 22. Southview Bridge reinforcement detail

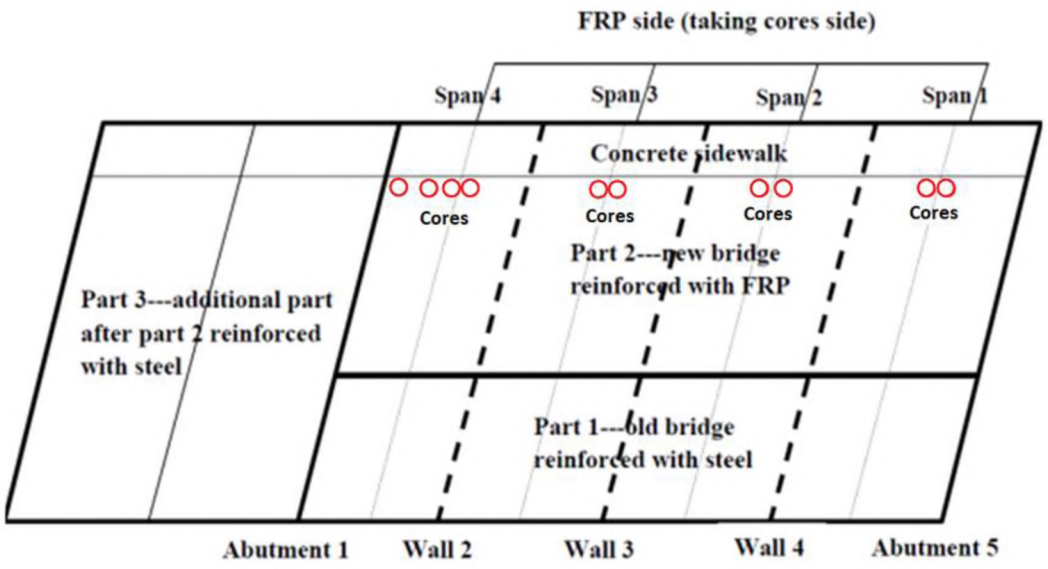


Figure 23. Southview Bridge extracted core locations

## 2.10. THAYER ROAD BRIDGE (IN)

The Thayer Road Bridge replacement project was completed in 2004. The bridge is located on Thayer Road crossing I-65 Newton County, Indiana and is exposed to approximately 95 freeze-thaw cycles per year (Haley 2011). The bridge, shown in Figure 24, was designed for 60-km/h (40-mph) traffic of cars and trucks and consists of five spans of 12.1 m (39.8 ft), 19.4 m (63.5 ft), 23.7 m (77.8 ft), 19.4 m (63.5 ft), and 12.2 m (40 ft), respectively, summing up to a total length of 86.6 m (284 ft) with a 10.5-m-wide (34.5-ft) deck. The project was a collaboration of the Indiana Department of Transportation and Purdue University and involved the replacement of a concrete deck. The deck is supported by seven wide-flange steel girders and is reinforced with GFRP bars on the top mat and epoxy-coated steel on the bottom mat, as shown in Figure 25

(Frosch and Pay 2006). The GFRP bars were made of E-glass fibers and vinyl-ester resin. Six concrete cores were extracted from the Thayer Road Bridge deck, as shown in Figure 26.

Figure 24 Thayer Road Bridge

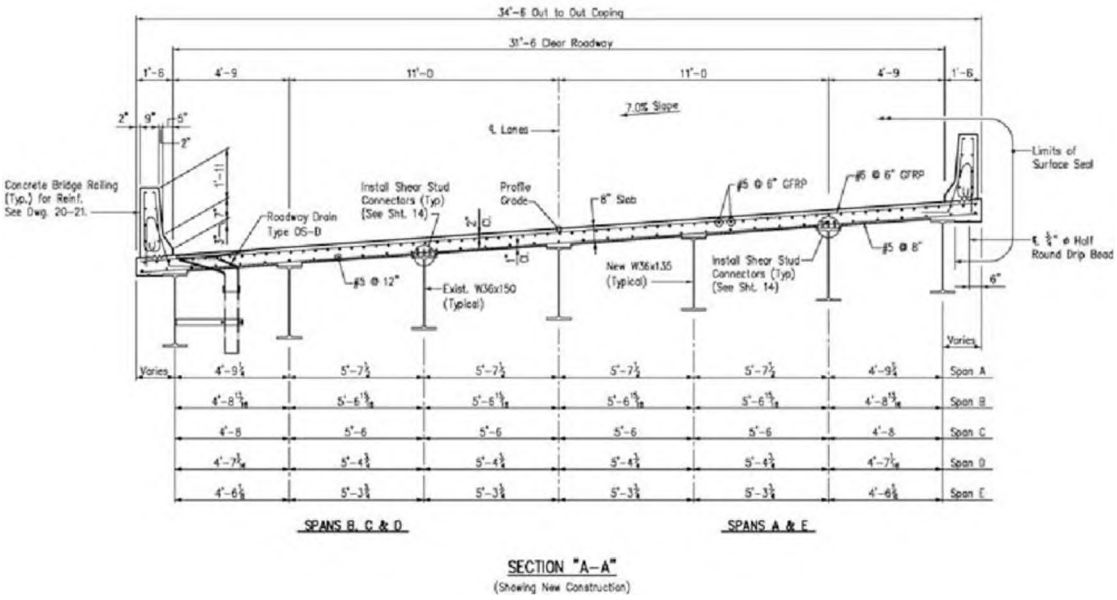


Figure 25. Thayer Road Bridge Reinforcement Detail

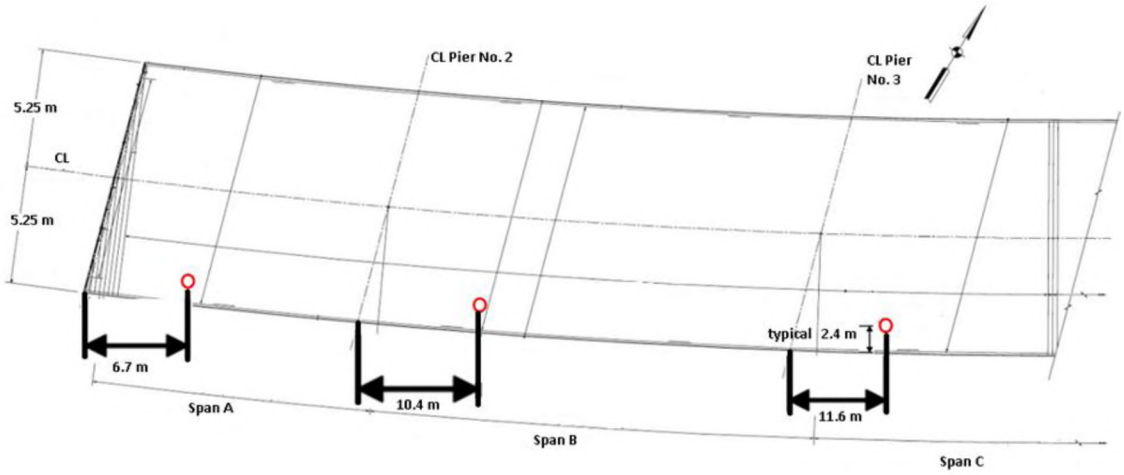


Figure 26. Thayer Road Bridge extracted core locations

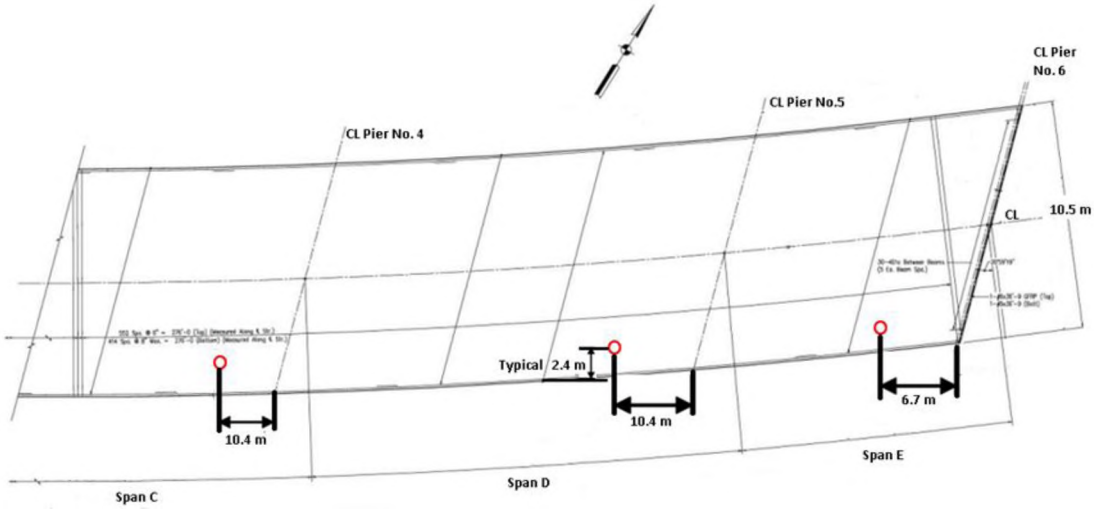


Figure 27. Thayer Road Bridge extracted core locations

## 2.11. WALKER BOX CULVERT BRIDGE (MO1)

The Walker Box Culvert Bridge replacement project was completed in 1999. The bridge is located on Walker Avenue in Rolla, Missouri (Gooranorimi et al. 2017) and is exposed to approximately 90 freeze-thaw cycles per year (Haley 2011). The original bridge became unsafe to operate due to excessive corrosion of the steel pipes (Nanni 2001). To replace the original bridge, GFRP bars made of E-glass fibers and polyester resin were used to reinforce the concrete box culvert. The new bridge, shown in Figure 27, is 11 m (36 ft) wide, consisting of 18 box culverts that are 1.50 × 1.50 m (4.92 × 4.92 ft) with a thickness of 150 mm (5.9 in.) (Wang et al. 2018). The RC boxes were entirely reinforced with M6 (#2) GFRP bars pre-bent and cut to size by the manufacturer (Alkhrdaji and Nanni 2001). Six concrete cores were extracted from Walker Box Culvert Bridge. The extracted cores were taken from the bottom of the two culverts, as shown in Figure 28.

Figure 28.Walker Box Culvert Bridge

## 3. SAMPLE EXTRACTION

To extract the concrete cores from the bridges, a barrel of 102 mm (4 in.) in diameter was used. The targeted locations for core extraction were, when possible, areas with cracks or signs of environmental deterioration. No non-destructive method for identifying bar location is yet available. As a result, some concrete cores had no GFRP bars and others had GFRP bars shorter than 51 mm (2 in.). An extracted core with a short bar is shown in Figure 29.

Figure 29. A core sample

## 4. SAMPLE INVENTORY AND DISTRIBUTION

Upon receipt of the concrete cores at UM, an inventory of all specimens was compiled. Concrete cores were measured and approximate GFRP bar lengths and concrete cover were determined. The core specimens are identified using a two-part

identification scheme NN_Cx, where NN is the state abbreviation of the bridge's location, and Cx indicates the x-th core number. For the GFRP bars, a three-part identification scheme is used, NN_Cx_Bx, where NN is the state abbreviation of the bridge's location, Cx indicates the x-th core number, and Bx indicates the x-th bar number. In cases where more than one specimen from a certain bar was tested, an extra (-x) suffix is used to identify the specimen number.

Once the inventory was compiled at UM, the cores were placed in sealed plastic bags for storage until testing or distribution to other laboratories. Consequently, a plan for carrying out the concrete and GFRP tests among the project partners was developed. Most concrete tests were performed at UM, while the GFRP tests were divided based on the testing capabilities of each laboratory.

## 5. CHALLENGES AND SOLUTIONS

One challenge in testing was the relatively small number of specimens that could be tested due to the limited number of cores that could be extracted, the small length of bars embedded in the cores, and the difficulty of locating GFRP bars prior to drilling the cores. The extracted bars, with the exception of witness bars extracted from the Sierrita de la Cruz Creek Bridge, had a maximum length of 95 mm (3.75 in.). An aim of the investigation was to run three repetitions for each material property. For GFRP tests that required bar lengths of 25 mm (1 in.) or less, the bars were cut to the required dimension so that a minimum of three test replicates could be achieved with one bar. For other tests,

however, in order to achieve a minimum of three replicates per test type, multiple bars of the same size extracted from the same bridge were assumed to have had identical exposure conditions.

Another challenge during this study was the lack of data on most of the materials at the time of installation. No information on the original concrete mix designs could be obtained. Thus, no comparison was made between the concrete quality before and after in-service exposure. In addition to the lack of information on concrete mixtures, the cores were not sealed hermetically upon extraction from the bridges, which may have affected some concrete properties such as moisture content.

# 6. CONCRETE TESTS PROCEDURE

## 6.1. CHLORIDE PENETRATION DEPTH

Chloride penetration is a major concern in concrete structures with steel reinforcement as it can accelerate corrosion. GFRP bars, on the other hand, have been reported to be highly resistant to chloride ions (Zhou et al. 2018). To evaluate the chloride penetration depth of the extracted concrete cores and understand how chloride presence may have influenced the durability of reinforcement, the calorimetric method using silver nitrate ($AgNO_3$) was employed. According to Meck and Sirivivatnanon (2003), this method was popularized by Otsuki et al. (1992) and Collepardi (1995). In this method, a 0.1 N $AgNO_3$ solution is sprayed on a freshly broken concrete surface, where chloride ions are present. The silver ions react with the chloride ions and form a

white precipitate, and in areas containing few or entirely free of chloride ions, a brown precipitate forms (Yuan et al. 2008). Additionally, there is a distinguished boundary between the white and brown regions.

Although this method can be influenced by many factors such as the sprayed volume and concentration of $AgNO_3$ solution, which can result in high variability (Meck and Sirivivatnanon 2003, He et al. 2012), chloride penetration resistance varies significantly with concrete mixture. For instance, increasing fly ash and fly ash fineness, and reducing water-to-binder ratio can increase chloride penetration resistance (Chindaprasirt et al. 2007).

To determine the presence of chlorides in the concrete cores and to observe if chlorides reached the depth of the GFRP bars, the concrete cores were split to expose a fresh surface and compressed air was used to remove dust particles from this surface. The silver nitrate solution was sprayed onto the surface and allowed to dry. The chloride penetration depth was measured with a ruler, as the lighter color indicates areas of chloride penetration, and a darker color indicates areas not affected by chlorides. At least three exposed surfaces were tested for samples from each bridge.

## 6.2. CARBONATION DEPTH

Carbon dioxide that penetrates the surface of concrete can react with alkaline components in the cement paste. The chemical reaction of $Ca(OH)_2$ and calcium–silicate–hydrate (C–S–H) with $CO_2$ forms $CaCO_3$ and water (Chang et al. 2006). As a result, the pH value of the pore solution decreases, destroying the passivity of embedded steel

reinforcement bars (Chang et al. 2006). For GFRP bars, on the other hand, carbonated concrete was found to be less aggressive than non-carbonated concrete (Rajput and Sharma 2017). The most common method to determine the depth of carbonation is by using a phenolphthalein indicator solution. This method was carried out by spraying the solution over a fresh-cut concrete surface and then monitoring the change in surface color. The solution mixture has 1% phenolphthalein, 70% ethyl-alcohol, and 29% distilled water per volume ratio. The concrete turns shades of purple when pH is above 9 and remains colorless when pH is below 9 (Chang et al. 2006).

### 6.3. pH

The pH of ordinary Portland cement concrete is generally between 12.5 and 13, but deterioration mechanisms such as chloride ingress and carbonation can decrease the pH of concrete (Behnood et al. 2016). Behnood et al. (2016) show that even with nearly zero concentration of chloride ions near the bars, a concrete pH level of less than 11 in the area of the steel bars can initiate corrosion. Although a low pH is detrimental for steel, some researchers suggest that the high pH of concrete can reduce the durability of GFRP bars (Chen et al. 2006).

To measure the pH of the concrete from the selected bridges, cores from each bridge were tested at three or more different locations. Two different procedures were used: one according to Grubb et al. (2007) and the other one by using a rainbow indicator. The Grubbet al. (2007) procedure was used in cores from eight bridges to determine the pH at various depths. Cores were split and then drilled to collect 5 g (77

grains) of concrete dust for each test. Split cores were drilled at three varying depths from 13 mm (0.5 in.) below the surface of the concrete to 13 mm (0.5 in.) above where the GFRP bar had been located. The concrete dust was then mixed with 10 ml (0.34 oz.) of fresh distilled water at a temperature of 23 °C (73.4 °F). The mixture was stirred for 30-second intervals three times over seven minutes and then filtered through No. 40 filter paper. A calibrated pH probe was then used to read the pH of the mixture.

The rainbow indicator procedure was used in the evaluation of specimens from three bridges: Roger's Creek, Thayer Road, and McKinleyville Bridges. This procedure is very simple and consists of spraying a rainbow indicator (Germann Instruments, Inc.) on a fresh concrete surface. The concrete cores were cut to expose a fresh surface, dust was removed with compressed air, and the indicator was sprayed on the concrete surface. Once the indicator dried, changes in color could be observed on the concrete surface. This color indicated the pH value according to the color pallet.

# 7. CONCRETE TESTS RESULTS

## 7.1. CHLORIDE PENETRATION DEPTH

Chloride penetration testing was performed in 10 of the 11 bridges (excluding Sierrita de la Cruz Creek). The difference in the color of the concrete due to the silver nitrate was difficult to identify in some of the specimens. For instance, for the McKinleyville, Roger's Creek, Thayer Road, Southview, and Walker Box Bridges, no chloride penetration was observed. All other bridges presented chloride penetration,

varying from approximately 6 mm (0.25 in.) to 64 mm (2.5 in.). The worst case of chloride penetration, approximately 64 mm (2.5 in.), was observed in concrete specimens from the Cuyahoga and Salem Ave. Bridges. Table 2 shows the average and highest chloride penetrations for each bridge.

Table 2. Average chloride penetration for each bridge

| **Bridge** | **Average Chloride penetration, mm (in.)** | **Highest Chloride Penetration Observed, mm (in.)** |
|---|---|---|
| Bettendorf | 19 (0.8) | 25 (1.0) |
| Cuyahoga | 38 (1.5) | 64 (2.5) |
| Gills Creek | 8 (0.3) | 13 (0.5) |
| McKinleyville | N/A | N/A |
| O'Fallon Park | 13 (0.5) | 13 (0.5) |
| Roger's Creek | N/A | N/A |
| Salem Ave. | 38 (1.5) | 64 (2.5) |
| Southview | N/A | N/A |
| Thayer Road | N/A | N/A |
| Walker Box Culver | N/A | N/A |

The chloride penetration observed in the extracted cores appeared to be due to deicing salt applications, as four out of the five bridges that showed chloride presence had the highest amount of snow per year. In terms of its effect on the extracted GFRP bars, Cuyahoga Bridge that presented chloride penetration reaching the level of reinforcement, also showed a significant reduction in shear strength and a glass transition temperature ($T_g$) lower than required by the latest ASTM standard (ASTM 7957) (Al-

Khafaji 2020). A reduction in shear strength would be indicative of fiber/matrix interface degradation (Benmokrane et al. 2015), and a reduction in $T_g$ would be indicative of resin degradation. However, these results could also be due to other factors such as the high moisture absorption rate (1.52%) observed for Cuyahoga Bridge (Al-Khafaji 2020).

In this study, the lack of information on the concrete mixes does not allow a comparison between results. To understand the obtained results, values from other studies in the literature can be considered. In the study of Xi et al. (2018), for example, bridge decks exposed to deicing salts presented chloride ingress at a depth of 50 mm (2 in.). However, the percentage of chloride by concrete weight can be minor and possibly not detected when using silver nitrate solution. The chloride content at 50 mm appears to increase with concrete age. For example, for a bridge deck with 14 years of service, chloride concentrations of 0.061% at a depth of 50 mm (2 in.) was observed, while for a bridge deck of 21 years of service, 0.065% chloride penetration was observed at the same depth (Xi et al. 2018).

The observed chloride penetration using silver nitrate may indicate a high enough level of chloride content to break the passive layer of the steel reinforcement. The observed chloride penetration at 64 mm (2.5 in) would have reached the reinforcement and cause corrosion initiation for steel reinforcement.

## 7.2. CARBONATION DEPTH

Concrete cores from all 11 bridges were tested for carbonation depth. Most specimens presented some carbonation near the surface, but others such as

McKinleyville, Roger's Creek, Southview, Thayer Road and Walker Culvert presented no carbonation at all. This could be due to the degree of relative humidity of the specimens. According to the study of Chang et al. (2006), phenolphthalein indicator changes color (to white) when the area is fully carbonated (the level of carbonation is above 50%), which happens when the relative humidity is above 50%. Carbonation above 50% presents an opportunity for corrosion of steel reinforcement. Steel reinforcement would be unlikely to corrode in the bridges with less than 50% carbonation.

Some bridges presented significant depth of carbonation reaching into the central volume of the concrete core and possibly reaching the reinforcement. These results were consistent with the results from Sagues et al. (1997), where 18 bridges with 16 to 59 years of service were investigated for carbonation. Sixteen of the eighteen bridges studied by Sagues et al. (1997) presented carbonation. The average carbonation depth was approximately 10 mm (0.4 in.) and some bridges presented carbonation depth as high as 50 mm (2 in.). Table 3 shows the highest carbonation depth observed for each bridge. All bridges that presented chloride penetration also presented carbonation. The bridges that presented from the highest to the lowest carbonation depth are Salem Ave., Gills Creek, O'Fallon Park, Sierrita de la Cruz Creek, Cuyahoga and Bettendorf. Half of these bridges also presented GFRP bars with high volume of water retention. For some bridges, O'Fallon Park, Salem Ave. and Sierrita de la Cruz Creek, the depth of carbonation may have reached the reinforcement. Although carbonated concrete is considered a less aggressive environment than non-carbonated concrete, these bridges still presented a reduction in GFRP bar shear strength. Bar physical and chemical composition, on the

other hand, presented no signs of deterioration from SEM and EDS tests (Al-Khafaji 2020). If these bridges had been reinforced with steel bars, the observed carbonation depth could have resulted in corrosion initiation.

Table 3. Carbonation depth for each bridge

| **Bridge** | **Highest Observed Carbonation Depth, mm (in.)** |
|---|---|
| Bettendorf | 19 (0.8) |
| Cuyahoga | 25 (1.0) |
| Gills Creek | 51 (2.0) |
| McKinleyville | N/A |
| O'Fallon Park | 38 (1.5) |
| Roger's Creek | N/A |
| Salem Ave. | 76 (3.0) |
| Sierrita de la Cruz Creek | 38 (1.5) |
| Southview | N/A |
| Thayer Road | N/A |
| Walker Box Culver | N/A |

### 7.3. pH

All eleven bridges were tested for pH. Out of the eleven bridges, eight were tested according to the procedure from Grubb and co-workers (Grubb et al. 2007), and three bridges were tested using the rainbow indicator. The bridges presented pH extreme values as low as 7 and as high as 13 with an average between 10 and 12. The lowest average pH value observed was 10 for the Roger's Creek and McKinleyville Bridges, the two oldest bridges in the investigation. While the highest average pH was 12.2 for Cuyahoga and Gills Creek Bridges. The pH values observed during this test were

consistent with the values obtained by Grubb and co-workers (2007), who recorded a pH value of approximately 10.5 for a 20-year old specimen and a 12-pH value for a 2-month-old specimen.

The average results for each bridge can be observed in Table 2. Most bridges presented high pH, above 11.5, which according to some authors would be detrimental to FRP bars (Ceroni et al. 2006, Demis et al. 2007). However, based on the results obtained in Al-Khafaji et al. (2020), no direct correlation between GFRP bar degradation and pH was identified. The condition of the GFRP bars from McKinleyville and Roger's Creek Bridges that presented an average pH of 10 was comparable to the bars from the other bridges with higher pH. On the other hand, a pH lower than 11 would be representative of corrosion initiation of steel reinforcement even with low presence of chloride ions near the bars (Behnood et al. 2016).

Table 4. Average pH for each bridge

| Bridge | Average pH | Bridge | Average pH |
|---|---|---|---|
| Bettendorf | 12.1 | Salem Ave | 11.6 |
| Cuyahoga | 12.2 | Sierrita de la Cruz Creek | 11.5 |
| Gills Creek | 12.2 | Southview | 11.5 |
| McKinleyville* | 10 | Thayer Road* | 12 |
| O'Fallon Park | 12.1 | Walker | 11.5 |
| Roger's Creek* | 10 | | |

*Bridges tested with the rainbow indicator

# 8. CONCLUSIONS

Concrete cores with embedded GFRP bars were extracted from eleven bridges with 15 to 20 years of service to investigate their performance and durability. The investigated bridges are located across the United States and exposed to varying environmental conditions (e.g., deicing salts, wet and dry cycles, and freeze-thaw cycles) that influence the durability of reinforced concrete structures. Experiments were performed on the concrete to evaluate its condition and its influence on the durability of in-service GFRP bars. The concrete tests included chloride penetration depth, carbonation depth, and pH tests. The results were compared with the information given from the bridges and to the results obtained in part II of this two-part series of paper. The following observations were made:

- Carbonation was observed in most concrete cores. Some bridges presented carbonation depth larger than 38 mm (1.5 in), which may indicate that carbonation reached the GFRP bars.
- Chloride penetration tests were performed on specimens from ten bridges. In some bridges, no chloride penetration was observed; in the worst case, chloride may have reached the reinforcement at about 64 mm (2.5 in.) depth. The chloride penetration observed in the bridges suggests it was due to the application of deicing salts.
- Concrete pH values were recorded on specimens from all bridges. Most bridges presented relatively high pH, above 11, which according to literature (Ceroni et al.

2006, Demis et al. 2007) are conditions detrimental to GFRP bars. The two oldest bridges in the investigation presented an average pH of 10, an indicator of corrosion initiation for steel reinforcement. No correlation between pH and degradation of GFRP bars could be concluded.

The work presented in this paper is relevant to the interpretation of the test results on GFRP samples extracted from the cores and discussed in Part II of this two-paper series.

## ACKNOWLEDGMENTS

The authors are grateful to the Strategic Development Council (SDC) of the American Concrete Institute (ACI) and NSF I/U CRC CICI for providing the funding that allowed the extraction of the cores and the distribution of specimens to four laboratories for the performance of the tests and the Tier 1 ReCAST University Transportation Center for supporting a portion of laboratory testing and evaluation. Similarly, the authors acknowledge the collaboration and help provided by the state and local authorities that have jurisdiction on the selected bridges for allowing this research to take place.

Several other individuals provided technical support to this endeavor. In particular, the authors thank Jason Cox of Missouri S&T, and Ryan Koch, Bryan Barragan, Doug Gremel, Mala Nagarajan and Nelson Yee of Owens Corning Infrastructure Solutions.

# REFERENCES


Alkhrdaji, T., and A. Nanni. 2001. "Design, Construction, and Field-Testing of an RC Box Culvert Bridge Reinforced with GFRP Bars." In *Proc., 5th International Symposium on Fiber-Reinforced Polymer Reinforcement for Concrete Structures (FRPRCS-5),* Edited by C. Burgoyne, Thomas Telford, 1055-1064. Cambridge, UK.

Al-Salloum, Y. A., El-Gamal, S., Almusallam, T. H., Alsayed, S. H., & Aqel, M. 2013. "Effect of harsh environmental conditions on the tensile properties of GFRP bars." *Composites Part B: Engineering*, *45*(1), 835-844.

ASTM C1218/C1218M-17. 2017. *Standard Test Method for Water Soluble Chloride in Mortar or Concrete*. ASTM International, West Conshohocken, PA.

ASTM D7957/D7957M 2017. *Standard Specification for Solid Round Glass Fiber Reinforced Polymer Bars for Concrete Reinforcement*. ASTM International, West Conshohocken, PA.

Behnood, A., K. V. Tittelboom, and N. De Belie. 2016. "Methods for measuring pH in concrete: A review." *Construction and Building Materials.* 105: 176-188.

Benmokrane, B., P. Wang, T. M. Ton-That, H. Rahman, and J.Robert. 2002. "Durability of glass fiber-reinforced polymer reinforcing bars in concrete environment." *Journal of Composites for Construction* 6 (3): 143-153.

Benmokrane, B., Elgabbas, F., Ahmed, E. A., & Cousin, P. 2015. "Characterization and comparative durability study of glass/vinylester, basalt/vinylester, and basalt/epoxy FRP bars." *Journal of Composites for Construction*, *19*(6), 04015008.

Broomfield, J. P. 2003. *Corrosion of steel in concrete: understanding, investigation and repair, 2nd Edition*. USA and Canada: RCR Press.

Cady, P. D., and R. E. Weyers. 1983. "Chloride penetration and the deterioration of concrete bridge decks." *Cement, concrete and aggregates.* 5 (2): 81-87.

Camata, G., & Shing, B. 2005. "Evaluation of GFRP honeycomb beams for the O'Fallon park bridge." *Journal of Composites for Construction. 9* (6): 545-555.

Ceroni, F., E. Cosenza, M. Gaetano, and M. Pecce. 2006. "Durability issues of FRP rebars in reinforced concrete members." *Cement and Concrete Composites*. 28 (10): 857-868.

Chang, C., and J. Chen. 2006 "The experimental investigation of concrete carbonation depth." *Cement and Concrete Research.* 36 (9): 1760-1767.

Chen, Y., Davalos, J. F., & Ray, I. .2006. "Durability prediction for GFRP reinforcing bars using short-term data of accelerated aging tests." *Journal of Composites for Construction*, *10*(4), 279-286.

Chen, Y., J. F. Davalos, I. Ray, and H.Kim. 2007. "Accelerated aging tests for evaluations of durability performance of FRP reinforcing bars for concrete structures." *Composite Structures*. 78 (1): 101-111.

Chen, Y., P. Liu, and Z. Yu. 2018. "Effects of environmental factors on concrete carbonation depth and compressive strength." *Materials*. 11 (11): 2167.

Chindaprasirt, P., C. Chotithanorm, H. T. Cao, and V. Sirivivatnanon. 2007. "Influence of fly ash fineness on the chloride penetration of concrete." *Construction and Building Materials.* 21 (2): 356-361.

Collepardi, M. 1995. "Quick method to determine free and bound chlorides in concrete. Chloride penetration into concrete." In *Proc., International RILEM Workshop*, 10. St. Remy-les-Chevreuse, France.

Davalos, J. F., Chen, Y., & Ray, I. 2012. "Long-term durability prediction models for GFRP bars in concrete environment." *Journal of Composite Materials*, *46*(16), 1899-1914.

Dejke, V., and Tepfers, R. 2001. "Durability and service life prediction of GFRP for concrete reinforcement." In *Proc., 5th international conference on fiber-reinforced plastics for reinforced concrete structures (FRPRCS-5)*. 505-516.

Demis, S., K. Pilakoutas, and E. Byars. 2007. "Durability of fibre reinforced polymers in concrete-procedures for reduced alkalinity exposures." In *Proc.,8th International Symposium on Fiber-Reinforced Polymer Reinforcement for Concrete Structures (FRPRCS-8)*, 534-535. Patras, Greece.

Eitel, A. 2005. "Performance of a GFRP reinforced concrete bridge deck." PhD diss., Case Western Reserve University, Cleveland, OH.

Fico, R., N. Galati, A. Prota, and A. Nanni. 2006. *Southview bridge rehabilitation in Rolla, Missouri.* Report No. UTR 103.Center for Infrastructure Engineering Studies University Transportation Center Program, University of Missouri–Rolla, Rolla, Missouri, USA.

Frosch, R. J., and A. C. Pay. 2006. *Implementation of a Non-Metallic Reinforced Bridge Deck, Volume 2: Thayer Road Bridge*. Publication FHWA/IN/JTRP-2006/15-2. Joint Transportation Research Program, Indiana Department of Transportation and Purdue University, West Lafayette, Indiana. https://doi.org/10.5703/1288284314223.

Gooranorimi, O., and A. Nanni. 2017. "GFRP reinforcement in concrete after 15 years of service." *Journal of composites for construction.* 21 (5): 04017024.

Gooranorimi, O., Bradberry, T., Dauer, E., Myers, J., Nanni, A., & Tier, R. C. 2016. *FRP reinforcement for concrete: performance assessment and new construction: volume I: Sierrita De La Cruz Creek bridge* (No. RECAST UTC# 00042134-04-103A). RE-CAST Tier-1 University Transportation Center.

Gooranorimi, O., J. Myers, and A. Nanni. 2017. "GFRP Reinforcements in Box Culvert Bridge: A Case Study After Two Decades of Service." In *Concrete Pipe and Box Culverts*. ASTM STP1601, J.J.Meyer and J. Beakley, Eds., ASTM International, West Conshohocken, PA, 75–88, http://dx.doi.org/10.1520/STP160120160119.

Grubb, J. A., H. S. Limaye, and A. M. Kakade. 2007. "Testing pH of concrete." *Concrete international.*29 (4): 78-83.

Haley, J. S. 2011. "Climatology of freeze-thaw days in the conterminous United States: 1982-2009." PhD diss., Kent State University, Kent, OH.

Harik, I. E., P. Alagusundaramoorthy, V. Gupta, C. Hill, and C. C. Chiaw. 2004. *Inspection and Evaluation of a Bridge Deck Partially Reinforced with GFRP Rebars.* Report No. KTC-04-21/FRPDeck-1-97-1F. Kentucky Transportation Center Research Report. http://dx.doi.org/10.13023/KTC.RR.2004.21

He, F., C. Shi, Q. Yuan, C. Chen, and K. Zheng. 2008. "$AgNO_3$-based colorimetric methods for measurement of chloride penetration in concrete." *Construction and Building Materials*. 26 (1): 1-8.

Holdener, D., J. Myers, and A. Nanni. 2008. "An Overview of Composites Usage in Bridge Facilities in The State of Missouri, USA." In *Proc., International Conference and Exhibition on Reinforced Plastics, ICERP, Mumbai, India.*

Kumar, S. V., H. K. Thippeswamy, and H. V. S. Gangarao. 1997. "McKinleyville Bridge: Construction of the Concrete Deck Reinforced with FRP Rebars." In *Prec., International Composites Expo '97,* 6-F. Nashville, Tennessee.

Lee, Y., T. Hosteng, U. Deza, J. S. Nelson, T. Wipf, B. Phares, D. Wood, and W. Klaiber. 2009. "Structural Field Testing and Evaluation of Two Demonstration FRP Deck Bridges: Case Studies on FRP Panel Deck Bridge and Temporary Bypass Bridge. No. 09-2503." In *Proc., TRB 2009 Annual Meeting*. Washington D.C.

Lindquist, W. D., D. Darwin, J. Browning, and G. G. Miller. 2006. "Effect of cracking on chloride content in concrete bridge decks." *American Concrete Institute Journal.* 103 (6): 467-473.

Marks, Vernon J. 1977 *Detection of Steel Corrosion in Bridge Decks and Reinforced Concrete Pavement*. Iowa Research Board No. Project HR-156 Final Rpt. Iowa Department of Transportation.

Meck, E., and V. Sirivivatnanon. 2003. "Field indicator of chloride penetration depth." *Cement and Concrete Research.* 33 (8): 1113-1117.

Mertz, D. R., M. J. Chajes, J. W. Gillespie, D. S. Kukich, S. A. Sabol, N. M. Hawkins, W. Aquino, and T. B. Deen, 2003. *Application of fiber reinforced polymer composites to the highway infrastructure*, NCHRP Report 503, Transportation Research Board Washington, DC.

Micelli, F., Nanni, A., & La Tegola, A. 2001. "Effects of conditioning environment on GFRP bars." In *International Conference, CNIT Paris*.

Mufti, A.A., Onofrei, M.B.N.M.J.B.G., Benmokrane, B., Banthia, N., Boulfiza, M., Newhook, J.P., Bakht, B., Tadros, G.S. and Brett, P. 2007. "Field study of glass-fibre-reinforced polymer durability in concrete." *Canadian Journal of Civil Engineering. 34* (3): 355-366.

Myers, J. J., J. S. Volz, E. Sells, K. Porterfield, T. Looney, B. Tucker, and K. Holman. 2012. *Report E: Self-Consolidating Concrete (SCC) for Infrastructure Elements: Hardened Mechanical Properties and Durability Performance*. No. cmr 13-003. Missouri University of Science and Technology, Rolla, Missouri.

Nanni, A. 2001. "Relevant field applications of FRP composites in concrete structures." In *Pro., International Conference Composites in Construction–CCC2001,* 661-670. Portugal.

Nanni, A., & Faza, S. 2002. "Design and Construction of Concrete Reinforced with FRP Bars: An Emerging Technology." *Concrete International. 24*: 53-58.

Nkurunziza, G., A. Debaiky, P. Cousin, and B. Benmokrane. 2005. "Durability of GFRP bars: A critical review of the literature." *Progress in Structural Engineering and Materials.* 7 (4): 194-209.

Otsuki, N., S. Nagataki, and K. Nakashita. 1992. "Evaluation of AgNO 3 solution spray method for measurement of chloride penetration into hardened cementitious matrix materials." *Materials Journal*. 89 (6): 587-592.

Phelan, R. S., W. P. Vann, and J. Bice. 2003. *FRP Reinforcing Bars In Bridge Decks Field Instrumentation And Short-Term Monitoring*. No. FHWA/TX-06/9-1520-4.Texas Tech University, Lubbock, Texas.

Phillips, K. A., M. Harlan, C. L. Roberts-Wollmann, and T. E. Cousins. 2005. *Performance of a bridge deck with glass fiber reinforced polymer bars as the top mat of reinforcement*. VTRC 05-CR24, Virginia Center for Transportation Innovation and Research, Charlottesville, VA.

Price, R. K. 1985. *Determination of Chloride Ion Content in Concrete*. Texas State Department of Highways and Public Transportation. Materials and Tests Division, 1.

Rajput, A. S., & Sharma, U. K. 2017. "Durability and serviceability performance of GFRP rebars as concrete reinforcement." *Indian Concrete Journal*, *91*(7), 51-60.

Reising, R. MW, B. M. Shahrooz, V. J. Hunt, M. S. Lenett, S. Christopher, A. R. Neumann, A. J. Helmicki, R. A. Miller, S. Kondury, and S. Morton. 2001. "Performance of five-span steel bridge with fiber-reinforced polymer composite deck panels." *Transportation research record* 1770, no. 1: 113-123.

Sagues, A. A., E. I. Moreno, W. Morris, and C. Andrade. 1997. *Carbonation in concrete and effect on steel corrosion*. No. WPI 0510685. University of South Florida.

Shekar, V., S. H. Petro, and H. VS GangaRao. 2003. "Fiber-reinforced polymer composite bridges in West Virginia." *Transportation Research Record.* 1819 (1): 378-384.

Van Den Einde, L., L. Zhao, and Frieder Seible. 2003. "Use of FRP composites in civil structural applications." *Construction and Building Materials.* 17 (6-7): 389-403.

Wang, W., O. Gooranorimi, J. J. Myers, and A. Nanni. 2018. "Microstructure and Mechanical Property Behavior of FRP Reinforcement Autopsied from Bridge Structures Subjected to In Situ Exposure." In *International Congress on Polymers in Concrete*. 585-591. Springer, Cham.

Wipf, J.T., B. M. Phares, F. W. Klaiber, and U. Deza, 2006. *Evaluation of the Bettendorf Bridge, Iowa*. Final Report, Center for Transportation Research and Education, Iowa State University, Ames, IA.

Xi, Y., Y. Jing, and R. Railsback. 2018. *Surface Chloride Levels in Colorado Structural Concrete*. No. Report No. CDOT-2018-05. Colorado. Dept. of Transportation. Research Branch.

Yuan, Q., C. Shi, F. He, G. De Schutter, K. Audenaert, and K. Zheng. 2008. "Effect of hydroxyl ions on chloride penetration depth measurement using the colorimetric method." *Cement and Concrete Research.* 38 (10): 1177-1180.

Yunping X., Y. Jing, R. Railsback. 2018. *Surface Level Chlorides in Colorado Structural Concrete.* Report No. CD0T-2018-05. Colorado Department of Transportation. Research Branch.

Zhou, Y., B. Gencturk, K. Willam, and A. Attar. 2015. "Carbonation-induced and chloride-induced corrosion in reinforced concrete structures." *Journal of Materials in Civil Engineering*. 27 (9): 04014245.

Zhou, A., Chow, C. L., & Lau, D. 2018. "Structural behavior of GFRP reinforced concrete columns under the influence of chloride at casting and service stages." *Composites Part B: Engineering*, *136*, 1-9.

# APPENDIX B

# BOND ASSESSMENT OF GFRP BARS EMBEDDED IN FIBER-REINFORCED ECO-CONCRETE

# ABSTRACT

Steel corrosion is a major problem in the civil engineering industry, thus finding an effective alternative has been of main interest. One of these alternatives is glass fiber-reinforced polymer (GFRP) bar, as it has multiple advantages including: corrosion-free, nonconductive, and high strength-to-weight ratio. On the other hand, conventional concrete (CC) is not environment-friendly concrete due to its high CO2 emission. Therefore, other replacements of Portland cement have been on the lookout. Some of the alternatives include fly ash and silica fume that can be added either partially or fully to make the concrete. In addition, adding fibers to the concrete has been of main interest, as it offers several advantages including crack control, and tensile capacity increase. In this study, a bond investigation was carried out to assess the bond-slip behavior between GFRP bars and fiber-reinforced eco-concrete (High-volume fly ash (HVFA) concrete) following the RILEM recommendations. The parameters of the study involved: concrete type (CC and HVFA), fiber type (steel and synthetic), bar type (GFRP and steel), bar size (13 and 19 mm), and embedment length (6.4 mm, and 12.7 mm). To make the assessment, the bond results of the GFRP-reinforced specimens were compared to those resulted from steel-reinforced specimens. The test results showed that the bond strength of GFRP bar was less than that of steel bar. Also, the addition of fibers to the concrete decreased the bond strength.

# 1. INTRODUCTION

One of the major issues in the bridge industry is corrosion of reinforcement, as it is considered costly and requires continuous monitoring. Therefore, other alternative to replace steel reinforcement is of main need, one of these valid options is glass-fiber reinforced polymer (GFRP) bars (Nanni, De Luca, & Zadeh, 2014). GFRP bars present itself as a solid solution to replace steel reinforcement owing to its fantastic characteristics including corrosion resistivity, electrical non-conductivity, and high-strength-to-weight ratio (Ali F Al-Khafaji et al., 2020)(Benmokrane et al. 2018). On the other hand, conventional concrete (CC), which is a cement-based concrete, is not considered as environment friendly concrete owing to the high carbon dioxide (CO2) emissions (Al-Khafaji et al. 2019)(Volz et al. 2012). Therefore, other types of materials such as fly ash and silica fume have been put in focus to fully or partially replace Portland cement. Fly ash is a by-product obtained from the coal combustion in electric power generating plants. Fly ash is categorized into three main classes which are class C, F, and N (ASTM 618, 2010). A concrete can be considered as a high-volume fly ash (HVFA) concrete only when the fly ash percentage covers 50% or more of the cementitious material (Alghazali & Myers, 2019). Several studies have been carried out to assess the fly-ash based concrete, but most of them have addressed the low-volume fly ash concrete (around 20% or 30%) rather than the high-volume content (Jalal et al. 2013; Siddique et al. 2012). Naik et al. (1989) conducted a bond assessment investigation using a 10%, 20%, and 30% fly ash-based concrete where they found that the bond strength

reached its highest value with 20% fly ash and then exhibited a decrease when the 30% fly ash concrete was used. In addition to the use of fly ash, the use of fibers in concrete have been seeing an increasing demand (Garcia-Taengua et al. 2016). ASTM C1116 (2010) categorizes the fibers implemented in concrete into majorly four kinds including: Type 1 steel-fiber, Type 2 glass fibers, Type 3 synthetic fibers, and Type 4 natural fibers. Song et al. (2006) carried out a study to assess the mechanical properties of high-strength steel fiber reinforced concrete using different volume fractions including 0.5, 1.0, 1.5, and 2.0%. Their study concluded that the compressive strength increased by 15%, the tensile strength and rupture modulus increased up to 98% and 126% respectively. Kwak et al. (2002) investigated the shear strength of steel fiber-reinforced concrete beams without stirrups by involving three levels of volume fractions of fibers including 0.0%, 0.50%, and 0.75%. Their research showed that the nominal stress at shear cracking and the ultimate shear strength increased with increasing fiber volume, decreasing shear span-to-depth ratio, and increasing concrete compressive strength. Joshi et al. (2018) studied the efficiency of steel and synthetic fibers on the performance of prestressed concrete beams under shear and flexure. The test results showed that, in compared to synthetic fibers, the post cracking response was stiffened more efficiently when steel fibers were used.

In this study, pullout tests were carried out to assess the bond performance of HVFA and fiber-reinforced HVFA concrete reinforced with GFRP bars and compared with specimens of the same kind of concrete but reinforced with steel bars. Two types of fibers were implemented including steel and synthetic fibers, as well as two types of

concrete were used including 70% HVFA concrete and conventional concrete (CC). Two bar sizes were used, 13 mm (0.5 in.) and 19 mm (0.75 in.).

## 2. PULLOUT BOND EXPERIMENT

Bond between reinforcement and concrete can be accessed via several techniques including pullout, beam-end specimens, and beam splice. In this investigation, pullout test was conducted to make the bond assessment owing to its feasibility and the ability to provide reliable results. The pullout test was performed on thirty-two full-size cylinder specimens weighing between 20 to 35 kg (50 to 70 lb). To carry out the test, RILEM7-11-128, Reunion Internationale des Laboratoires et Experts des Materiaux, (1994) was implemented. In this setup, the selected embedment length was ten times the rebar diameter in order to avoid splitting of concrete failure. In addition, Polyvinyl chloride pipe (PVC) was used to cover the needed debonded section of the rebar. In order to meet the RILEM's cover requirements, a specimen diameter of 300 mm (12 in.) was used. The test setup is shown in Figure 1.

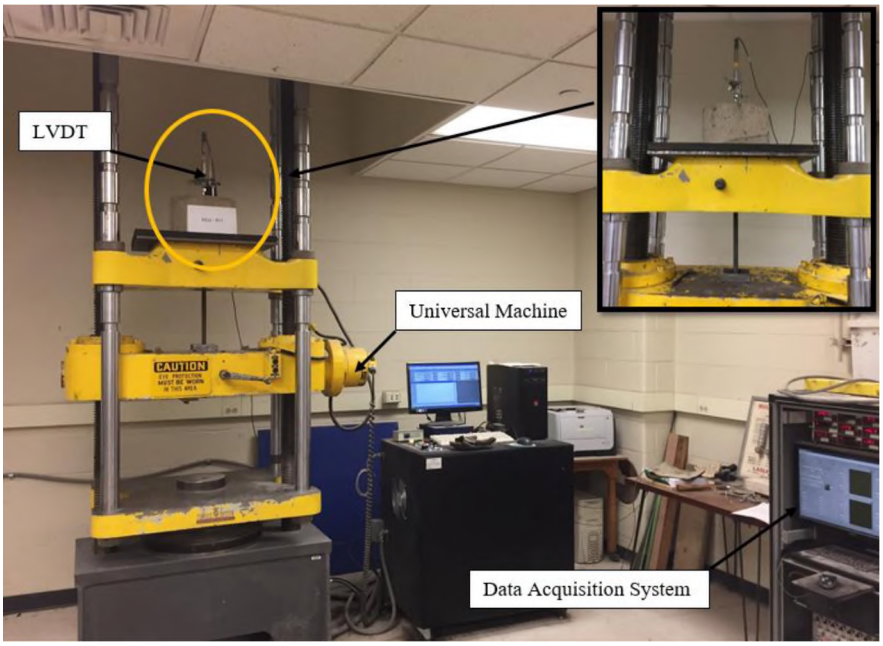


Figure 1. Pullout test setup

## 3. MIXTURES AND MATERIALS

In this investigation, the type of cement used was ASTM Type I/II Portland cement and the fly ash implemented was an ASTM Class C. The physical and chemical characteristics of cement and fly ash are shown in Table 1. The sources of fine and coarse aggregates were natural sand and crushed dolomite, which had a 19 mm (0.75 in.) approximate diameter, respectively. Two types of reinforcements were used, steel and glass fiber-reinforced polymer (GFRP) bars respectively, and, for each type, two sizes were used, 13 mm (0.5 in.) and 19 mm (0.75 in.). Steel reinforcement had a yield strength of 414 MPa (60 ksi) while GFRP bars were 100 Aslan from Owens Corning and had an ultimate tensile strength of about 725 MPa (105 ksi). The steel bar's deformation spacing,

height, and relative area were in agreement with ACI 408R-03 (2003) and ASTM A615-09 (2018). On the other hand, GFRP bars' specifications were in agreement with the ASTM D7205 standards (2011). The mechanical and physical properties of the GFRP bars are shown in Table 2.

Table 1. Chemical and physical properties of cementitious materials

| Properties | Unit | Cement | Fly Ash |
|---|---|---|---|
| $SiO_2$ | % | 19.4 | 35.17 |
| $Al_2O_3$ | | 4.58 | 21.07 |
| $Fe_2O_3$ | | 3.20 | 6.58 |
| CaO | | 62.7 | 26.46 |
| MgO | | 3.27 | 6.22 |
| $SO_3$ | | 3.19 | 1.43 |
| $Na_2O$ | | - | 1.91 |
| $K_2O$ | | - | 0.44 |
| $Na_2O$ eq. | | 0.50 | 1.31 |
| Loss in ignition | | 2.31 | 0.12 |
| Fineness (+325 Mesh) | | 98.4 | 15.2 |
| $C_3S$ | | 58.0 | - |
| $C_2S$ | | - | - |
| $C_3A$ | | 7.00 | - |
| $C_4AF$ | | - | - |
| Vicat set time, initial | Minutes | 90.0 | - |
| Vicat set time, final | | 195 | - |
| Specific gravity | - | 3.15 | 2.68 |

In concrete, the selected compressive strength was 35 MPa (5 ksi) which is representative for most concrete used in 3 to 6 story-buildings (Mahzuz et al. 2020). In addition to the Portland cement-based concrete (also called conventional concrete (CC)), Fly ash-based concrete contained 70% fly ash and 30% Portland cement was made. Also,

two types of fibers were used to reinforce the concrete including steel fibers used only with specimens contained steel bars, and synthetic fibers used only with specimens contained GFRP bars. Table 3 depicts the fresh and hardened concrete properties. Besides the pullout specimens, companion cylinders were collected and tested for compressive and tensile strength. For compressive strength measurements, cylinders were tested at ages of 3, 7, 28, and 56 days, while, for tensile strengths, cylinders were tested at 28 and 56 days. In GFRP-reinforced specimens, a steel tube was used to protect the gripped region of the bar from the crushing forces resulted from the testing machine's grips. Sika-Dur 30 epoxy was utilized to attach the steel tube to the GFRP bar. Figure 2 shows the materials used in this study.

Table 2. Manufacturer's, Owens Corning, mechanical and physical properties of GFRP rebars

| Rebar size mm (in.) | Nominal Area $mm^2$ ($in^2$) | Guaranteed Tensile Strength MPa (ksi) | Ultimate Tensile Load kN (kips) | Modulus of Elasticity GPa (ksi) | Ultimate Strain (%) |
|---|---|---|---|---|---|
| 13 (1/2) | 127 (0.20) | 758 (110) | 95.90 (21.55) | 46 (6672) | 1.64% |
| 19 (3/4) | 285 (0.44) | 690 (100) | 196.60 (44.20) | 46 (6672) | 1.49% |

## 4. SETUP AND PROCEDURE OF PULLOUT TEST

The test was carried out using a universal machine. The pullout specimens were rotated in a way where the bar side faced down. To make sure the specimen rested evenly

with no eccentrics, a thin rubber mat was used beneath the specimen. Universal machine's grips embraced the free end of the bar. A linear variable differential transformer (LVDT) was positioned on the exposed piece of the bar and utilized to record the slippage. A loading rate of 2.5 mm/min (0.01 in./min) was used to make sure enough data stored to draw the force-slip diagram and to avoid any appearance of dynamic-related forces that could influence the interpretation of the overall bond performance. The specimens were loaded in tension until a complete slippage took place.

Table 3. Fresh and hardened concrete properties

| Property | Specification | Age of Test, Days | CC | 70% HVFAC | FRCC | FR-70% HVFAC |
|---|---|---|---|---|---|---|
| Slump, mm (in.) | ASTM C143 | - | 114 (4.5) | 127 (5.0) | 127 (5.0) | 152 (6.0) |
| Air Content, % | ASTM C231 | - | 3 | 4 | 4.5 | 5.5 |
| Splitting Tensile Strength, MPa (psi) | ASTM C496 | 28 | 2.60 (377) | 1.72 (249) | 2.9 (428) | 2.1 (310) |
| | | 56 | 2.66 (387) | 1.73 (251) | 3.0 (432) | 2.2 (314) |
| Compressive Strength, MPa (psi) | ASTM C39 | 28 | 34 (4890) | 30 (4300) | 33 (4795) | 31 (4495) |
| | | 56 | 35 (5131) | 34 (4938) | 35 (5058) | 33 (4811) |

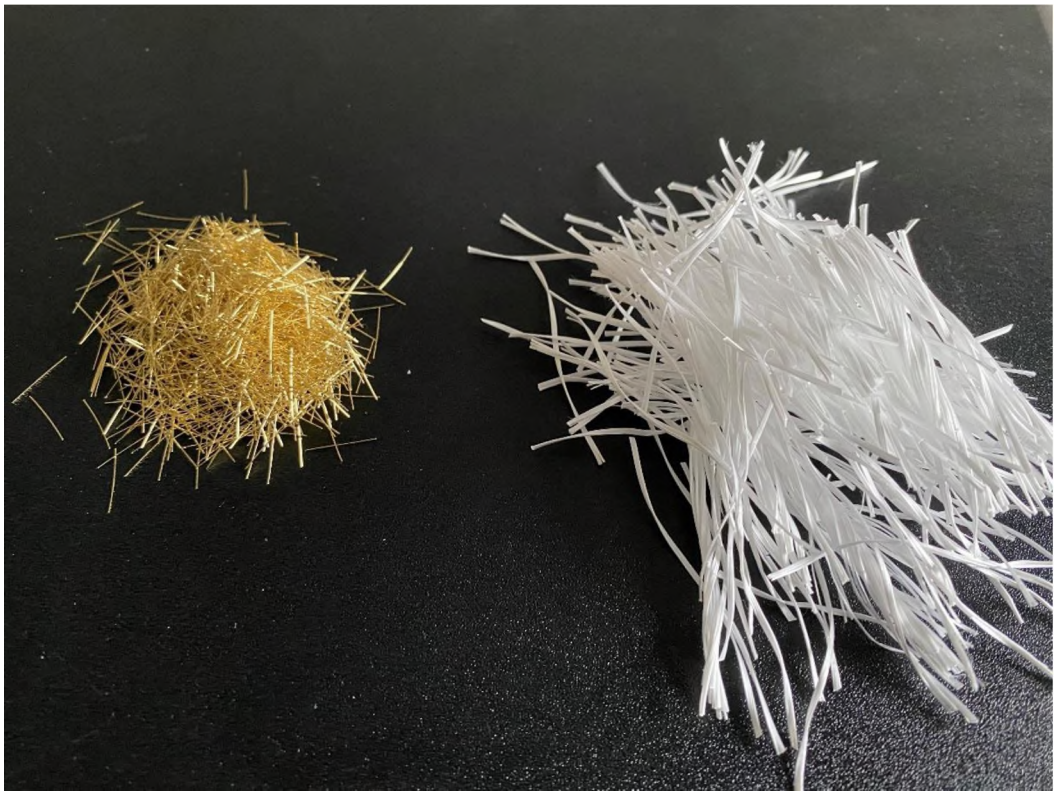

Figure 2. Fibers used, steel fiber (gold color) and synthetic fiber (white color)

## 5. TEST RESULTS AND DISCUSSIONS

The pullout tests results showed that regardless the type of concrete or addition of fibers, GFRP bars exhibited less bond strength than that of mild steel bars. All the specimens failed in pure pullout as planned. Figure 3 depicts a failed specimen. The compressive strengths used were normalized to mitigate the differences in compressive strength between the laboratory and filed ones. The inverse square root for normalization was endorsed by the ACI 318 (2014) while the fourth root was recommended by the ACI 408R-03 (2003). The results are depicted in Table 4. The design compressive strength of all concrete was 35 MPa (5000 psi), but the laboratory tests yielded some slight shifts in

their results from the design one and that was reflected on the bond strength results. When conventional concrete (CC) was used, a higher bond strength was observed than that resulted from using the 70% HVFA concrete owing to the higher bond strength noticed in CC.

Adding fibers to the concrete regardless of their type (steel or synthetic) or concrete type had led to reduce the bond strength. The addition of fibers was accompanied with an increase in the level of entrapped air in concrete and that behavior was also reported in other studies (Kobayashi et al. 2010; Naaman et al. 1993). It is believed that adding fibers disturbs the concrete and introduces more voids (Söylev, 2011). Voids surrounding the bar tend to create spacing between the bar and surrounding concrete and thus reduce the contact area between the concrete and bar. As a result of that reduction in contact area, a decrease in bond strength is resulted.

Steel fibers were used only with steel bars, while synthetic fibers were used with GFRP bars. The reason for this combination is to present/investigate a more sustainable concrete including all sustainable/green elements represented by noncorrosive bar (GFRP), synthetic noncorrosive fibers, and HVFA concrete. The results showed that the more fly ash added, the less the bond strength reduction resulted regardless the fibers and reinforcement types. In addition, CC had the highest reduction with 18%, while 70% HVFAC had 12% reduction only. Fly ash particles are smaller than Portland cement particles, as the earlier has an average size of around 75 μm while Portland cement has an average size of around 10 μm (Bentz et al. 2011). The finer the particle size was, the better the concrete-to-sand coated bar engagement was noticed.

In CC, when mild steel bars used, the reduction rates were 24% for 13 mm (0.5 in.) bar size and only 4% for 19 mm (0.75 in.) bar size. On the other hand, when GFRP bars used, the reduction rates of the 13 mm (0.5 in.) and 19 mm (0.75 in.) bars were 22% and 23% respectively. The reason that 19 mm steel bars had the lowest bond strength reduction rate is that 19 mm (0.75 in.) bar is the least susceptible to voids generated by the fiber addition among all bars used in this investigation.

Figure 3. GFRP bar after pullout test

Table 4. Test results of pullout

| Concrete Type | Rebar Size mm | Fiber Type | Rebar Type | P (kN) | Norm. P (kN) | P avg. (kN) | Coefficient of Variation (%) |
|---|---|---|---|---|---|---|---|
| CC | #13 | - | Steel | 66 | 66 | 63 | 8 |
| | | | | 59 | 59 | | |
| | | - | GFRP | 54 | 54 | 49 | 14 |
| | | | | 44 | 44 | | |
| | #19 | - | Steel | 171 | 172 | 160 | 11 |
| | | | | 148 | 148 | | |
| | | - | GFRP | 110 | 110 | 115 | 6 |
| | | | | 119 | 119 | | |
| 70% HVFAC | #13 | - | Steel | 71 | 71 | 73 | 5 |
| | | | | 76 | 76 | | |
| | | - | GFRP | 34 | 34 | 36 | 8 |
| | | | | 38 | 38 | | |
| | #19 | - | Steel | 158 | 157 | 157 | 0 |
| | | | | 159 | 158 | | |
| | | - | GFRP | 79 | 79 | 83 | 8 |
| | | | | 89 | 88 | | |
| CC + Fiber | 13 | Steel | Steel | 43 | 43 | 47 | 14 |
| | | | | 52 | 52 | | |
| | | Synthetic | GFRP | 41 | 41 | 38 | 9 |
| | | | | 36 | 36 | | |
| | 19 | Steel | Steel | 158 | 158 | 153 | 5 |
| | | | | 148 | 147 | | |
| | | Synthetic | GFRP | 89 | 89 | 87 | 2 |
| | | | | 86 | 86 | | |
| 70% HVFAC + Fiber | 13 | Steel | Steel | 57 | 56 | 59 | 7 |
| | | | | 63 | 62 | | |
| | | Synthetic | GFRP | 30 | 29 | 32 | 13 |
| | | | | 36 | 35 | | |
| | 19 | Steel | Steel | 138 | 136 | 136 | 0 |
| | | | | 137 | 136 | | |
| | | Synthetic | GFRP | 70 | 69 | 76 | 12 |
| | | | | 83 | 82 | | |

# 6. CONCLUSIONS

Corrosion is a major issue in the civil engineering industry, therefore other non-corrosive materials, such as GFRP bars, have been used as an effective solution to replace steel bars. Portland cement is also not an environment-friendly material owing to its high level of carbon dioxide emissions, thus alternative such as fly ash has been of main interest to replace Portland cement fully or partially. In this investigation, a bond strength assessment was carried out on specimens made from HVFA concrete and Fiber-Reinforced HVFA concrete and reinforced with GFRP bars. Fly ash Type-C has been used to partially replace Portland cement where the fly ash replaced 70% of the overall cementitious material and the rest was Portland cement. In addition, two types of reinforcement and two bar sizes were used, namely steel and GFRP bars, and 13 mm (o.5 in.) and 19 mm (0.75 in.) respectively. Furthermore, the addition of fibers in concrete was assessed too, where two types of fibers were implemented, namely steel and synthetic fibers. The following was concluded from the study:

- All specimens showed a clear slippage mode of failure.
- GFRP bars showed less bond strength than that of steel bars.
- The bigger the bar size was, the more bond strength yielded.
- The higher the compressive strength (even if it is slightly high or low) was, the bigger the bond strength.

- The ribs of steel bars were the reason for the higher bond strength owing to bearing forces generated from the existence of ribs in addition to the friction forces. Sand-coated GFRP bars had only friction resistance.
- CC with or without fibers had a higher bond strength than HVFA.
- The addition of fibers reduced the bond strength, regardless the concrete or bar type, due to the increase in the level of air entrapped in concrete that disrupts the concrete and create more voids.
- The bond reduction after adding fibers was the highest in CC with 18% reduction and the lowest in HVFA with 12%.
- In fiber-reinforced CC, 19 mm (0.75 in.) steel bars had the lowest reduction of bond among the other types and sizes of bars owing to the low voids susceptibility of the steel bar's ribs. The larger the bar rib was, the less voids susceptibility was noticed and thus less bond reduction.
- In fiber-reinforced HVFA, GFRP bars, regardless of their size, showed less bond reduction than steel bars owing to the better engagement of the fine particles of HVFAC with sand coating of the GFRP bars.

# REFERENCES

ACI 318. (2014). *Building code requirements for structural concrete (ACI 318-14) : an ACI standard : commentary on building code requirements for structural concrete (ACI 318R-14).*

ACI 408R. (2003). ACI 408R-03. *American Concrete Institute*, 1–49.

Al-Khafaji, Ali F., Myers, J. J., & Alghazali, H. (2019). The evaluation of bond-slip behaviour of GFRP bars in conventional and sustainable concrete. In *Advanced Composites in Construction, ACIC 2019 - Proceedings of the 9th Biennial Conference on Advanced Composites in Construction 2019* (pp. 178–182).

Al-Khafaji, Ali F., Myers, J. J., Nanni, A., Myers, J. J., Committees, T., & Nanni, A. (2020). Assessment Study of Gfrp Reinforcement Used in Two Concrete Bridges After More Than Fifteen Years of Service, (M), 1–34. https://doi.org/10.14359/51725980

Alghazali, H. H., & Myers, J. J. (2019). Bond performance of high-volume fly ash self-consolidating concrete in full-scale beams. *ACI Structural Journal*, *116*(1), 161–170. https://doi.org/10.14359/51706920

ASTM-C1116. (2010). Standard Specification for Fiber-Reinforced Concrete. *Merican Society for Testing and Materials*, 1–7. https://doi.org/10.1520/C1116

ASTM-D7205. (2011). Standard Test Method for Tensile Properties of Fiber Reinforced Polymer Matrix. *ASTM*, *i*(Reapproved 2011), 1–13. https://doi.org/10.1520/D7205

ASTM 618. (2010). Standard Specification for Coal Fly Ash and Raw or Calcined Natural Pozzolan for Use in Concrete. *Annual Book of ASTM Standards*, 3–6. https://doi.org/10.1520/C0618

ASTM A615. (n.d.). Standard Specification for Deformed and Plain Carbon-Steel Bars for Concrete Reinforcement. *ASTM*. https://doi.org/10.1520/A0615

Au, C., & Büyüköztürk, O. (2006). Peel and shear fracture characterization of debonding in FRP plated concrete affected by moisture. *Journal of Composites for Construction*, *10*(1), 35–47. https://doi.org/10.1061/(ASCE)1090-0268(2006)10:1(35)

Benmokrane, B., Nazair, C., Loranger, M. A., & Manalo, A. (2018). Field Durability Study of Vinyl-Ester-Based GFRP Rebars in Concrete Bridge Barriers. *Journal of Bridge Engineering*, *23*(12), 1–13. https://doi.org/10.1061/(ASCE)BE.1943-5592.0001315

Bentz, D. P., Hansen, A. S., & Guynn, J. M. (2011). Optimization of cement and fly ash particle sizes to produce sustainable concretes. *Cement and Concrete Composites*, *33*(8), 824–831. https://doi.org/https://doi.org/10.1016/j.cemconcomp.2011.04.008

Garcia-Taengua, E., Martí-Vargas, J. R., & Serna, P. (2016). Bond of reinforcing bars to steel fiber reinforced concrete. *Construction and Building Materials*, *105*, 275–284. https://doi.org/10.1016/j.conbuildmat.2015.12.044

Jalal, M., Ramezanianpour, A. A., & Pool, M. K. (2013). Split tensile strength of binary blended self compacting concrete containing low volume fly ash and TiO2 nanoparticles. *Composites Part B: Engineering*, *55*, 324–337. https://doi.org/10.1016/j.compositesb.2013.05.050

Joshi, S. S., Thammishetti, N., & Prakash, S. S. (2018). Efficiency of steel and macro-synthetic structural fibers on the flexure-shear behaviour of prestressed concrete beams. *Engineering Structures*, *171*, 47–55. https://doi.org/https://doi.org/10.1016/j.engstruct.2018.05.067

Kobayashi, K., Iizuka, T., Kurachi, H., Concrete, K. R.-C. and, & 2010, undefined. (n.d.). Corrosion protection performance of high performance fiber reinforced cement composites as a repair material. *Elsevier*. Retrieved from https://www.sciencedirect.com/science/article/pii/S0958946510000429

Kwak, Y. K., Eberhard, M. O., Kim, W. S., & Kim, J. (2002). Shear strength of steel fiber-reinforced concrete beams without stirrups. *ACI Structural Journal*, *99*(4), 530–538.

Mahzuz, H. M. A., Choudhury, M. R., Ahmed, A. R., & Ray, S. (2020). Effect of material strength on the cost of RCC building frames. *SN Applied Sciences*, *2*(1), 1–8. https://doi.org/10.1007/s42452-019-1830-4

Naaman, A., Alkhairi, F., & Hammoud, H. (1993). *Mechanical Behavior of High Performance Concretes, Volume 6: High Early Strength Fiber Reinforced Concrete*. Retrieved from https://trid.trb.org/view/404937

Naik TR, Singh SS, S. V. (1989). Concrete compressives strength, shrinkage and bond strength as affected by addition of fly ash and temperature. *The University of Wisconsin*.

Nanni, A., De Luca, A., & Zadeh, H. (2014). *Reinforced Concrete with FRP Bars*. CRC Press.

RILEM, & Materials, T. R. for the T. and U. of C. (1994). RILEM 7-II-128. RC6: Bond Test for Reinforcing Steel - Pullout Test.

Siddique, R., Aggarwal, P., & Aggarwal, Y. (2012). Influence of water/powder ratio on strength properties of self-compacting concrete containing coal fly ash and bottom ash. *Construction and Building Materials*, *29*, 73–81. https://doi.org/10.1016/j.conbuildmat.2011.10.035

Söylev, T. A. (2011). The effect of fibers on the variation of bond between steel reinforcement and concrete with casting position. *Construction and Building Materials*, *25*(4), 1736–1746. https://doi.org/10.1016/j.conbuildmat.2010.11.093

Volz, Jeffery; Myers, John; Richardson, David; Arezoumandi, Mahdi; Beckemeier, Karl; Davis, Drew; Holman, Kyle; Looney, Trevor; and Tucker, B. (2012). *Design and evaluation of a high-volume fly ash (HVFA) concrete mixes*. *Microwave and Optical Technology Letters* (Vol. 52). https://doi.org/10.1002/mop.24993

# REFERENCES

Ali F. Al-Khafaji; John J. Myers; Hayder H. Alghazali. "Evaluation of bond performance of glass fiber rebars embedded in sustainable concrete" Journal of Cleaner Production, 28, 2020.

Ali F. Al-Khafaji; John J. Myers; Antonio Nanni. "Assessment Study of Glass Fiber-Reinforced Polymer Reinforcement Used in Two Concrete Bridges after more than 15 Years of Service." ACI Materials, 117, 5, 2020.

NACE, 2013. Corrosion costs and preventive strategies in the United States," Corrosion Costs Prev. Strategy. United States, No. NACE. FHWA-RD-01-156.

Ali F. Al-Khafaji; Rudy T. Haluza; Vanessa Benzecry; John J. Myers; Charles E. Bakis; Antonio Nanni, "Durability assessment of 15-to-20-year-old GFRP bars extracted from bridges in the US II: GFRP Bar Assessment" ASCE Journal of Composites for Construction, 25, 2, 2021.

Vanessa Benzecry; Ali F. Al-Khafaji; Rudy T. Haluza; Charles E. Bakis; John J. Myers; Antonio Nanni, "Durability assessment of 15-to-20-year-old GFRP bars extracted from bridges in the US I: Bar Extraction, and Concrete Assessment" ASCE Journal of Composites for Construction, 25, 2, 2021.

El-Salakawy, E. F., B. Benmokrane, and F. Brière. "Glass FRP composite bars for concrete bridge barriers." Sci. Eng. Compos. Mater. 12 (3): 167–192. 2005.

Ahmed, E., B. Benmokrane, and M. Sansfaçon. "Case study: Design, construction, and performance of the La Chancelière parking garage's concrete flat slabs reinforced with GFRP bars." J. Compos. Constr. 21. 2017(1): 05016001. https://doi.org/10.1061/(ASCE)CC.1943-5614.0000656.

Mohamed, H., and B. Benmokrane. "Design and performance of rein- forced concrete water chlorination tank totally reinforced with GFRP bars: Case study." J. Compos. Constr. 18 (1) 2014: 05013001. https://doi.org /10.1061/(ASCE)CC.1943-5614.0000429.

T. Hemalatha, Ananth Ramaswamy "A review on fly ash characteristics e Towards promoting high volume utilization in developing sustainable concrete" Journal of Cleaner Production, 147, 2017.

ASTM, 2010. Standard Specification for Coal Fly Ash and Raw or Calcined Natural Pozzolan for Use in Concrete. Annu. B. ASTM Stand., pp. 3e6. https://doi.org/10.1520/C0618

Sahmaran, M., Li, V.C., 2009. Durability properties of micro-cracked ECC containing high volumes fly ash. Cem. Concr. Res. 39, 1033e1043.

EPA, 2008. Study on Increasing the Usage of Recovered Mineral Components in Federally Funded Projects Involving Procurement of Cement or Concrete. Environmental Protection Agency, 2008.

# VITA

Ali was born in Baghdad, Iraq. He received his Bachelor's degree in Civil Engineering from the University of Baghdad, Iraq, in 2009. He earned his Master's of Science degree in Civil Engineering (Structures) from the University of Kansas, USA, in 2013. After that, he worked as a Material Engineer at Geotechnology Inc. in Kansas City, Missouri, USA. In 2014, he moved to Tulsa, Oklahoma, USA, to work for B+T Group as a Project Engineer where he analyzed and modified telecommunication towers structurally. In 2015, he started working for BlueScope Building in Kansas City, Missouri, USA, as a Structural Engineer where he was responsible for design and analyses many prefabricated metal buildings across the North America. In 2016, he earned his Masters of Engineering degree in Engineering Management from Ohio University, USA. In August 2017, he was accepted as a PhD student at Missouri University of Science and Technology, Missouri, USA. Besides his PhD studies, Ali was involved in several Civil Engineering Organizations such the ASCE and ACI. He also served as an Associate Member in ACI 440 – FRP committee and Voting Member for ACI 440-L FRP-Durability. In addition, during his PhD studies, he became a licensed professional engineer (PE) in the State of Missouri in 2019 and certified project management professional (PMP) in 2020. In May 2021, he received his PhD in Civil Engineering from Missouri University of Science and Technology.